DESIGN AND DEVELOPMENT OF AN ENVIRONMENTAL CELL FOR DYNAMIC *IN SITU* OBSERVATION OF GAS-SOLID REACTIONS AT ELEVATED TEMPERATURES

by

Pushkarraj Vasant Deshmukh

BE, Padmabhooshan Vasantraodada Patil Institute of Technology, India, 2000

MS, University of Kentucky, 2003

Submitted to the Graduate Faculty of

Swanson School of Engineering in partial fulfillment

of the requirements for the degree of

Doctor of Philosophy

University of Pittsburgh

2008

UNIVERSITY OF PITTSBURGH

SWANSON SCHOOL OF ENGINEERING

This dissertation was presented

by

Pushkarraj Vasant Deshmukh

It was defended on

April 3, 2008

and approved by

Dr. Roy D. Marangoni, Emeritus Professor, Department of Mechanical Engineering and Materials Science, University of Pittsburgh

Dr. Laura Schaefer, Associate Professor, Department of Mechanical Engineering and Materials Science, University of Pittsburgh

Dr. Judith C. Yang, Associate Professor, Department of Mechanical Engineering and Materials Science, University of Pittsburgh

Dissertation Director: Dr. Michael Lovell, Professor, Department of Industrial Engineering, University of Pittsburgh

DESIGN AND DEVELOPMENT OF AN ENVIRONMENTAL CELL FOR DYNAMIC *IN SITU* OBSERVATION OF GAS-SOLID REACTIONS AT ELEVATED TEMPERATURES

Pushkarraj Vasant Deshmukh, PhD

University of Pittsburgh, 2008

In situ monitoring of events in transmission electron microscopy provides information on how materials behave in their true state while varying environmental conditions (i.e. temperature and pressure) and exposure to reactant gas mixtures. In-situ results are usually different from static, post-reaction observations because they provide valuable real time – rather than post mortem - information. To facilitate applications that demand *in situ* observations, a transmission electron microscope specimen holder assembly has been developed in this dissertation. This assembly incorporates a gas flow and heating mechanism along with a novel window-type environmental cell. A controlled mixture of up to four different gases can be circulated through the cell during an experiment. In addition, the specimen can be heated up to a temperature of 1500 °C using a specially designed carbon dioxide laser mechanism. This heating technique provides major advantages over conventional methods in terms of product life, specimen heating time and design size. The cell design incorporates a gas reaction chamber less than 1 mm in height, enclosed between a pair of 20 nm thick silicon nitride windows. The chamber can accommodate a specimen or a grid having a diameter of 3 mm and thicknesses in the range of 50 to 100 microns. The volume for the gas environment within the chamber is approximately 3 mm^3 and the gas path length is less than 1 mm. This holder has been designed by incorporating cutting edge heating and Si_3N_4 window fabrication technology to achieve excellent resolution along with a low thermal drift. Successful application of the holder has been shown to provide scientists

with an economical alternative to dedicated transmission electron microscopes for a vast array of *in situ* applications. These applications include understanding the basic material properties, catalysis reactions, semiconductor device development, and nano structure fabrication.

TABLE OF CONTENTS

LIST OF TABLES

LIST OF FIGURES

ACKNOWLEDGEMENTS

This research benefitted from the insight and direction of many people. I would like to take this opportunity to express my immense gratitude for their invaluable assistance.

First, my research committee members, Dr. Michael Lovell, Dr. Roy Marangoni, Dr. Juidth Yang and Dr. Laura Schafer for their expert guidance throughout the course of this research. Dr. Michael Lovell and Dr. Roy Marangoni, exemplify the high quality scholarship to which I aspire. In addition, Dr. Lovell provided timely and instructive comments and evaluation at every stage of the research process, allowing me to complete this dissertation on schedule. The infrastructure provided by Dr. Judith Yang, especially the transmission electron microscope was essential towards the successful completion of this project.

I would also like to thank our graduate administrator, Miss. Glinda Harvey for all her help and encouragement.

A major part of this research was carried out at E.A. Fischione Instruments, Inc. The vast and varied experience of the team members of this organization provided an exceptional platform for intellectual interactions. Mr. Paul Fischione, the president of E.A. Fischione Instruments, Inc., provided constructive guidance throughout the design process. I was highly motivated by his patient and practical approach towards this research. Special thanks to Mr. Jeffrey Gronsky, who helped make this design prototype a reality.

I would also like to take this opportunity to thank Dr. Nigel Browning and Dr. Mitra Taheri, for all the help extended during the preliminary testing of the *in situ* holder assembly.

Finally I would like to thank my family and friends. Even though they were not directly involved with my research, their emotional support went a long way in overcoming difficult situations.

This work was supported by the United States, Department of Defense Small Business Innovation Research Program (SBIR-Grant No: DE-FG02-04ER83932).

1.0 INTRODUCTION

Transmission electron microscopy is an imaging technique whereby a beam of electrons is transmitted through a thin specimen, interacting with the specimen as it passes through it. An image is formed from the electrons transmitted through the specimen, magnified and focused by an objective lens and appears on a fluorescent screen or on a layer of photographic film or to be detected by a sensor such as the CCD camera (Figure 1). This technique has revolutionized our understanding of materials by providing us with an extraordinary ability to obtain their structural (phase and crystallographic) data and elemental composition. This microscope was first developed by Knoll and Ruska in 1932 for which Ruska received the Nobel Prize in 1986.

The smallest distance between two points that can be resolved by human eyes is 0.1-0.2 mm. Any instrument that has a resolution of less than 0.1 mm could be described as a microscope. The smallest distance that can be resolved by a light microscope is approximately given by

$$\delta = \frac{0.61\lambda}{\mu \sin \beta} \qquad 1.1$$

In this equation, λ is the wavelength of radiation, μ the refractive index of the viewing medium and β is the semi angle of collection of the magnifying lens. If $\mu \sin \beta$ is approximated to be equal to unity, the resolution becomes equal to half the wavelength of light. This resolution increases with the decrease in wavelength. For green light in the middle of the visible spectrum,

λ is equal to 550 nm, so the resolution of a good light microscope is about 300 nm. This corresponds to about 1000 atom diameter, making it unsuitable for use in the field of material science where atomic scale resolution is a necessity. The features that control the properties of materials are on a scale well below the resolution of the light microscope.

The limitations of the light microscope were overcome based on Boglies idea about particle wave density. Being a charged particle, an electron could be easily refracted in a magnetic field and accelerated by an electrical potential. The stronger the potential the faster the electron will move, and as per the de Broglie relationship, the shorter the wavelength therefore the better the resolution. Some of the basic properties of an electron are listed in Table 1.

Table 1: Fundamental constants and definitions [1]

Charge (e)	(-) 1.602 X 10^{-19} C
Kinetic energy (1 eV)	1.602 X 10^{-19} J
Rest mass (m_0)	9.109 X 10^{-31} kg
Rest energy (m_0c^2)	511 KeV
Kinetic energy (charge X voltage)	1.602 X 10^{-19} Nm (1 V potential)
Plank's constant (h)	6.626 X 10^{-34} N m s
1 ampere	1 C/sec
Speed of light in vacuum (c)	2.998 X 10^{8} m/sec

The wavelength of electron beam is calculated to be equal to

$$\lambda = \frac{h}{\left[2m_0eV\left(1+\frac{eV}{2m_0c^2}\right)\right]^{1/2}} \qquad 1.2$$

Where h is the Plank's constant, m_0 is the rest mass of the electron, eV is the Kinetic energy and c is the speed of light in vacuum.

The electron wavelength for a given accelerating voltage is listed in Table 2 [1]. It can be seen that the wavelength of electrons is more than 10^5 times smaller than light waves. Within a transmission electron microscope (TEM) we impart momentum to the electron by accelerating it through a potential drop, V, giving it a kinetic energy eV. From the above equation it is seen that by increasing the accelerating voltage we decrease the wavelength of the electrons. Thus for a 100 KeV TEM the theoretical resolution that can be achieved is approximately 0.04 Å. However, due to the limitations of the lenses this resolution has never been attained. Recent developments in high resolution TEM's (HRETM's) has allowed the production of images with sufficient resolution to show carbon atoms in diamond separated by only 0.89 Å (1 angstrom is 10^{-10} m) and atoms in silicon by 0.78 angstroms at magnifications of 50 million times [1]. The record for the highest-resolution images ever seen was achieved by the TEAM (Transmission Electron Aberration-corrected Microscope) group wherein they crossed the 0.5 Å imaging milestone [62].

Table 2: Electron properties as a function of accelerating voltage [1]

Accelerating voltage (kV)	Wavelength (nm)
100	0.00370
120	0.00335
200	0.00251
300	0.00197
400	0.00164
1000	0.00087

1.1 TRANSMISSION ELECRON MICROSCOPY

1.1.1 Working principle

Figure 1 shows the basic principle of TEM. The electron gun produces a stream of electrons. This stream is focused to a small, thin, coherent beam by the use of condenser lenses 1 and 2. The first lens which is usually adjusted by the spot size control largely determines the spot size, i.e. the general size range of the final spot that strikes the sample. The second lens which is usually adjusted by the intensity or brightness control actually changes the size of the spot on the sample; changing it from a wide dispersed spot to a pinpoint beam. The beam is restricted by the condenser aperture, knocking out high angle electrons (those far from the optic axis, the dotted line down the center). The coherent beam is then transmitted through the specimen and focused by the objective lens into an image. Optional objective and selected area metal apertures can further restrict the beam; the objective aperture enhances contrast by blocking out high-angle diffracted electrons, the selected area aperture enables the user to examine the periodic diffraction of electrons by ordered arrangements of atoms in the sample. The image is passed down the column through the intermediate and projector lenses, being enlarged all the way. Finally, the electrons strike the phosphor image screen and light is generated, allowing the user to see the image.

This complete assembly is mounted in a column which is maintained under high vacuum with the help of pumps. The vacuum prevents the scattering of electrons by gas particles and helps to reduce the contamination of the electron source.

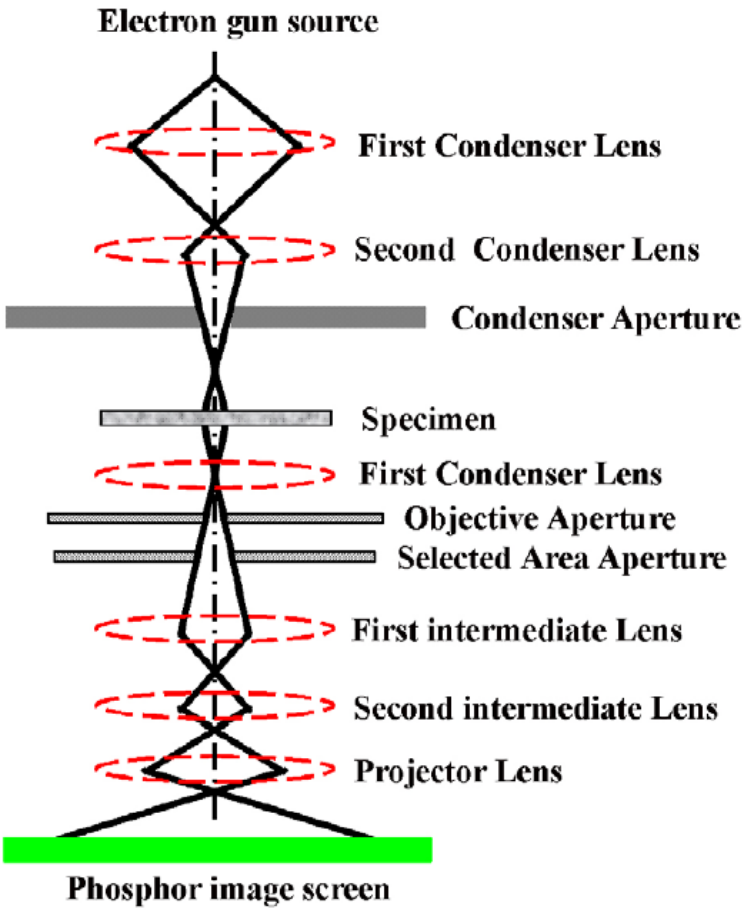

Figure 1: Schematic diagram of TEM

Electrons being a type of ionizing radiation generate a wide range of secondary signals when they strike the specimen as seen in Figure 2. These electrons are capable of removing one of the tightly bond inner-shell electrons from the attractive field of the nucleus. The electron wave can change both its amplitude and its phase as it traverses the specimen and both these kinds of change can give rise to image contrast. Thus a fundamental distinction we make in the TEM is between amplitude contrast and phase contrast. In most cases, both types of contrast actually contribute to an image, although one will tend to dominate. Amplitude contrast includes two principle types, namely mass-thickness contrast and diffraction contrast.

Mass-thickness contrast arises from incoherent (Rutherford) elastic scatter of electrons. It was found the cross section for incoherent scatter is a strong function of the atomic number as well as the thickness of the specimen. Generally speaking, a region with high atomic number element is expected to scatter more electrons than low atomic number region of the same thickness; thick regions scatter more electrons than thin region of the same elements. As a consequence, for the case of a bright field image, thicker and/or higher mass areas will appear darker than thinner and/or lower mass areas. The reverse will be true for dark field imaging form diffracted beam. Diffraction contrast is simply a special form of amplitude contrast because the scattering occurs at special angles (Bragg diffraction) which are controlled by the crystal structure and orientation of the specimen.

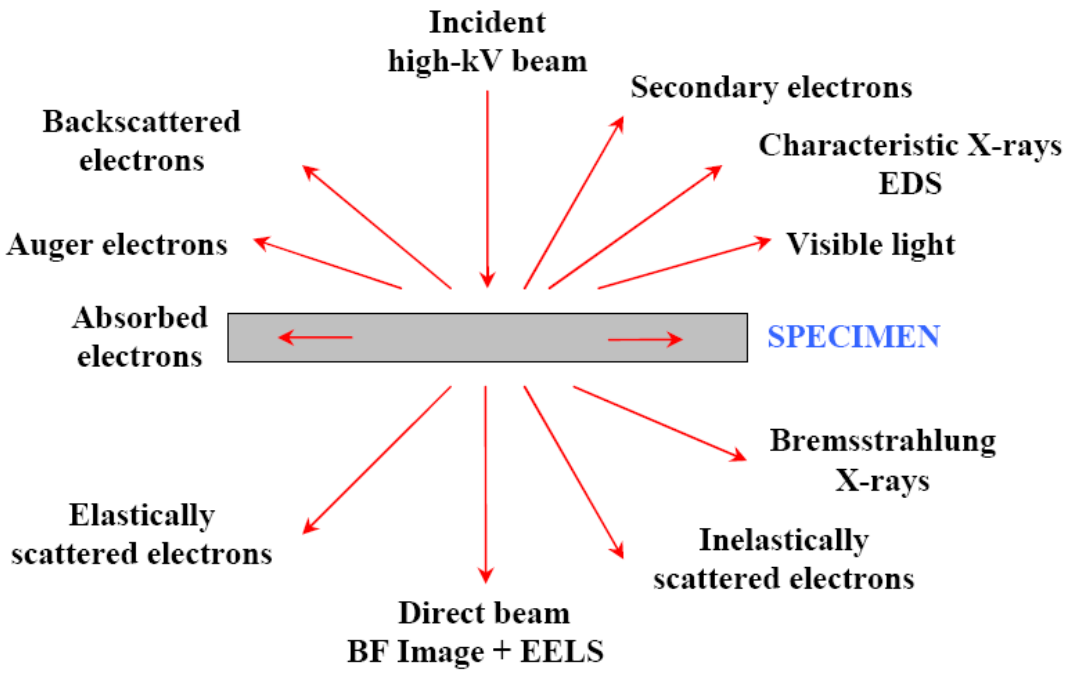

Figure 2: Signals generated when a beam of electron interacts with a specimen [1]

1.1.2 Applications

Ever since its invention, a TEM has been a primary tool of research in the field of physical and life sciences. Typical life science (biological) applications include tomographic reconstructions of small cells or thin sections of larger cells. In addition, cell structure and morphology are commonly determined while the localization of antigens or other specific components within cells is readily undertaken using specialized preparative techniques.

Using a TEM, material scientists have also been able to provide structural (phase and crystallographic) data and elemental composition, allowing them to tailor the microstructure of the materials to achieve specific sets of properties. Faults in crystals affect both the mechanical and electronic properties of materials, so understanding how they behave gives a powerful insight. By carefully selecting the orientation of the sample, it is possible not just to determine the position of the defects but also to determine the types of defects (line or planar) present. Generation of 3-D images using computer modeling has added a new layer of understanding to the study of crystalline materials. In analytical TEM's the element composition of the specimen can be determined with the help of energy dispersive X-ray analysis (EDXA) or energy loss spectrometry (EELS) [1].

1.1.3 Specimen Preparation

To achieve optimum results using electron microscopy, a sample that is both representative of the bulk and free of artifacts is imperative. There are several preparation methods that are used to produce high-quality specimens, with large, representative electron transparent areas for microanalysis [1-7]. The specimen thickness required for electron transparency depends on the

accelerating voltage of the TEM. For a 120 kV TEM, it is required that the specimen thickness be on the order of 100 to 800 Ångstroms. Materials that have dimensions small enough to be electron transparent, such as powders or nanotubes, can be quickly produced by the deposition of a dilute sample containing the specimen onto support grids. However, a standard TEM specimen consists of a 3mm disk and requires extensive work for it to be suitable for studies within a TEM. The rim of the specimen is relatively thick and total area of the material is usually small and confined to the center of the disk. The steps involved in the preparation of this specimen are

1. Creation of a thin slice from the bulk of the specimen

This is usually done using chemical wire/string saw, a wafering saw or spark erosion. Diamond saws are preferred in case of brittle materials. A thin slice which is approximately 200 microns thick is generated by this process.

2. Cutting the disk

This step involves generating a 3mm disk using a mechanical punch, ultrasonic drill or a grinding drill, depending on the nature of the material. Care should be taken to avoid shear transformation due to shock and to minimize the damage around the perimeter of the specimen.

3. Prethinning the Disk (Dimpling)

The aim of this process is to thin the center of the disk while minimizing damage to the center of the surface of the sample. This is usually carried out by simultaneous rotation of both the specimen and the grinding wheel containing abrasive slurry whose axes are orthogonal and intersecting. This process generates a region ~10 microns thick within the specimen disk.

4. Final Thinning

Electropolishing or ion milling is used for the generation of the final electron transparent specimen. Electropolishing is used in electrically conducting specimens, wherein a certain

applied voltage creates a polished surface due to the anodic dissolution of the specimen. Ion milling involves a momentum transfer process, wherein the specimens are bombarded with energetic ions or neutral atoms until it is thin enough to be studied in a TEM.

There are various other techniques that have been developed over the years in order to optimize the specimen preparation process. The focused ion beam (FIB) milling is one such technique. The FIB uses a liquid metal (typically Ga^{+}) ion beam, focused onto a spot which is as small as 5nm in diameter and possessing accelerating voltages ranging from 1 kV to 30 kV. The liquid metal source is often combined with a scanning electron microscope (SEM) to allow direct observation of the milling area (DB-FIB). Because the FIB can be used to micro-machine samples very precisely, it is possible to mill very thin membranes from a specific area of a sample, such as a semiconductor or metal. The final thinning is carried out by low eV milling such as nanomilling.

1.1.4 Specimen Holders

For observations to be carried out within a TEM, the specimen must be placed within the objective lens of the microscope. This area is represented by the goniometer, which allows for five possible movements of the specimen holder, X, Y, Z, α and β. X and Y are movements within the plane of the specimen and the Z is the movement perpendicular to it. α, is the tilt along the axis of the holder and β is the tilt of the specimen surface with respect to the tip of the holder. Specimen holders are a critical component of a TEM as the final resolution attained, invariably depends on the stability of the holder with respect to environmental conditions such as temperature and vibrations.

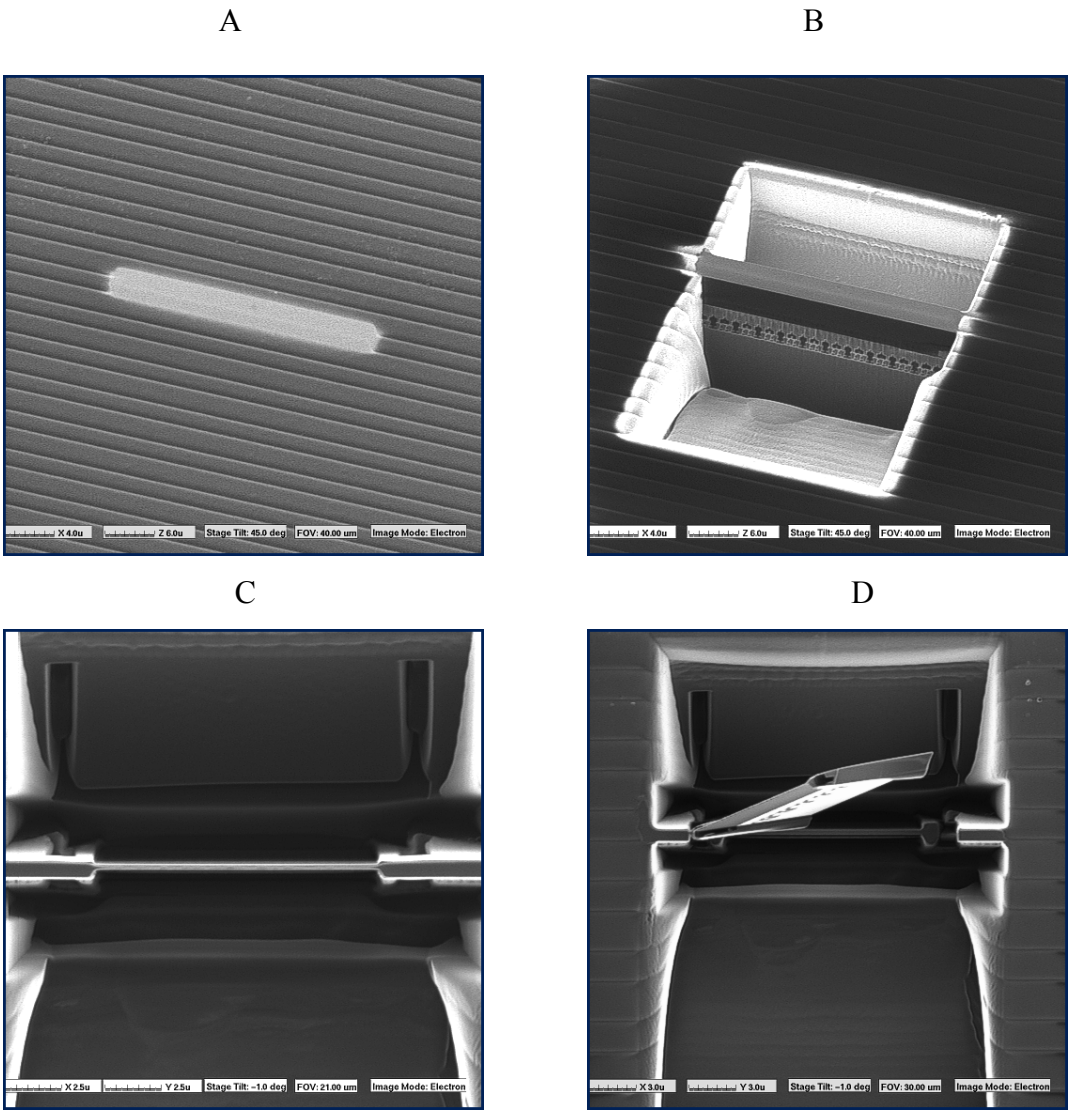

Figure 3: Steps involved in focused ion beam milling A) Deposit protective metal layer on the area of interest, B) Mill and thin central membrane, C) Polish mill for electron transparency D) FIB-mill to free membrane from trenches (Ref. www.fibics.com)

The key parts of a standard holder consists of

1. O-Ring

This acts as a seal between atmosphere and the TEM column and helps maintain the high vacuum inside the microscope.

2. Jewel bearing

This provides the mechanical link to the microscope column and is used to locate the specimen at a desired position between the objective lens. Some microscopes use the holder barrel to serve this purpose.

3. Specimen cup and clamping mechanism

The cup is used to hold the specimen. The clamping mechanism is designed to hold the specimen firmly in place within the cup. Material selection of the cup and the clamping mechanism is critical to avoid inducing a magnetic field which in turn might affect the resolution of the TEM. The material should also be able to conduct stray electrons in order to avoid charging of the specimen.

Varieties of holders are available for positioning the specimen within the TEM and its selection depends on the desired application.

1. Single tilt holders

This is the most basic holder. In this holder the specimen can be tilted about the axis of the rod.

2. Double tilt holders

This holder can be used to tilt about two orthogonal axes, providing great flexibility in orienting the specimen. This is absolutely essential for imaging and diffraction studies of crystalline specimen.

Figure 4: Variety of TEM specimen holders. A) Rotation holder, B) Heating holder, C) Cooling holder, D) Double tilt holder, E) Single tilt holder

3. On-Axis rotation holders

This type of holder is ideal for rod-shaped or conically-shaped specimen prepared by focused ion beam milling. It allows 360^0 image acquisition and tomographic reconstruction of the image as seen in Figure 6.

4. Dual-Axis tomography holders

This holder allows for the planar rotation of the specimen as well as provides tilt about the axis of the holder. A typical application of this holder is illustrated in Figure 8.

5. *In situ* holders

Biological applications require the specimen to be maintained below the vitrification point of water (-155 ^oC). Cooling holders are designed for this purpose. They use liquid N_2 or liquid He to regulate the low temperatures. These holders are also essential for *in situ* studies of

superconducting materials. Similarly a heating holder is designed to study the change in specimen properties at high temperatures.

Other types of specialized holders include nano indentation holders, straining holders, biasing holders and environmental cell holders. Each type of holder is critical for specific operations that require a regulated environment for atomic scale observations.

Figure 5: On-Axis holder (E.A. Fischione Instruments, Inc.)

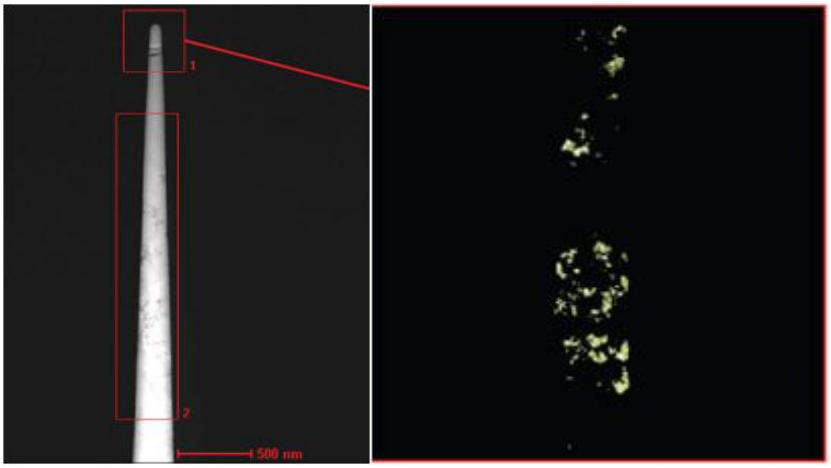

Figure 6: Reconstruction of alumina particles using On-Axis Rotation holder, Courtesy of P. Kotula, Sandia National Laboratories (U.S.A.), L.A. Giannuzzi, FEI Compnay (U.S.A.), and F. de Haas, FEI Company, (The Netherlands)

Figure 7: Dual-Axis holder (E.A. Fischione Instruments, Inc.)

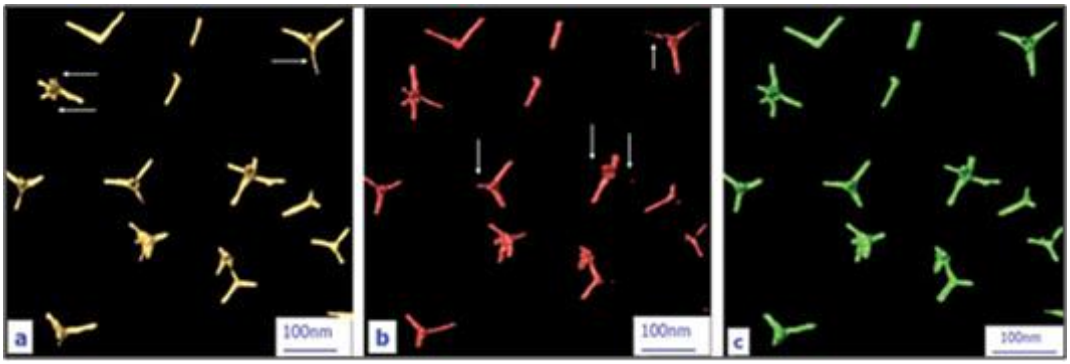

Figure 8: Dual-axis tomographic reconstructions of CdTe tetrapods, Courtesy of I. Arslan, J.R. Tong, and P.A. Midgley from the Department of Materials Science and Metallurgy, University of Cambridge (United Kingdom) and A.P. Alivisatos from the University of California at Berkeley and Lawrence Berkeley National Laboratory (USA) for the CdTe tetrapod specimen

1.1.5 Limitations

There are a few drawbacks associated with TEM's.

1. The TEM is a poor sampling tool. Its field of view is relatively small. It examines only 0.3 - 0.6 mm^3 of the specimen.
2. A single TEM image has no depth sensitivity. Generally all TEM information is averaged through the thickness of the specimen.

3. At higher voltages ionizing radiation can cause sample damage, particularly in materials such as polymers and biological specimens.
4. For a specimen to be transparent to electrons it must be thin enough to transmit sufficient electrons such that enough intensity falls on the screen or photographic film to give us an interpretable image in a reasonable time. This requires extensive sample preparation which may cause changes in the material structure.
5. In-situ examination of the specimen is limited. The processing examinations are usually carried out after the experiments.
6. High vacuum is necessary in the vicinity of the electron gun and within the TEM column.

1.2 STATEMENT OF PROBLEM

Ever since its invention, the use of TEM has spread rapidly among educational and research institutes. They provide an invaluable characterization technique in both life and physical sciences. Initially, experiments within the TEM had largely been two dimensional and static. However, over the last decade that has been an increased focus on moving from traditional imaging of atomic columns to individual atoms, from generation of two-dimensional to three-dimensional information and from static to dynamic experimentation.

Current developments in computer technology and specimen holders have helped scientists obtained three-dimensional data by 360^0 image acquisition and tomographic reconstruction and the research in the field of microscopy instrumentation have made it possible to synthesize, characterize and measure properties of active materials at the nanoscale*, in situ*, using transmission electron microscopy.

In situ is a Latin phrase meaning "in the place". The ability to study materials directly, close to their natural state as they undergo reactions is an important goal in different areas of science and engineering. Real time monitoring of the events in a transmission electron microscope (TEM) provides information on how the materials behave in their true state under various conditions. This is usually different from the static, post-reaction examination. *In situ* techniques have been successfully used to study chemical and physical properties such as melting behavior of nanoparticles, nanoindentation effects and calculating the stress-strain properties of nanoparticles such as carbon nanotubes using specialized holders described previously.

Some of the more advanced areas for the application of *in situ* techniques for nanoscience research have been summarized as:

1. Following the evolution of transformation mechanism at the atomic-level, allowing different steps of nucleation and growth processes to be identified from time resolved images and spectra [8].
2. Identification of both stable and meta-stable intermediate phases [8].
3. Determination of thermodynamic and kinetic data for individual nanostructures [8].
4. Synthesis and structural characterization is performed simultaneously and this dynamic feedback may allow synthesis conditions to be rapidly optimized [8].
5. *In situ* observations of mechanical, electronic and magnetic responses.

The majority of these experiments require a provision wherein the specimen is surrounded by specific gases at a certain pressure and elevated temperatures. This is a major challenge as the electron beam interacts strongly with matter. To avoid extraneous scatter, it is required to have a very low pressure beam path within the TEM column. A specimen immersed

in gases opposes this basic principle. Studies have been carried out in the past to examine the effect of gas path length on the electron scatter [9]. Based on this it is concluded that for any note worthy observations the gaseous environment height should be less than a few hundred microns. This makes it extremely challenging to incorporate a heating system within the confined space to fulfill the high temperature aspect. Apart from being a major design challenge, high temperatures also give rise to additional issues like specimen drift, due to uneven thermal expansion. The resolution issues caused by the presence of gases are further aggravated by the temperature, limiting the amount of useful information that can be gathered. Thermal conduction, convection and radiation all play a vital role in the heat transfer during *in situ* observations. Traditional heating holders employ resistive heating to elevate specimen temperatures; however, this technique has many drawbacks, namely limited working life, space constrains results in a complex heating mechanism and limits the localized heating of specimen, time required to attain steady state temperatures is usually very long and majority of the resistive coil cannot be used in oxidizing environments. Most of the heating holders available commercially can only heat the samples to 1000 ^{0}C, which is a low temperature especially to study reactions involving ceramic materials.

One approach devised to successfully carry out *in situ* gas flow and heating experiments is the use of modified TEM's, these include environmental transmission electron microscopes (ETEM), low energy electron microscope (LEEM), *in situ* high voltage electron microscope (HVEM) and environmental-high resolution transmission electron microscope (EHREM). The construction of such a TEM is not economically feasible for a dedicated set of applications and as a result; they are only available in a few laboratories.

The second means of carrying out *in situ* experimentation is with the help of environmental cell (E-Cell) that is part of the TEM specimen holder. It is a chamber built around the specimen to provide a controlled atmosphere for *in situ* experimentation. The basic requirement for such a device is to contain the gas within the cell so that the main microscope vacuum remains undisturbed. Environmental chambers generally fall into two categories, aperture type [14-23] and window type [24-26] cells. In the window type chamber, the gas is confined within the cell with the help of electron transparent membranes. In an aperture type cell, small differentially pumped apertures are located above and below the specimen to restrict flow of gas into the microscope. This type of E-Cell requires massive modifications to the TEM columns.

Even though various *in situ* holders have been developed over the last few decades they have not found a wide spread use due to their limitations in the maximum pressure that can be attained within the cell and/or the maximum specimen temperature that can be achieved.

1.3 RESEARCH OBJECTIVES

The objective of this research is to design and develop an environmental cell that would perform as a micro laboratory within the objective lenses of a transmission electron microscope. The design will incorporate a novel heating and gas flow mechanism for the dynamic *in situ* observations of gas solid reactions at elevated temperatures.

Based on the required needs of industry, the following technical design specifications have been developed.

Designing a environmental cell holder with primary focus on

a. External cell height of less than 4 mm in order to achieve four degrees of freedom with an accuracy of 0.005 degrees. These include translation in X, Y and Z directions and +/- 15 degrees tilt about the holder axis. (α-tilt)
b. Ergonomic design incorporating quick and easy specimen loading and unloading mechanism along with a simple specimen clamping mechanism.
c. Portable holder and assembly design aimed towards compatibility with all major commercially available TEM's.
d. Optimized specimen cup design to attain specimen temperatures of up to 1500 ^{0}C.
e. Provision to maintain a sealed gaseous environment around the specimen at pressures as high as 760 torr.

To attain these requirements we will utilize the following approach

a. Use of a safe and precisely controlled articulated arm to transmit the laser beam up to the holder on the goniometer.
b. Use of optics within the holder to reduce the laser beam spot size to less than 500 microns.
c. Utilize finite element analysis in order to optimize the heat distribution within the cell taking into consideration thermal conduction, convection and radiation.
d. A gas flow mechanism consisting of a set of four mass flow controllers and regulators to accurately control the flow of gases into the environmental cell.
e. Computerized control unit with feedback mechanism to monitor the gas flow, pressure and the specimen temperature.

1.4 OVERVIEW OF THE THESIS

The contents of the dissertation are described as follows. Chapter 2 gives a theoretical background on the design of different types of environmental cells. The literature relevant to this research is also categorized and critically reviewed. Chapter 3 describes the formulation of the finite element problem specific to this research. Various aspects of the problem such as modeling, constitutive material model, boundary conditions and the general theoretical aspects are described here. The results obtained from the analyses are presented and used for the optimization of the environmental cell holder designed and discussed in Chapter 4. The application data obtained from the preliminary tests using the designed assembly are discussed in Chapter 5. Chapter 6 provides the summary of the present work and discusses the possible areas of future research involving the successful application of the complete *in situ* holder assembly.

2.0 BACKGROUND

Observing transient behavior—how a chemical reaction, structural deformation or phase transformation takes place—is key to understanding many of the basic phenomena at the heart of chemistry, biology and materials science. The ability to directly observe and characterize these complex events leads to a fundamental understanding of properties such as reactivity, stability, and strength. It also allows us to define models that aid in the design of new and improved materials and devices. The primary requirement of such observations is the means by which the desired environment can be created around the specimen within the TEM. Over the years various approaches have been tried and tested and new tools have been developed in order to facilitate *in situ* observations.

This chapter gives an overview of the past and present research, which is directly related to the tools and techniques devised to carry out *in situ* experiments.

2.1 GAS FLOW

The greatest challenge that has intrigued the research community is the means by which the specimen can be exposed to reactive gases within the TEM. A TEM requires the presence of a high vacuum within the column in order to function. Presence of gas molecules in the electron beam path causes the electrons to scatter prematurely which directly affects the quality of the

image obtained. Gases also pose a threat to the electron gun which generates the electron. All microscopes are very sensitive to the column pressure and in order to avoid damage, critical rise in column pressure automatically initiates a full microscope shut down sequence.

2.1.1 Gas injection holders

The controlled flow of gas into the microscope column - without adversely affecting the microscope vacuum - has been reported in literature [27, 28]. In such cases, a gas injection needle is typically used to locally leak small volumes of gas directly into the region of the sample of interest. Here the pressure rise is limited only to the specimen volume around the tip of the injection needle. This small additional gas load can usually be handled with the existing pumping system of the microscope.

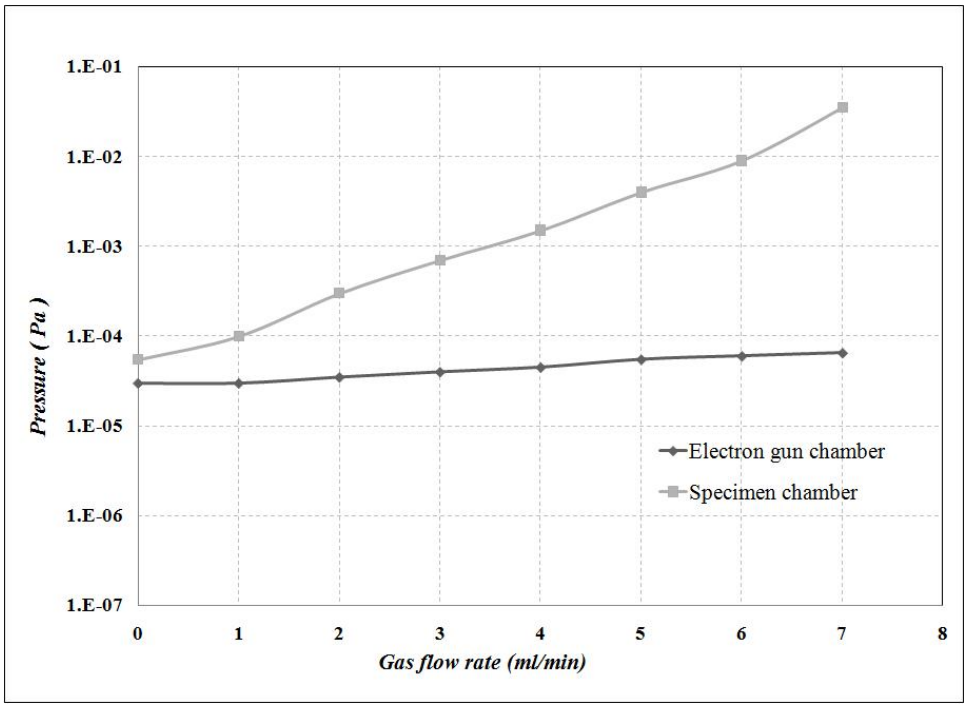

Figure 9: Pressure in the specimen chamber and the electron gun chamber as a function of gas flow rate of the specimen holder [28]

One such gas injection holder was developed by Kamino et. al. [28]. It was a side entry holder designed for use with any conventional Hitachi microscope. Using this holder they obtained a maximum gas pressure of 1E-2 Pa in the vicinity of the specimen, while the electron gun chamber pressure was kept at 2E-4 Pa. Figure 9 shows the variation in the pressure of the specimen chamber as a function of the gas flow rate. The pressure of the specimen chamber increases in proportion to the increasing gas flow rate.

Although this holder was successfully used to study gas solid reactions, it has several limitations that include:

1. Reactive gases released in the microscope can cause severe damage to its components. This limits the type of gases that can be used for observations using the gas injection holder.
2. Some reaction rates are a complicated function of pressure. In order to replicate real life conditions it is often desired to obtain high, uniformly distributed pressure around the specimen. There is a limitation on the maximum pressure that can be obtained using this holder as well as the pressure is not uniformly distributed around the specimen.

2.1.2 Environmental cell holders

An environmental cell (E-Cell) is a chamber built on a holder around the specimen to provide a controlled atmosphere for *in situ* experimentation. They were devised as a means to observe structural changes at the atomic level. The E-cells generally include the use of electron transparent windows to completely seal the specimen [24-26] or the use of multiple small bore apertures above and below the specimen [14-23].

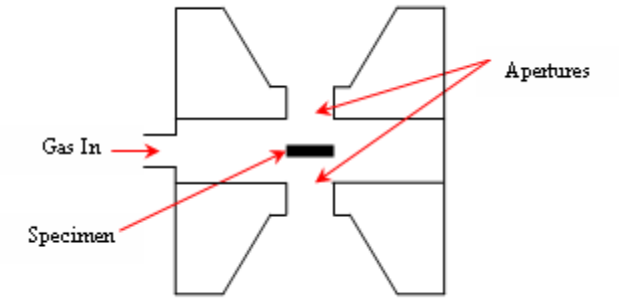

Figure 10: Schematic diagram of an aperture type E-Cell

1. Aperture type E-Cell

In this type of E-Cell, gas leakage from around the specimen into the column vacuum occurs, but it is controlled by the size of the apertures, supplemented in some instances by the provision of differential pumping (Figure 10). Successful microscope operation depends on the effective microscope pumping speed exceeding the leak rate. Usually multiple layers of apertures having diameters 100 - 200 microns are used in order to slow the leak rate.

The major considerations for this cell include:

a. The mass thickness of the environment must be kept to a minimum to achieve sufficient electron transmission through the cell so that images of satisfactory quality can be achieved (Gas path length of the beam should be kept short).

b. There should be adequate space for sample tilting and translation.

c. It should fit between the pole pieces of the microscope. The pole pieces are usually modified in order to accommodate the pumping mechanism.

Swann and Tighe [10-11] outlined the basic principles for the design of a differentially pumped E-Cell in the early 70's. They carried out various experiments in order to study the fall in electron transmission with the increase in gas pressure. Table 3 lists the maximum acceptable gas pressure inside the E-Cell for a given TEM.

Table 3: Maximum environmental cell gas pressure for useful microscopy [11]

Gas pressure (torr) at a given KV (path length 5.5 mm)						
Gas	100	200	400	600	800	1000
He	419	668	>760	>760	>760	>760
Air	38	64	103	128	145	156
CO_2	24	43	74	97	109	114
SF_6	7	11	18	23	26	29

With the advent of medium voltage high-resolution electron microscopes, the last decade has seen a renewed interest in the differentially pumped E-Cell [14-23]. The progress in the field of differentially pumped systems has been successfully used to understand chemical processes in several research areas including catalysis, metallurgy, semiconductor processing and polymerization. However, these cells still face many challenges which have limited further advancement in its applications.

The major disadvantages of aperture type cell include:

a. Pressure attained within the E-Cell is often lower than real life conditions; hence the kinetic data obtained from these studies may not be compatible to real life situations.
b. Differentially pumped systems have a complex design which includes modifying the TEM pole pieces to incorporate a pumping system.
c. Gas path length in the cell is of the order of 4-7 mm. This leads to a huge reduction in the intensity of the electron beam, thus reducing the overall efficiency of the

microscope [9]. The image resolution is usually improved with the help of imaging filters; however, this is a very expensive addition.

d. The size of the aperture controls the leak rate, hence the pressure in the sample area. For higher gas pressure, these apertures must be small. But the lower aperture also effects the diffraction information thus restricting the structural information available in the image. There is also a considerable amount of difficulty associated with the alignment of small apertures with the optic axis of the microscope.

e. Most differentially pumped E-Cells cannot be used for liquid-solid interactions.

2. Window type E-Cell

This type of cell consists of two thin film windows which completely seal the space around the specimen (Figure 11). These windows prevent the leakage of gas into the microscope column. Initially these types of cells were limited to wet biological analysis. However, with the advent of high energy transmission electron microscopes (HRTEM), window type cells became more widely accepted [24-26]. Their beams had a greater penetrating power thus allowing the use of more rigid windows.

The major considerations for such an E-Cell include:

a. The mass thickness of the cell environment must be kept to a minimum to achieve sufficient electron transmission through the cell so that images of satisfactory quality can be achieved (Gas path length of the beam should be kept short).

b. Cell design should accommodate sample tilting and translation.

c. The windows should be thin enough to permit electron penetration.

d. The window should be thick enough to withstand the temperature as well as pressure differential in and around the chamber.

e. The window should be inert to the gases flowing through the chamber.

f. The window seal should prevent the gas from leaking into the TEM.

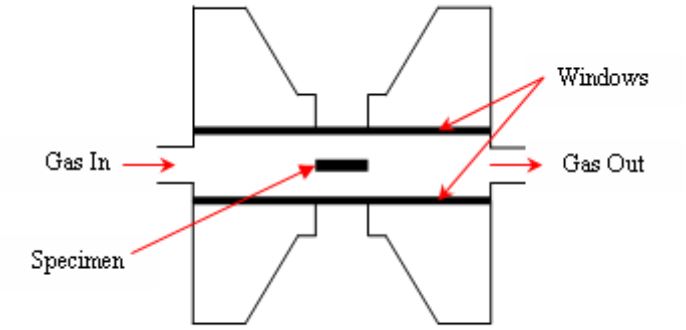

Figure 11: Schematic diagram of a window type E-Cell

The major disadvantage associated with a window type environmental cell is the leakage of gas within the microscope column due to the rupture of the windows. This can usually be avoided by carefully inspecting the windows before the experiments. Window failure within the TEM usually leads to a rise in column pressure and this initiates the shut down sequence of the microscope which protects the electron gun from any damage.

The thickness of the windows has a major effect on the resolution of the microscope. Konishi et al [26] carried out experiments to determine the optimum thickness of windows for sealed cell microscopy. They used carbon film windows fabricated by using vapor deposition techniques. Windows having a thickness of 0.15 nm were found to be adequate to withstand 1 atmospheric pressure. To reduce the inelastic scattering of gas around the specimen there is a need to minimize the gas filled gap in the sealed cell. Konishi et al [26] found that the electron transmittance of air sandwiched between 22 nm thick carbon films exponentially decreased with the cell pressure as listed in Table 4.

Table 4: Decrease in electron transmittance for various gas path lengths [9]

Cell height (microns)	Decrease in electron transmittance for the given cell pressure	
	$<10^{-6}$ torr	760 torr
50	92%	82%
150	92%	75%
250	92%	65%
500	92%	40%

Table 5: Major differences between a differentially pumped and window type E-Cell [9]

	Window	**Aperture**
Construction and Design	Generally straightforward	More difficult
Ease of Installation	Generally easy	Can be complex
Alignment	Generally straightforward	Coaxial alignment can be difficult
Ease of operation and dependability	Poor; specimen changing tedious	Good
Possible to vary gas path length	Yes	No
Maximum area of specimen viewable at one time	~0.8 mm^2 with 1 mm window	~ 10^{-2} mm^2 limit because of small apertures
Electron gun protection	Good; as long as window remains intact	Good; continuous monitoring of vacuum required
Pressure measurement and variability	Pressure measurement possible with low variability	Pressure around specimen variable and may not correspond to pressure measured at gas inlet
Temperature Capabilities	Limited if amorphous windows are used	Not limited
Most likely cause of breakdown	Rupture of a window	Blockage of an aperture

Komatsu et al. [25] successfully observed oxidation of copper and reduction of copper oxides that occurs through-gas solid reaction, using a window type environmental cell. The window consisted of commercially available copper 200 line/line mesh grid with double-layer polyvinyl-formvar/carbon thin films formed by vapor deposition. Additional layers of nylon and amorphous carbon were evaporated on this to improve its mechanical strength and heat resistance. The total thickness of the window was 50nm. A 2 MeV HVEM was used to achieve a few nanometer resolution at a maximum cell pressure of ~1.3 X 10^4 Pa. One such E-Cell holder is commercially made by JEOL Inc. This *in situ* holder is capable of circulating dry or water saturated gas through the specimen chamber using two/four lines for gas circulation at room temperatures. Windows for the E-Cell are fabricated from 15-20 nm thick amorphous carbon films which cover seven hexagonally arrayed, 0.15 mm apertures on a 3.5 mm Cu disk. The window grids were tested to withstand a pressure differential of 250 torr for 1 min. This holder was successfully used for analyzing hydrated bacteria [24].

2.1.3 Environmental TEM

Advances in aperture type environmental cell gradually gave rise to environmental high resolution electron microscope (ETEM). This is a term coined for TEM's modified to include a differentially pumped E-Cell. Recently an atomic resolution *in situ* ETEM has been pioneered by Gai and Boyes [18-20]. This ETEM consists of radial holes incorporated in the objective lens pole pieces for the first stage of differential pumping. The regular sample area of the ETEM is the controlled environment volume. Differential pumping systems are connected between the apertures using molecular drag pumps. This permits high gas pressure in the sample region, while maintaining high vacuum conditions in the rest of the TEM. A conventional reactor-type

gas manifold system enables inlet of flowing gases into the ETEM, and a sample stage with a furnace allows samples to be heated. This design was adopted by commercial TEM manufacturers [FEI Inc.] and is used in several laboratories around the world including Haldor Topsoe, a chemical company in Denmark.

Robertson and Teter [23] described the design of a similar controlled environmental electron microscope (JEOL 4000EX) installed at the University of Illinois. Sharma et al. [15-17] modified a Philips 400-T and 430 TEM to incorporate a differentially pumped E-Cell. It can accommodate a cooling (-170 ^{0}C) and a heating holder (1300 ^{0}C). This has been used successfully to obtain atomic level information of the structural and chemical changes during dynamic processes using high resolution imaging and electron-energy loss spectroscopy.

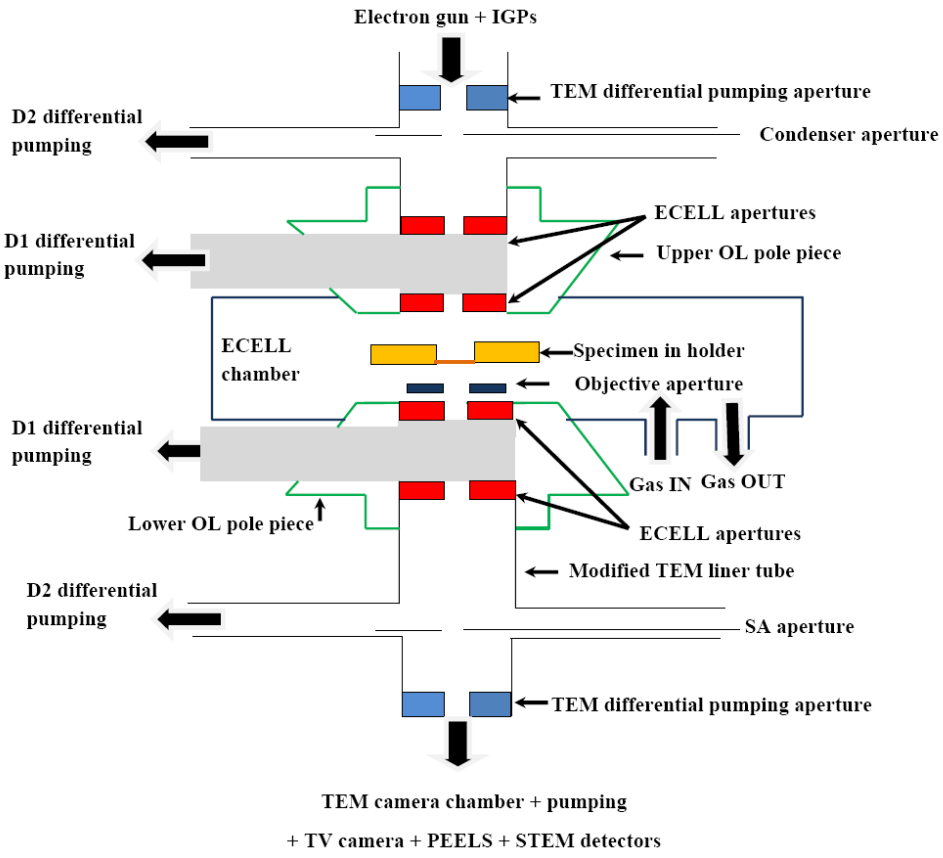

Figure 12: Schematic representation of the basic geometry of an ETEM [18]

Apart from the above mentioned ETEM's, only a few of these exist around the globe. It is hard to justify the high installation and operation cost of ETEM to carry out a dedicated set of experiments. In addition to this it also suffers from all the drawbacks associated with aperture type E-Cells, most important being the limited pressure that can be attained.

2.2 HEATING

Heat is the oldest and most commonly used way of modifying the properties of a material. In the presence of gaseous environment, heat results in various surface reactions such as oxidation and reduction, annealing, tempering, curing and ageing. *In situ* experiments provide the opportunity to characterize the microstructure changes that take place when the material is heated.

2.2.1 Heating Stages

Heating stages are widely used types of special treatment devices incorporated within the TEM. Over the years two main types of heating stages have been developed [9]. During the early years of microscopy high voltage electron beam was used to heat the specimen without the need for a special stage. This technique was discontinued because of the difficulty in controlling the specimen temperature and due to the steep thermal gradient that was generated across the specimen.

1. Direct Heating

The first types of heating stages developed consisted of a specimen sandwiched between two grids or ribbons which were resistance heated by the passage of electric current. The grids

were generally made of stainless steel or tungsten and mica was used for insulation. These designs were capable of heating the specimen up to a 1000^0 C with limited tilting. Although this technique was widely used, it suffered from many drawbacks. The grid heaters had current leads near the electron beam. This generated an electromagnetic field which caused huge beam deflections as the current was applied. Insulation of the leads did not cause a major difference. Asymmetrical heating of the specimen generated considerable amounts of thermal drift. The maximum temperature that could be attained using this holder was also limited and the temperature stability and reproducibility from experiment to experiment were not very good. Controlling the drift required a separate cooling mechanism to maintain low temperatures at the interface between the stage and the specimen rod. This made the design very complicated.

2. Indirect Heating

An indirect type of heating stage consisted of a miniature coil furnace surrounding the holder into which the specimen was inserted. The furnace was wound non-inductively using bifilar or spiralized wire so that beam deflection due to the electromagnetic field could be minimized. The symmetric nature of the furnace also helped to minimize the drift. As compared to direct heating type stages these furnaces had a very complex design and more power was required to reach the same specimen temperature. Some idea of the complexity of the design can be appreciated from the photograph of the stage component parts shown in Figure 13. The heating wire evaporated eventually limiting the productive life of the stage. The heating leads also break very easily due to repeated bending or tilting of the holder.

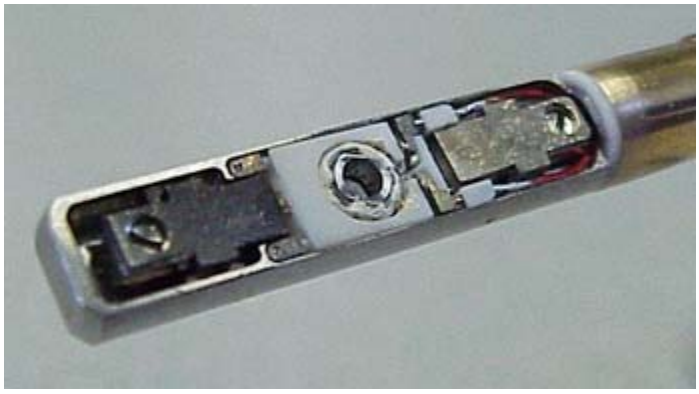

Figure 13: Typical furnace heating type specimen holder

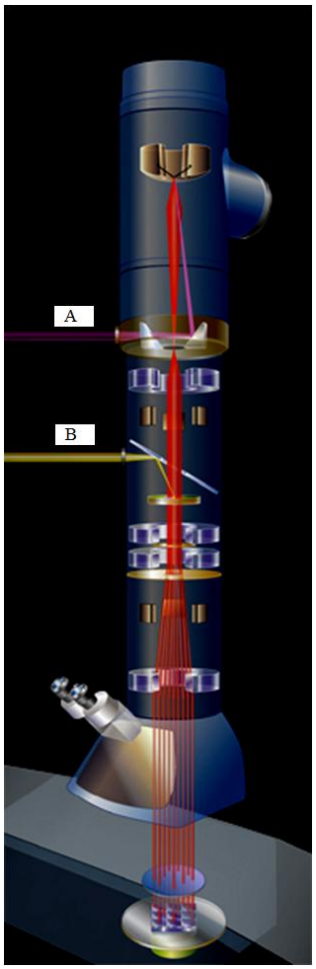

Figure 14: DTEM installed at Lawrence Livermore nation laboratories. A and B show the incident laser beam used to pulse the electron beam and ablate the specimen [34]

3. Laser heating

With the advent of high power laser systems, lasers have easily surpassed the traditional heating technology, with respect to high precision and local thermal action. They have brought about a rapid advancement in a large number of applications ranging from material processing to medical surgeries. Medical procedures using high power lasers to alter or vaporize body tissues are increasingly common. Some examples include enlarged prostate surgery, laser lithotripsy or stone fragmentation; endovenous laser therapy, laser angioplasty, laser trabeculotomy and dental/oral surgeries [60-61]. Even in traditional realms of technology such as welding cutting and drilling, lasers are used to attain productivity levels comparable to classic methods with far greater precision [42].

The use of lasers in electron microscopy can be traced to Hodgson [29]. Recent use of lasers within the TEM's has been concentrated in the field of laser induced spectroscopy.

Laser-induced breakdown spectroscopy (LIBS) is a type of atomic emission spectroscopy which utilizes a highly energetic laser pulse as the excitation source. LIBS operates by focusing the laser onto a small area at the surface of the specimen; when the laser is discharged it ablates a very small amount of material, in the range of nanograms to picograms, which instantaneously generates a plasma plume with temperatures of about 10,000–20,000 K. At these temperatures, the ablated material dissociates into excited ionic and atomic species. During this time, the plasma emits a continuum of radiation which does not contain any useful information about the species present, but within a very small timeframe the plasma expands at supersonic velocities and cools. At this point the characteristic atomic emission lines of the elements can be observed. Bostanjoglo [30-31] attached a Q-switched Nd-YAG laser system to a TEM to investigate the crystallization of amorphous Ge films by time resolved microscopy. Takaoka [32] heated

specimens locally to a temperature greater than 1000 ^{0}C by introducing a laser diode and small lens system into the vacuum space in the TEM. Some prominent laboratories have modified commercial TEM's by setting up an elaborate network of laser optics in order to pulse the electron beam as well as ablate the specimen. Lobastov and Zewail [33] employed a diode-pumped mode-locked Ti:Sapphire laser oscillator to develop a 4D ultra fast electron microscope. Here the laser is used to generate ultra fast electron pulse derived from a train of femtosecond pulses and concurrently heat the sample and induce melting of metals. Similarly, Browning et al. [34] modified a commercial JEOL2000 TEM and designed a dynamic transmission electron microscope (DTEM) with the help of an Nd-YAG laser system. This DTEM is used for vast arrays of applications including the *in situ* analysis of Nano wire catalysis and growth.

Light emitted by laser is electromagnetic radiation. This radiation has a wave nature consisting of oscillating electric and magnetic field. When radiation interacts with matter, it evolves change from one energy level to another. The energy difference between the levels must be balanced by emission or absorption of the radiant energy. The relevant equation is

$$\frac{hc}{\lambda} = E_2 - E_1 \qquad 2.1$$

Where E_2 and E_1 are the energies of the two states involved, h is the Planck's constant, c is the velocity of light and λ is the wavelength of the radiation. There are three different ways in which the radiation can interact with energy levels, fluorescence, absorption and simulated emission. The energy that is absorbed begins to heat the surface. Compared to a conventional thermal source, a laser delivers very high values of irradiance to the matter. (Irradiance is defined as the incident laser power per unit area at the surface; it has units of Watts/cm^2).

For the successful implementation and efficient use of this laser it is necessary to understand the interaction of laser radiation with matter. The laser heating kinetics depends on

various parameters such as thermo physical properties metals, the optical properties of metal targets, the laser beam and target sizes, the distribution in space of laser beam and its temporal spatial intensity, polarization and angle of incidence, the composition of surrounding gas and pressure. Figure 15 shows the variation of specimen cup temperature based on the amount of laser beam energy absorbed by the cup.

In order to analytically determine the evolution in space and time of the temperature distribution within the specimen it is essential to know the radiation absorption rate of the metal. There are different mathematical models [36-41] and experimental techniques to measure the amount of laser energy absorbed, including:

1. An integrating sphere technique to measure directly the reflectance of a laser treated metal surface.
2. Calorimetry, which is an indirect method that measures the amount of heat absorbed by the work piece by the temperature change, and therefore the reflected amount, can be deduced [38].
3. An electrical resistivity model: Previous studies [41] have shown that absoptivity is related to the substrate resistivity and the wavelength of laser radiation. It was demonstrated that absorptivity of various polished metallic surfaces is a linear function of the square root of the electrical resistivity of the respective metals.

$$\varepsilon_\lambda(T) = 0.365\sqrt{\frac{\rho_r}{\lambda}} - 0.0667\left(\frac{\rho_r}{\lambda}\right) + 0.006\left(\frac{\rho_r}{\lambda}\right)^{3/2} \qquad 2.2$$

where

ε_λ : *Emissivity of substrate at T K*

ρ_r : *Electrical resistivity of substrate in ohm – m*

λ : *Wavelength of impinging radiation in m*

This theory is based on the fact that absorption of infrared radiation by metals largely depends on conductive absorption by free electrons. The absorptivity, therefore can be calculated from the knowledge of electrical resistivity of the substrate.

The second important consideration for the practical use of lasers in order to heat the work piece is a flexible delivery system for transmitting laser radiation onto the region of interest. Previous studies have successfully utilized hollow sapphire waveguides as an optical fiber [43-48] for transmitting CO_2 laser radiation. These wave guides have many advantages:

1. The attenuation associated with them is very low for a $C0_2$ laser. (0.46 db/m and 0.31 db/min for a tube having a diameter of 790 microns and 1060 microns respectively).
2. The hollow waveguides avoid surface and bulk laser damage problems associated with high peak power transmission in solid fibers.
3. Glass tubing is much smoother than either metal or plastic tubing and therefore the scattering losses are less.
4. Sapphire has a high melting temperature (2053 ^{0}C), high resistance to chemically hostile environment and has adequate mechanical properties.

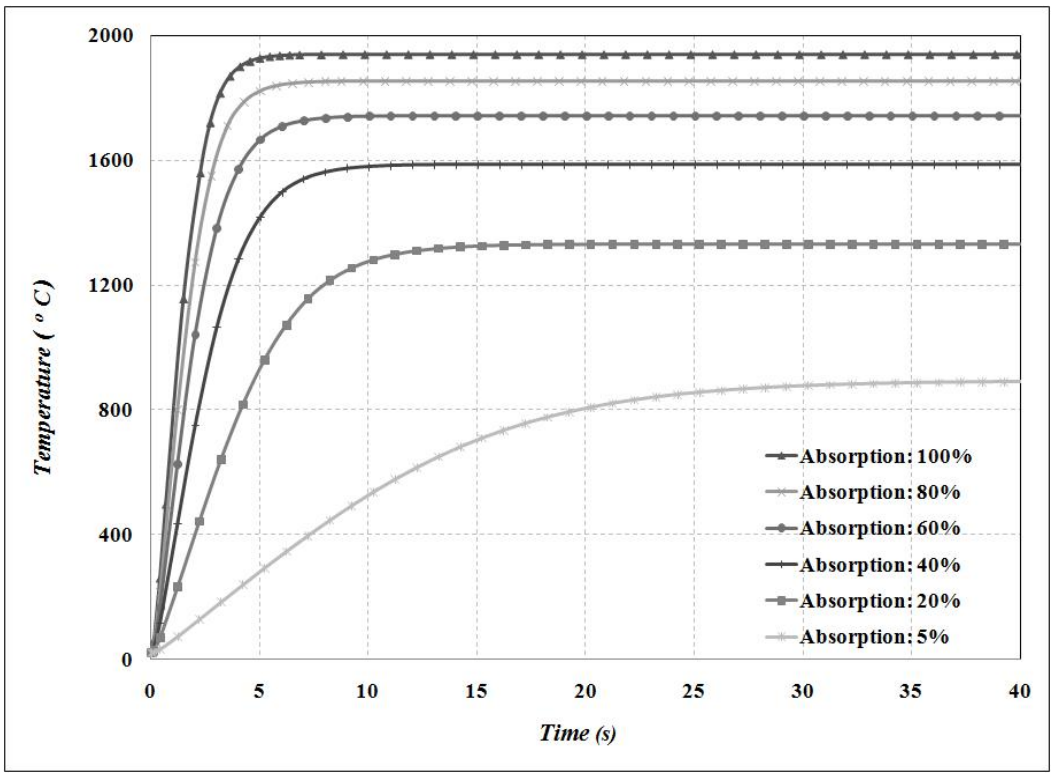

Figure 15: Effect of laser beam absorption on maximum steady state temperature of the specimen

The other means of laser beam delivery used commonly in medical surgeries and laser welding is an articulated arm. Articulated Arms provide a flexible solution when connecting a CO_2 laser to a moving system such as an X-Y flatbed machine or multi-axis robot. The arm has a constant distance beam path which delivers a fixed focal spot size across the full range of motion. The arm also provides a fully enclosed path and controlled atmosphere for propagating the beam. It consists of multiple ball bearing rotary joints and right angled mirror knuckles. Relative motion between the laser arm and the motion system causes no change in the focal point position or loss of power. This minimizes machine foundation and structural rigidity requirements of the motion system. Articulated Arms also significantly simplify system maintenance by eliminating alignment issues associated with conventional moving beam systems [53].

3.0 THERMAL ANALYSIS

Incorporating laser heating mechanism within the environmental call is an important aspect of this research. Heat distribution in space and time, within the environmental cell involves:

1. The amount of laser radiation absorbed by the specimen cup depending upon the complex interaction of the laser beam with matter
2. Conduction of heat through the specimen cup and the specimen
3. Heat radiation from the specimen cup and the specimen
4. Heat convection brought about by the flow of gases within the environmental cell
5. Thermal stresses induced within the specimen and the environmental cell due to the extreme operating conditions

Based on the complexity of the problem it is not possible to theoretically determine the evolution, in space and time, of the temperature distribution within the environmental cell. In order to overcome this limitation, Ansys [49], a general purpose finite element software, was used to carry out the transient heat flow analysis within the *in situ* specimen holder.

3.1 FUNDAMENTALS OF THERMAL ANALYSIS

3.1.1 Conduction and Convection

The first law of thermodynamics states that thermal energy is conserved. Specializing this to a differential control volume:

$$\rho c\left[\frac{\partial T}{\partial t}+\{V\}^T\{L\}^T\right]+\{L\}^T\{q\}=\ddot{q} \tag{3.1}$$

Where, ρ is the density, c is the specific heat, T is the temperature, t is time, {L} is the vector operator, {V} is the velocity vector for mass transport of heat and {q} is the heat flux vector and $\ddot{q}$ is the heat generation rate per unit volume

$$\{L\}=\begin{Bmatrix}\frac{\partial}{\partial x}\\ \frac{\partial}{\partial y}\\ \frac{\partial}{\partial z}\end{Bmatrix} \tag{3.2}$$

$$\{V\}=\begin{Bmatrix}V_x\\ V_y\\ V_z\end{Bmatrix} \tag{3.3}$$

Fourier's law is used to relate the heat flux vector to the thermal gradients

$$\{q\}=-[D]\{L\}T \tag{3.4}$$

Where, [D] is the conductivity matrix which is defined by the element conductivity, K_{xx}, K_{yy}, K_{zz}, in the x, y and z directions respectively.

$$[D] = \begin{bmatrix} k_{xx} & 0 & 0 \\ 0 & k_{xx} & 0 \\ 0 & 0 & k_{zz} \end{bmatrix} \quad 3.5$$

Three types of boundary conditions are considered. It is presumed that these cover the entire element.

1. Specified temperatures acting over surface S_1

$$T = T^* \quad 3.6$$

Where, T* is the specified temperature

2. Specified heat flows acting over surface S_2

$$\{q\}^T \{\eta\} = -q^* \quad 3.7$$

Where, $\{\eta\}$ is the unit outward normal vector and q^* is the specified heat flow

3. Specified convection surfaces acting over surface S_3 (Newton's law of cooling)

$$\{q\}^T \{\eta\} = h_f (T_S - T_B) \quad 3.8$$

Where, h_f is the heat transfer coefficient evaluated at $\{(T_B+T_S)/2\}$, T_B is the bulk temperature of the adjacent fluid and T_S is the temperature at the surface of the model.

3.1.2 Radiation

Radiation is the transfer of energy via electromagnetic waves. The waves travel at the speed of light, and energy transfer requires no medium. Thermal radiation is just a small band on the electromagnetic spectrum (i.e. wavelength λ ranges between 0.1 and 100 μm). Radiant energy exchange between neighboring surfaces of a region or between a region and its surroundings can

produce large effects in the overall heat transfer problem. Though the radiation effects generally enter the heat transfer problem only through the boundary conditions, the coupling is especially strong due to nonlinear dependence of radiation on surface temperature. Extending the Stefan-Boltzmann Law for a system of N enclosures, the energy balance for each surface in the enclosure for a gray diffuse body is given the following equation, which relates the energy losses to the surface temperatures:

$$Q_i = \sigma \varepsilon_i F_{ij} A_i (T_i^4 - T_j^4) \tag{3.9}$$

Where, N is the number of radiating surfaces, ε_i is the effective emissivity of the surface i, F_{ij} are the radiating view factors, A_i is the area of surface i, Q_i is the energy loss of surface i, σ is the Stefan-Boltzmann constant and T_i and T_j are the absolute temperature of surface i and j respectively.

The view factor, F_{ij}, is defined as the fraction of total radiant energy that leaves surface i which arrives directly on surface j, as shown in Figure 16. It can be expressed by the following equation:

$$F_{ij} = \frac{1}{A_i} \int_{A_i} \int_{A_j} \frac{\cos\theta_i \cos\theta_j}{\pi r^2} d(A_j) d(A_i) \tag{3.10}$$

Where, A_i, A_j are the areas of surface i and surface j respectively, r is the distance between differential surfaces i and j, θ_i is the angle between N_i and the radius line to the surface $d(A_i)$, θ_j is angle between N_j and the radius line to the surface $d(A_j)$ and N_i, N_j are surface normal of $d(A_i)$ and $d(A_j)$ respectively.

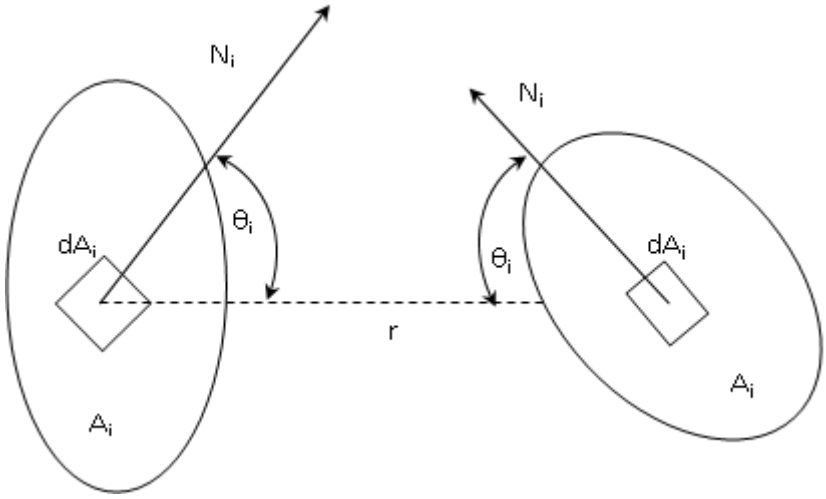

Figure 16: View factor calculation terms

3.2 INTERACTION OF CO_2 LASER RADATION WITH MATTER

For the successful implementation and efficient use of a CO_2 laser it is necessary to understand the interaction of the lasers radiation with matter. The laser heating kinetics depends on various parameters such as thermo physical properties of metals, the optical properties of metal targets, the laser beam and target sizes, the distribution in space of laser beam and its temporal spatial intensity, polarization and angle of incidence and the composition of surrounding gas and pressure [42].

For accurate thermal analysis of the environmental cell, it is first required to quantify the amount of laser energy available to heat the specimen cup. In order to achieve this, theoretical calculations were performed and the results were validated by comparing them with experimental and analytical observations.

3.2.1 Theoretical calculations

The model described by Bramson [41] was used to calculate the absorption coefficient for the specimen cup. This model was chosen because of its simplicity in obtaining the absorbtivity of the substrate. The objective was to utilize these results in order to optimize the relative heat distribution profile within the E-cell. It was not desired to calculate the precise specimen temperature during the analysis. For a given wavelength of radiation, electrical resistivity was found to play a vital role in determining the amount of radiation absorbed by the substrate.

$$\varepsilon_\lambda(T) = 0.365\sqrt{\frac{\rho_r}{\lambda}} - 0.0667\left(\frac{\rho_r}{\lambda}\right) + 0.006\left(\frac{\rho_r}{\lambda}\right)^{3/2} \qquad 3.11$$

Where, λ is the wavelength of radiation and ρ_r is the electrical resistivity of the substrate.

The results obtained using this equation for various materials is listed in Table 6.

Table 6: Absorption of laser radiation by various materials

Material	Wavelength of CO_2 laser radiation (m)	Electrical Resistivity (ohm-m)	Absorption (%)
316 Stainless steel	1.06E-7	7.20E-07	9.07
Inconel 625	1.06 E-7	1.29E-06	11.9
Tantalum	1.06E-7	1.25E-07	3.89

3.2.2 Experimental observations

An experimental assembly was built in order to perform the initial laser heating tests on the specimen cup. The complete setup is shown in Figure 17. A 10 watt CO_2 laser was mounted on

an optical breadboard and the laser beam was transmitted to the specimen cup using an articulated arm. This arm consisted of a series of mirrors and rotary joints to safely transmit the laser beam, with minimum (~1% per mirror) loss of power. A specimen cup, designed to hold a 3mm TEM specimen disk, was manufactured out of two different materials, inconel 625 and 316 stainless steel. A 'K' type thermocouple was attached on the specimen cup to record the variation of specimen temperature with time. This chromel-alumel thermocouple had an operating range of -200 ^{0}C to 1200 ^{0}C. The specimen cup was mounted on an insulator pin as shown in Figure 17. This pin was then attached on to an X-Y stage to precisely position the specimen cup along the laser beam path. The laser beam spot size was reduced to a diameter of 300 micron with the help of a convex lens made of zinc selenide, having a focal length of 100mm. The laser beam power at the specimen cup was measured to be 5.8 watts.

Figure 18 shows the variation of the specimen cup temperature with time. On heating the specimen cup in atmosphere, the inconel cup attained a maximum steady state temperature of 370 ^{o}C where as the stainless steel cup recorded a maximum temperature of 335 ^{o}C. Using a 5.8 watt laser beam, it took less than 25 seconds to reach the maximum temperature. From the theoretical calculations performed above it was found that approximately 10% of the laser energy was absorbed by steel and inconel and the rest was scattered on being reflected off the surface. Studies have been performed in the past [41] that showed an increase in the laser absorption rate with an increase in surface roughness of the metal substrate. However, this change was not significant.

Zirconium oxide and Aluminum oxide are ceramics having a melting point in excess of 2700 ^{o}C and 2000 ^{o}C. Aerosol cans containing particles of these ceramics are available commercially. The deposited oxide layers have high emissivity and surface roughness values.

Both these properties help increase laser absorption. Considering this, an experiment was conducted to validate the effect of laser beam absorption on a ceramic oxide coated specimen cup.

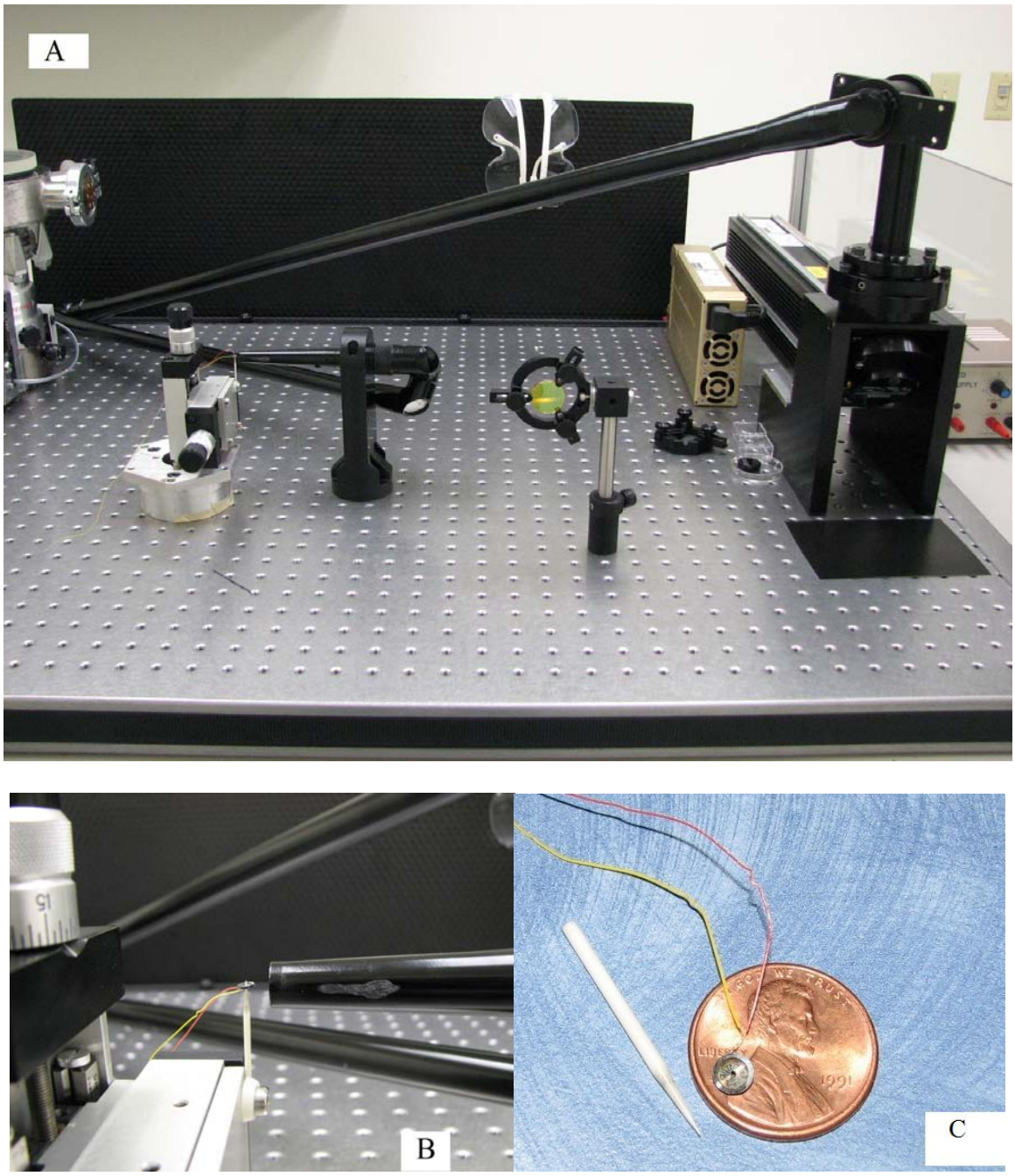

Figure 17: Experimental setup to study laser heating. (a) Laser along with the articulated arm assembly, (b) X-Y Stage, (c) Specimen cup

This unique experiment helped in considerably increasing the maximum temperature attained by the specimen cup, indicating an increase in laser absorption rate. Figure 19 shows the variation of the specimen cup temperature with time. The maximum temperature of the inconel cup increased by 27% when coated with aluminum oxide whereas the maximum temperature of the stainless steel cup increased by 98% when coated with zirconium oxide. The oxide coatings on the cup remained intact even after multiple cycles of heating and cooling. These coatings are also rated for vacuum making them compatible for use within a TEM.

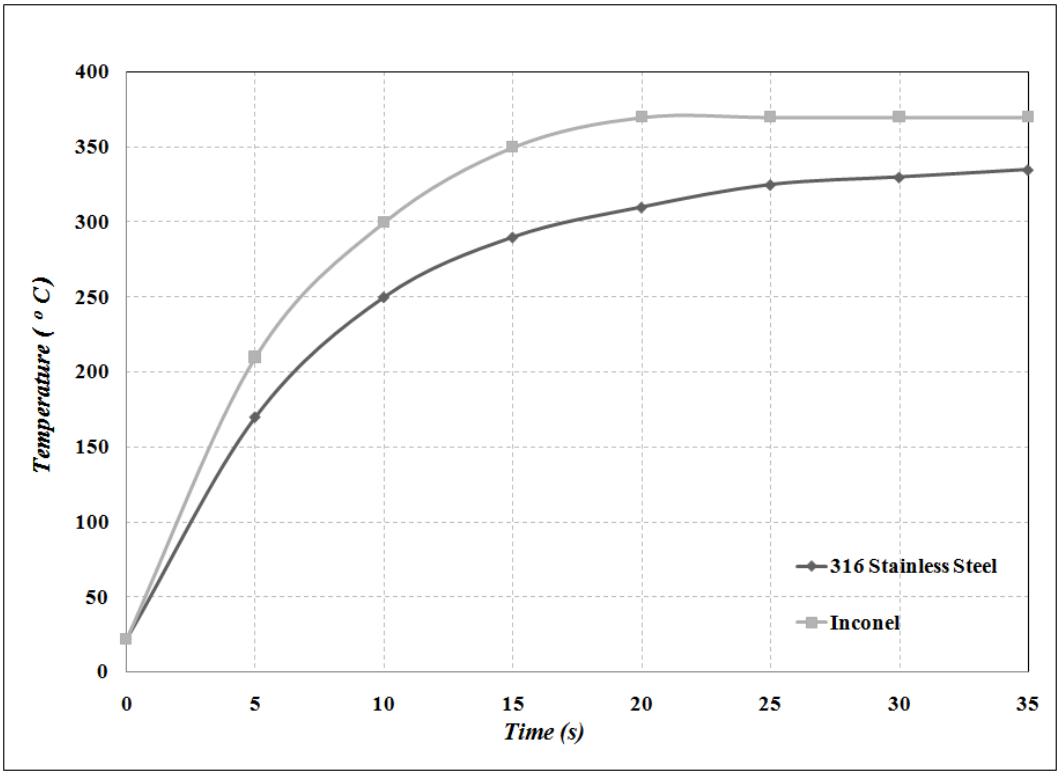

Figure 18: Experimental results: variation of specimen cup temperature with time

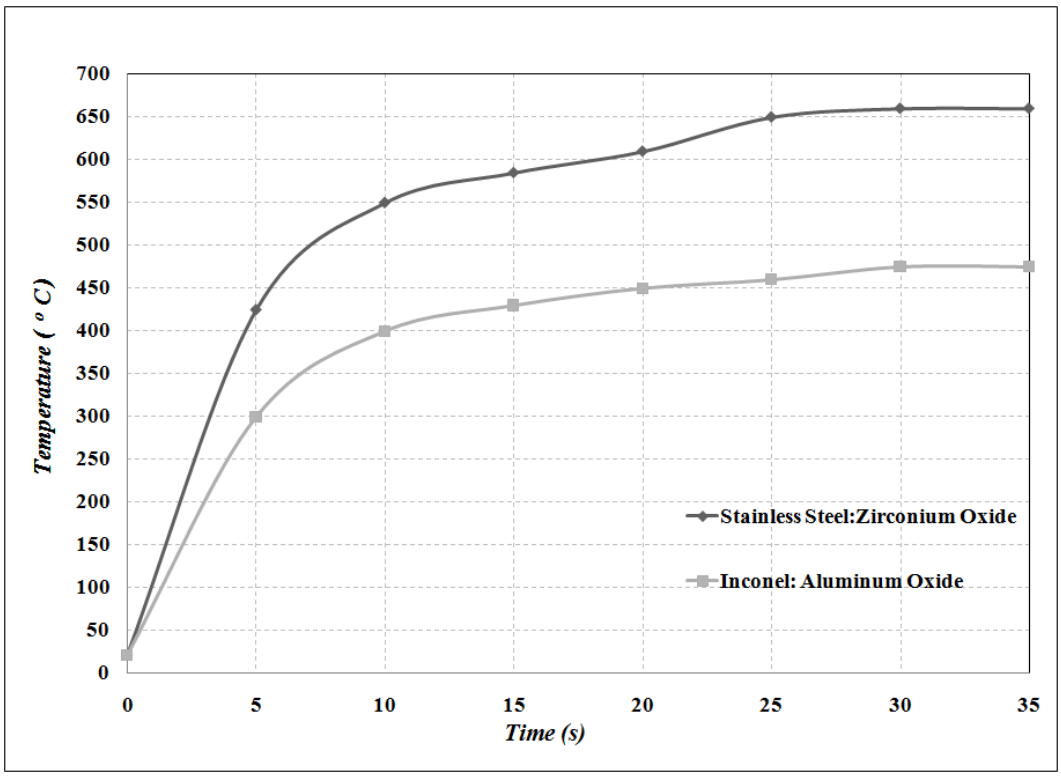

Figure 19: Effect of surface coating on the steady state temperature of the specimen cup

3.2.3 Finite Element Analysis

In order to correlate the experimental results with the analytical results, finite element analysis of the non coated specimen cup was carried out. Multiple analyses were performed assuming a laser power absorption rate of 5% to 40%. The model replicating the experimental specimen cup was generated using a solid modeling software, Solid Works [50] and was imported into Ansys [49] as an IGS file. The material properties incorporated into the finite element analysis code were imported from the online material library [51]. The model consisted of SOLID87 and SOLID90 elements. These elements are well suited to model irregular meshes (such as those produced from various CAD/CAM systems). These are 3-D tetrahedral elements, consisting of 10 and 20 nodes, respectively. These elements have one degree of freedom, temperature, at each node.

Three modes of heat transfer (conduction, convection and radiation) were included in this simulation. Convection heat transfer was applied as a surface load on the complete specimen cup. Because of the free convection condition prevalent in the laboratory, the heat convection coefficient was chosen to be 10 $W/m^2\ ^oC$.

Table 7: Material properties used for the finite element analysis

Property	Inconel	Stainless Steel	Zirconium Oxide
Youngs Modulus (N/m^2)	2E11	1.93E11	9.45E10
Density (Kg/m^3)	8440	8000	5680
Coefficient of Thermal Expansion ($m/m\ ^oC$)	12.8E-6	16.5E-6	7E-6
Specific Heat Capacity ($J/Kg\ ^oC$)	410	500	280
Thermal Conductivity ($W/m\ ^oC$)	9.8	16.3	1.675
Emissivity	0.2	0.15	0.5

Previous experiments and analysis carried out at low temperatures had shown a close correlation between the theoretical results and the analytical results as seen in Figure 21. Experiments were repeated in order to increase the fraction of absorbed power, by the generation of a keyhole in the substrate. Using this technique, the experimental and numerical results showed that 20% of the laser energy was absorbed by the substrate.

The results obtained from the present analysis are shown in Figure 22. These high temperature results followed the same trend as the previous results. Analytical results obtained

by assuming 20% laser beam absorption were in agreement with the experimental results. Figure 20 shows the steady state heat distribution within the specimen cup.

The above comparison showed a close correlation between the experimental and numerical values, thus verifying the theoretical value of absorption coefficient calculated using the electrical resistive model. These values of laser beam absorption were now incorporated into the finite element analysis code to fully understand the effect of heat conduction, convection and radiation within the specimen.

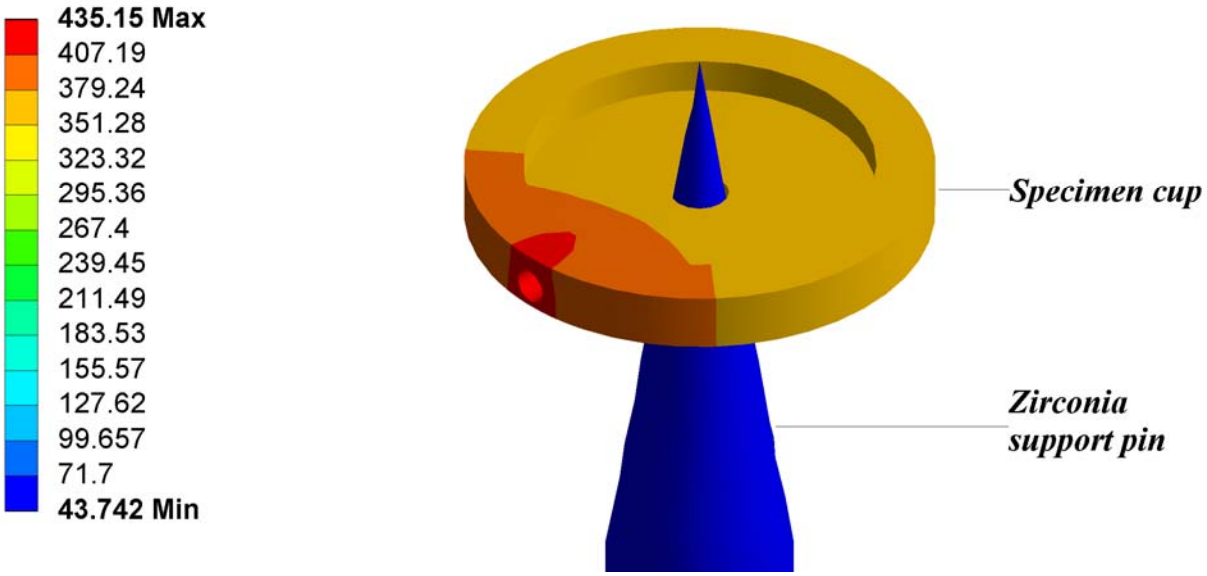

Figure 20: Steady state temperature (^{o}C) distribution within the specimen cup

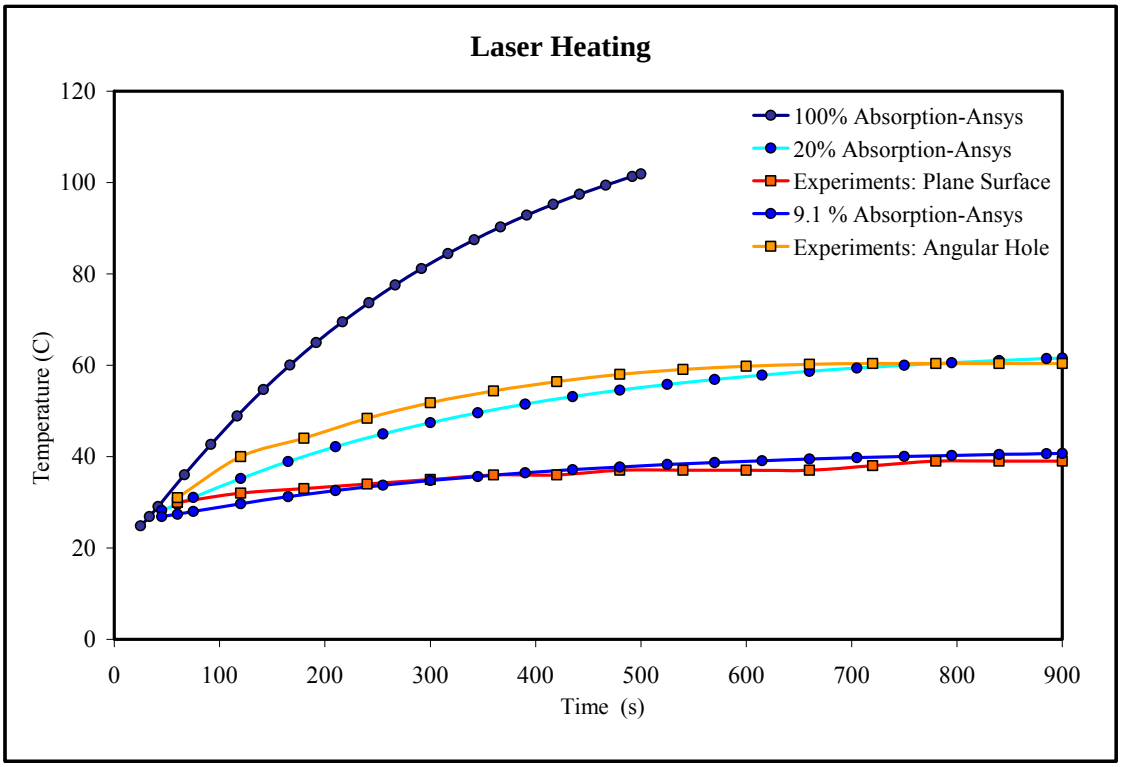

Figure 21: Effect of keyhole on laser absorption

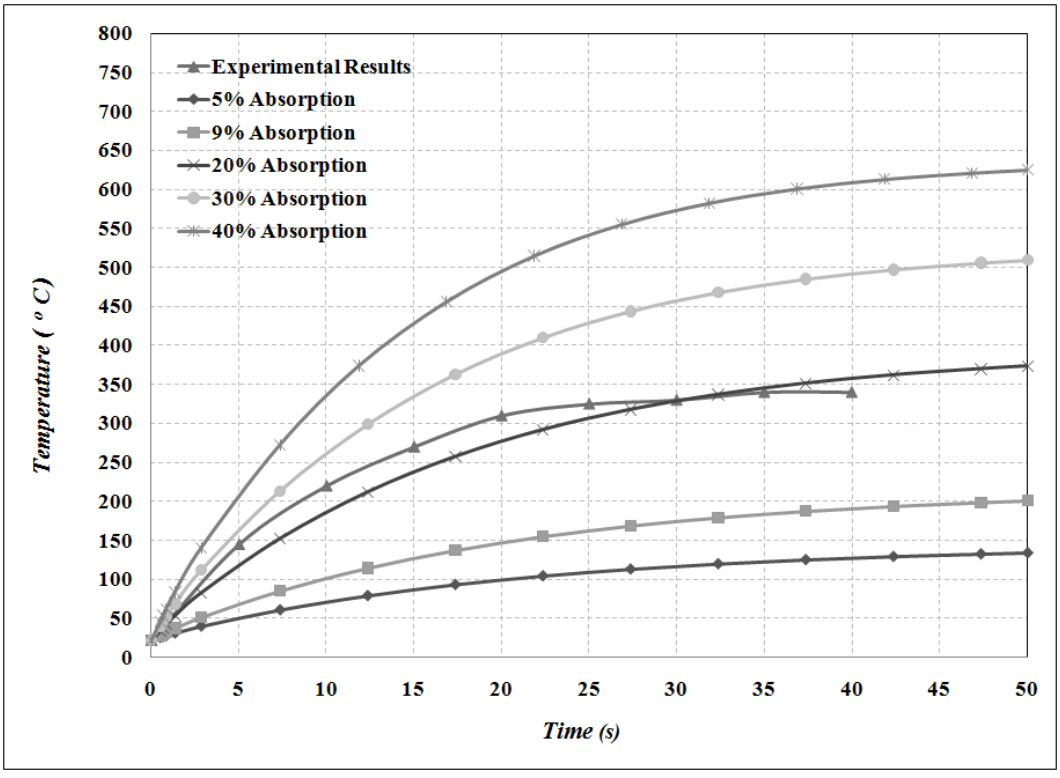

Figure 22: Comparison with various absorption rates

3.3 EFFECT OF RADIATION

The heat flow that radiation causes varies with the fourth power of the body's absolute temperature (see Eq. 3.9) and thus becomes very dominant at high temperatures. It is also very important to understand radiation in our application as it is the main cause of heat loss in vacuum. In order to avoid the thermal damage to the surrounding parts of the holder, the heated specimen was analyzed in the presence of a heat shield. Three sets of thermal analysis were carried out, Case I: No shield, Case II: Single shield and Case III: Multiple shields. The shields were placed within 200 microns of the specimen cup.

The results obtained from the analysis are shown in Figure 23. During the first case, in which the specimen cup was heated without the presence of radiation shield, the maximum steady state temperature attained by the cup was 990 ^{0}C after 100 s. This analysis was repeated in the presence of a single protective shield. In this case the shield reflected some part of the radiation back to the specimen cup. The maximum temperature of the cradle attained was 1100 ^{0}C, an improvement of 10%. The shield temperature attained was 696 ^{0}C. During the third analysis, when two shields were used, the cradle temperature remained at 1100 ^{0}C. The outer shield temperature, however was only 276 ^{0}C.

Although the presence of radiation shield helped raise the temperature of the specimen cup by 10%, the practical design consideration to assemble a sturdy shield within 200 microns of the cup was very complex. In the study it was seen that the shield lost its effectiveness completely once it was more than 500 microns away from the cup. Based on these results, it was decided that it was not practical to use a radiation shield.

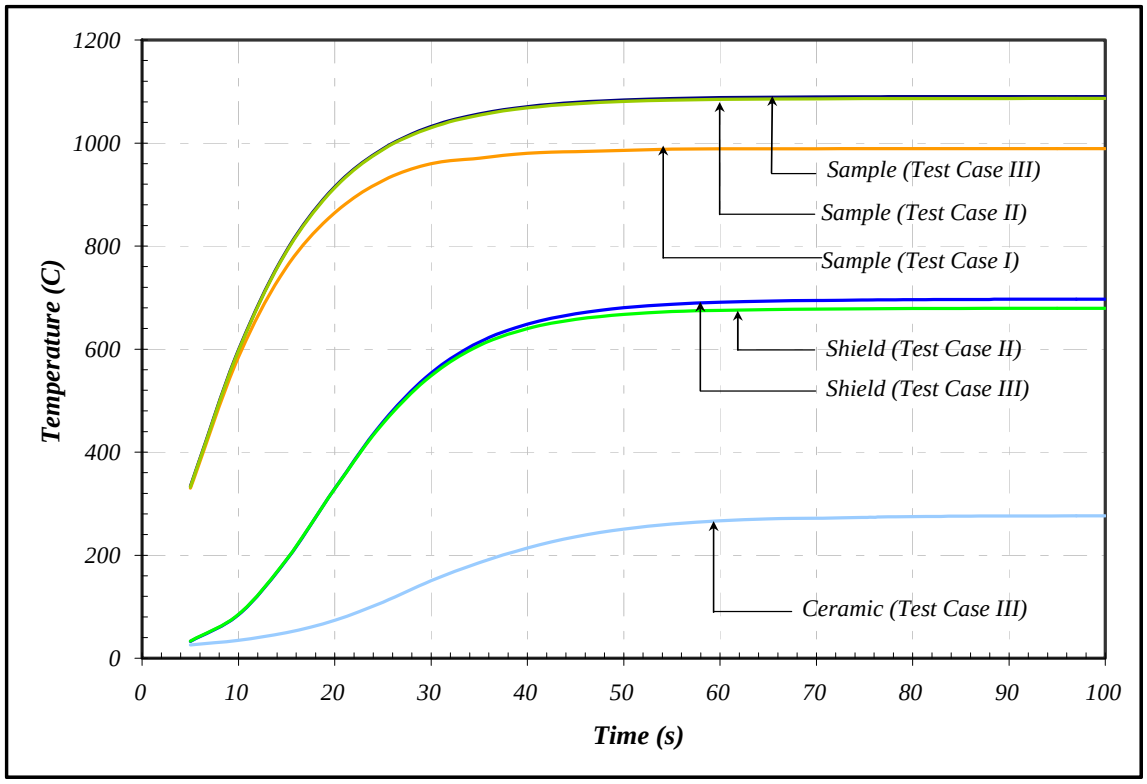

Figure 23: Variation of temperature distribution within the specimen cup. Case I: No Shield, Case II: 1 Shield, Case III: 2 Shields

The *In situ* specimen cup is sealed with the help of a pair of windows. These windows which are placed directly above and below the specimen to be heated, act as radiation shield. Based on the above results, it can be concluded that these windows may not provide considerable help in preventing the radiation heat loss from the specimen. However, it is essential to know what is the maximum temperature attained by these windows. This is required to optimize the design layout of the environmental cell so that the rigidity of the windows is maintained when the environmental cell is in use. For this purpose the FEA model was used to study the effect of windows layout on the maximum temperature attained by the windows. As shown in Figure 24, three test cases were studied, wherein the separation distance between each window and the specimen cup was 0.15mm, 0.05mm and 0.25mm respectively. From the results shown in Figure

25 it was observed that when the specimen cup reaches a temperature of 1500 ^{o}C, the temperature of the window was approximately 500 ^{o}C. These are silicon nitride windows deposited on silicon substrate and they have a working temperature of 1000 ^{o}C, which is well above the temperatures of the windows obtained in these studies. The temperature of the windows can be reduced by increasing its distance from the cup; however, this would increase the environmental cell height. An increased cell height would limit the resolution due to the increase in the gas volume present between the windows. Also, it should be noted that this is the worst case scenario, as the temperature of the window will be lower due to flow of heat between the windows and the cell body caused by conduction as well as due to convection in the presence of gas flow. This was taken into account when the complete cell was modeled.

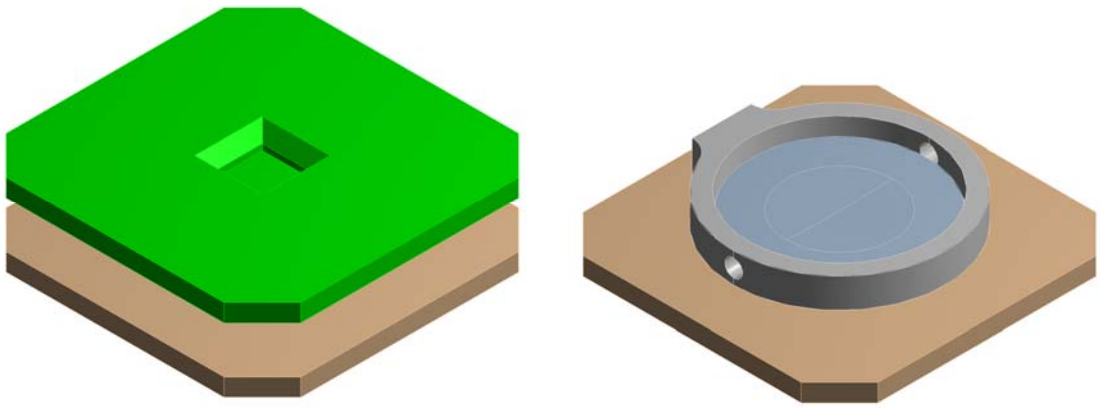

Figure 24: FEA model used to study the effect of heat radiation from the specimen cup to the windows

Another important consideration that attributes to the increase in the heat absorbed or radiated are the emissivity's of the window, the specimen and the specimen cup. Emissivity is a surface property defined as the ratio of the radiation emitted by the surface to the radiation emitted by a black body at the same temperature. To study the effect of emissivity, analysis was

repeated for various values of window and specimen emissivity and the maximum specimen temperature was recorded. The variation of specimen temperature with emissivity is shown in Figure 26 and Figure 27. From these results it was observed that for the above analysis the specimen temperature falls by 130 ^{o}C when the emissivity of the window is increased from 0.2 to 0.8 and the specimen temperature falls by 240 ^{o}C when the emissivity of the specimen and the cup is increased from 0.2 to 0.8. The variation in the temperature of the window was inconsequential. From these results it was shown that during the selection of the window and the cup, the materials having lower values of emissivity should be preferred to obtain higher specimen temperatures for a given laser power.

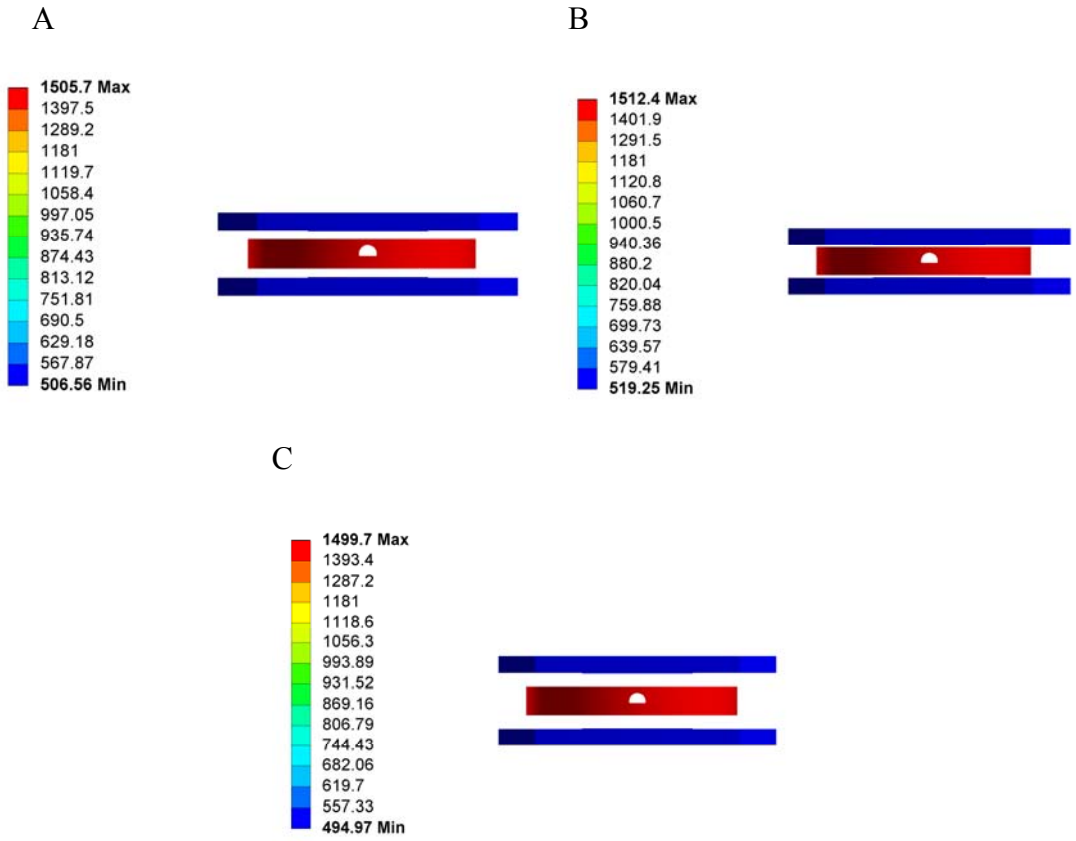

Figure 25: Maximum temperature (^{o}C) attained by the specimen cup and the window for various separation distances. (A) 0.15 mm, (B) 0.05 mm and (C) 0.25 mm

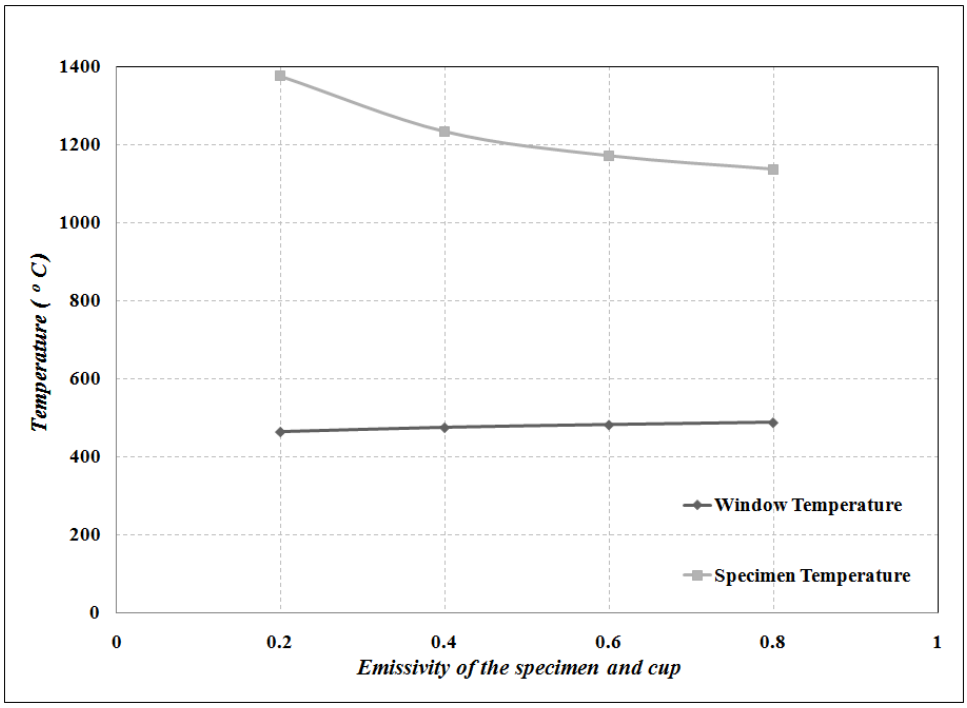

Figure 26: Variation of maximum specimen temperature with the increase in the emissivity of the specimen and cup

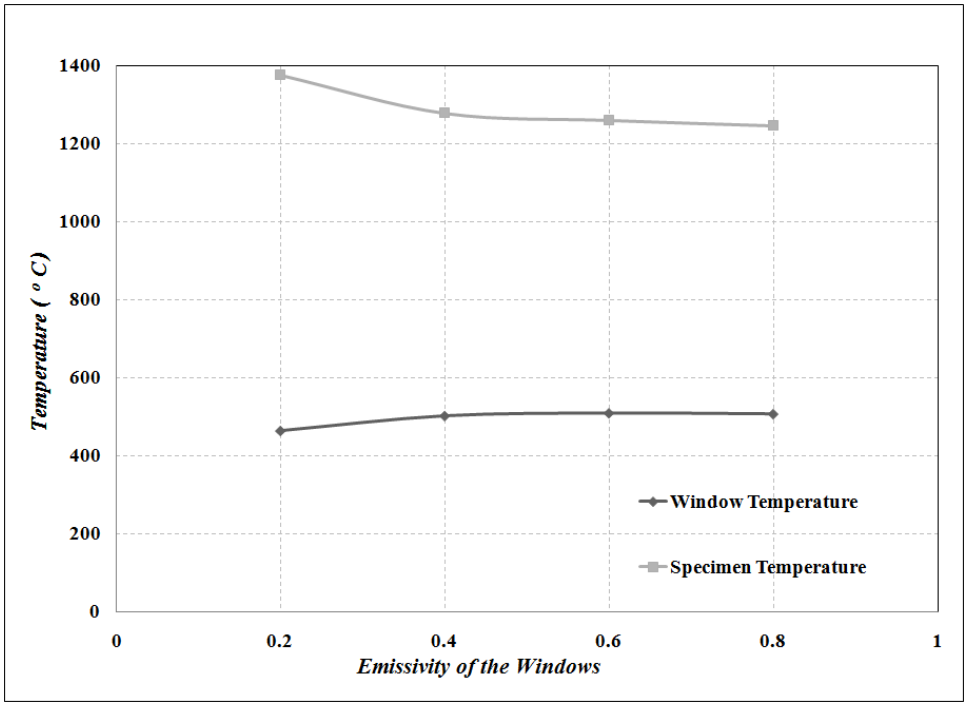

Figure 27: Variation of maximum specimen temperature with the increase in the emissivity of the specimen and cup

3.4 EFFECT OF HEAT CONVECTION

The circulation of gases within the environmental cell at high temperature would bring about a considerable loss of heat energy due to convection. Heat transfer by convection is difficult to analyze because convection varies from situation to situation, depending on the fluid velocity, fluid viscosity, flow rate of the gas, heat flux and the type of flow. In order to understand the effect of convection on the specimen temperature, analysis was carried out for various values of heat transfer coefficients. Figure 28 shows the dramatic change in maximum steady state temperature within the environmental cell with the increase in the value of coefficient of heat transfer. Depending on the specific nature of the application, detailed analysis will be carried out in the future to accurately simulate the effect of heat convection.

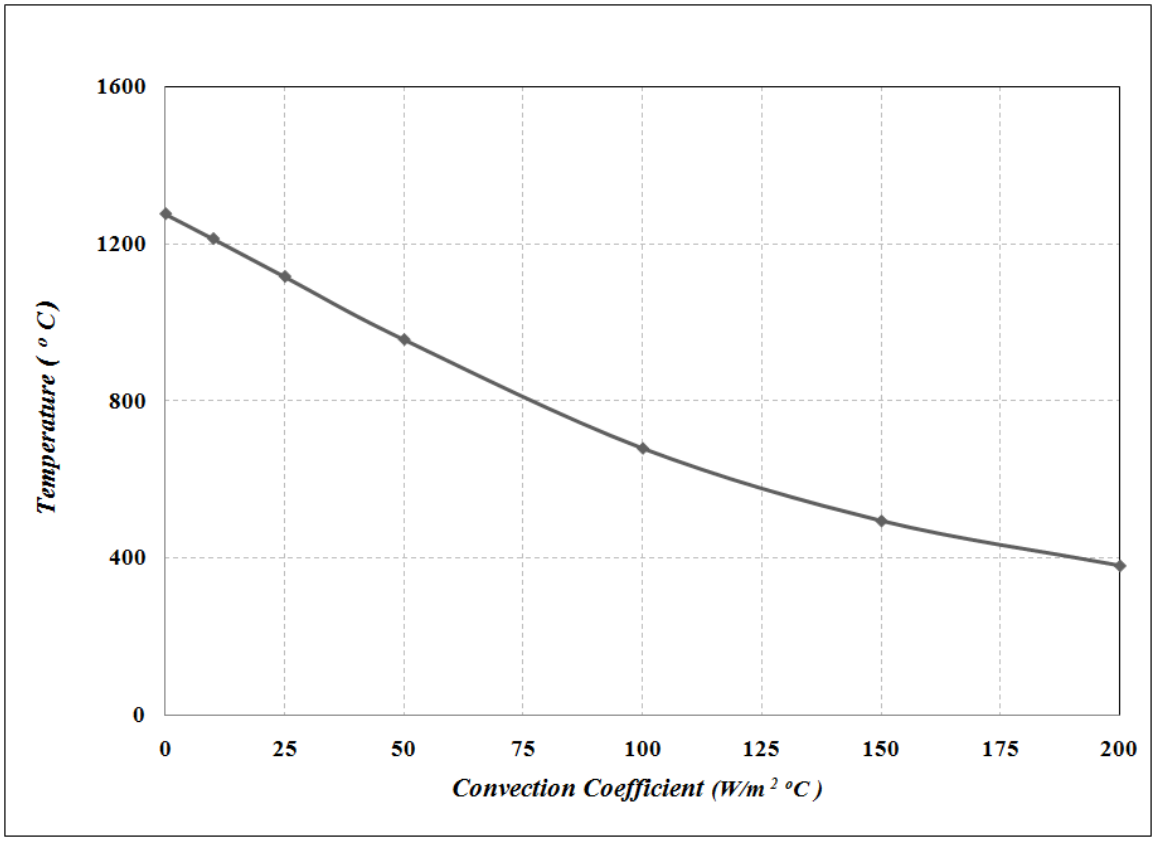

Figure 28: Variation of maximum specimen temperature with increase in convection coefficient

3.5 THERMAL CONTACT CONDUCTANCE

The conduction of heat through homogeneous, isotropic materials has been well understood, however the conduction of heat across interfaces formed by contacting surfaces is still a topic of investigation. The specimen in the environmental cell is placed within the heated specimen cup, and indirectly heated by conduction through the contact region. Thus it is essential to understand the heat flow behavior through the contact surface in order to obtain uniform temperature distribution within the specimen.

Surfaces that appear to be smooth are actually composed of microscopic asperities and depressions that deviate from an apparently smooth surface. Generally, the microscopic deviations are termed roughness and the macroscopic deviations are termed waviness. When two surfaces are in contact with each other, the actual area of contact is much smaller than the apparent area of contact. These areas of actual contact occur where the asperities of one surface are in contact with the asperities of the other surface. The number of these contact spots is further reduced when surface waviness and errors in form are taken onto account. Typically, there is some material or fluid in the interstitial spaces between the contacting surfaces, and heat is transferred through this interstitial material. If there are no interstitial materials or fluids, then most of the heat transferred across the interface formed by the two surfaces is transferred through these small contact spots. The amount of actual contact area is also dependent on the physical properties of the contacting materials. If one of the materials is softer than the other, then the asperities of the harder material are likely to penetrate the surface of the softer material and increase the contact area. At higher pressures, one would expect that the penetration of these asperities would increase. In the case of materials of nearly the same hardness, the asperities

would deform, and one might expect that the amount of deformation would increase with pressure. Interfaces with a higher mean thermal conductivity would be expected to have a lower resistance to heat transfer than those interfaces that have lower mean thermal conductivities.

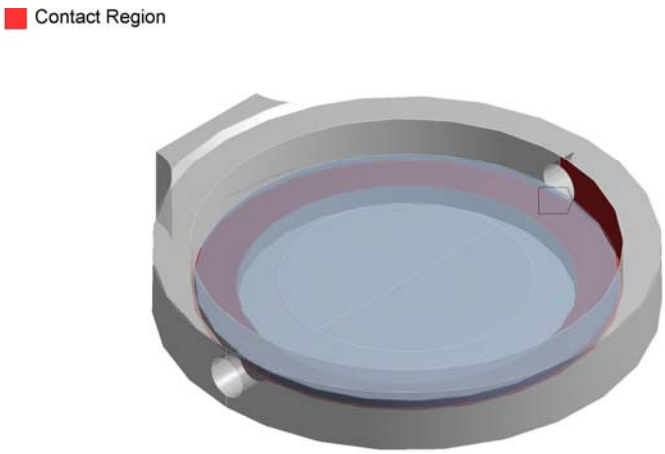

Figure 29: The contact region between the specimen and the specimen cup

Initial analysis was carried out assuming the surfaces between the specimen and the specimen cup are bonded, i.e. there is no loss of heat flow at the interface. The heat distribution result obtained is shown in Figure 30. The thermal gradient across the specimen was approximately 100 ^{o}C. However this optimum condition was not a representation of the real situation which the user may encounter during loading and unloading the specimen from the cup.

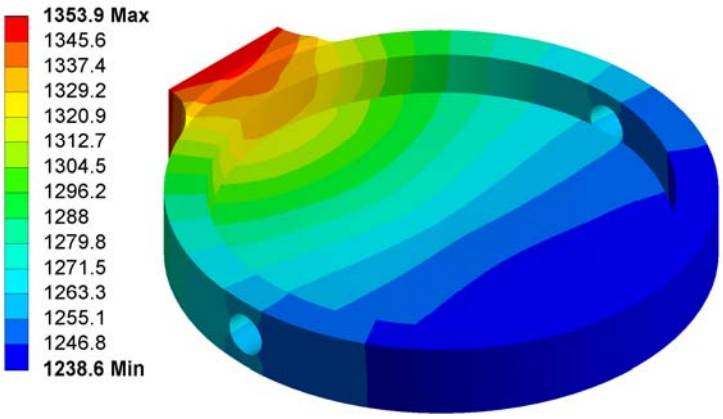

Figure 30: The heat distribution across the cup and the specimen assuming bonded contact

In order to represent a more practical condition the value of thermal contact conductance (TCC) was varied within the finite element code. For bonded contact, TCC takes a very large value, approaching infinity. The same simulation was repeated for a TCC value of 100 and 1000 $W/m^2\,^oC$. The results obtained are shown in Figure 31.

As expected these results show a decrease in the maximum specimen temperature with a decrease in the value of TCC, for a given laser power. The specimen temperature obtained was 815 ^oC when the thermal contact conductance was 100 $W/m^2\,^oC$, where as the specimen temperature was 1140 ^oC for when the thermal contact conductance was 1000 $W/m^2\,^oC$. This was considerably less than the 1238 ^oC obtained in case of bonded contact. Thus it is essential to clamp down on the specimen to generate sufficient contact pressure between the cup and the specimen to increase the thermal contact conductance. There was one significant advantage generated due to the contact interface. The heat distribution within the specimen was considerably uniform and this is one of the vital requirements for the heating cell.

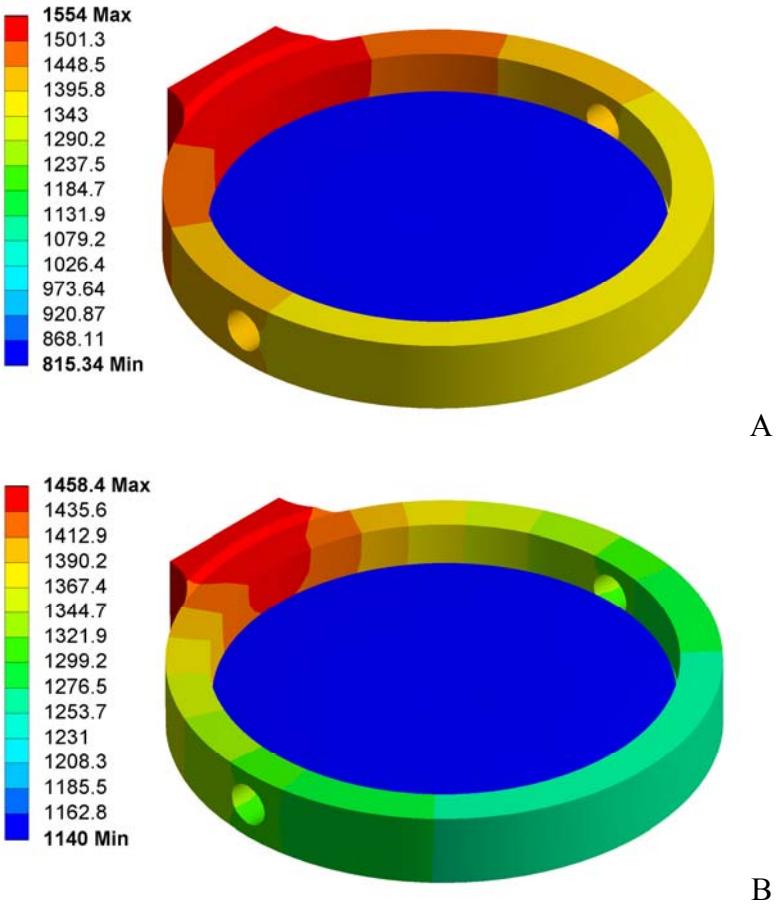

Figure 31: Heat distribution within the specimen and the cup for a TCC value of A) 100 W/m^2 ^{0}C and B) 1000 W/m^2 ^{0}C

3.6 OPTIMUM SPECIMEN CUP DESIGN

TEM specimens are typically disk-like having an outer diameter of 3mm and a thickness of 50 - 100 microns. They require a cylindrical cup to hold them between the pole pieces of the microscope. Since laser heating involves a point source of energy, it was critical to understand the heat distribution profile within the cup. This was required to minimize the thermal gradient across the specimen cup in order to reduce the generation of non uniform thermal stains and

stresses within the specimen. Thermal strain is one of the major causes of the image drifting during specimen observation within the TEM.

To simulate the heat flow within the traditional cylindrical cup, FEA was performed using a 3D model generated with the help of Solid Works [50]. The IGES file was imported into Ansys [49] and meshed using standard thermal elements described previously. The cup was made of tantalum and supported using zirconium oxide pins within the environmental cell. The purpose of selecting these materials is described in detail in the following chapter. One end of the cup was heated using a heat flux of 1E7 Watts/m^2. This simulates an absorption rate of 40% using 10 Watt laser beam. The simulation was performed assuming only conduction and radiation with no convection (vacuum)

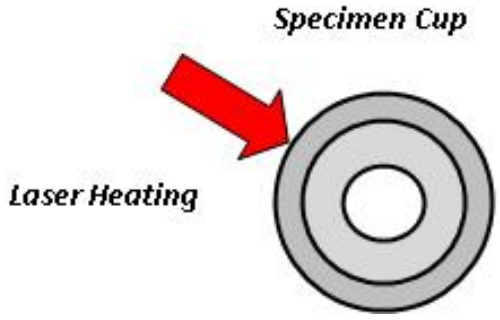

Figure 32: Schematic of the specimen cup used for the analysis

Simulation results presented in Figure 33 show the temperature distribution within the cup. The cup reached a maximum steady state temperature of 1698.4 ^oC within 60 seconds. The thermal gradient across the extreme ends of the specimen cup was 580 ^oC. It is important to note that this does not directly correlate with the specimen temperature within the specimen cup due to the complex nature of the thermal contact conductance described previously. However, any reduction in the thermal gradient across the specimen cup will optimize the final image quality obtained when using the environmental cell holder.

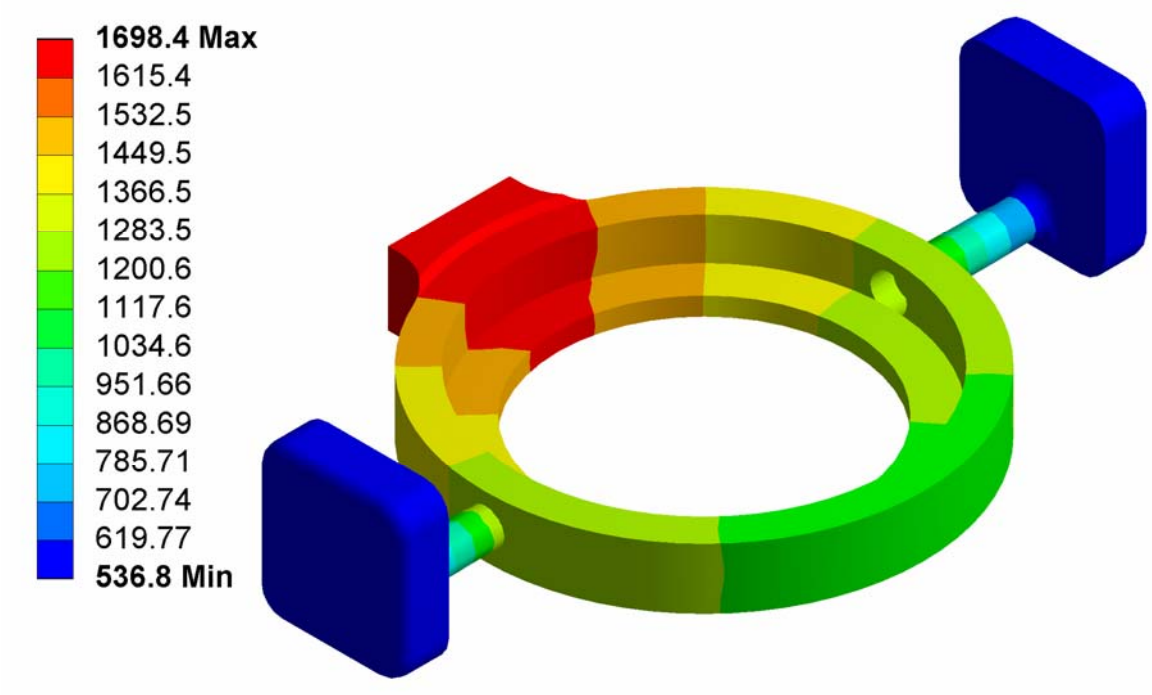

Figure 33: Steady state temperature (^{o}C) distribution with the cylindrical cup

In order to reduce the thermal gradient across the cup, the simulation was repeated on two modified cup designs. The schematic of the modified cups is shown in Figure 34. The objective was to reduce the heat flow resistance across the cup. The thin wall of the cup is the primary source of heat flow resistance. In the new designs the wall thickness was progressively changed across the width of the cup. Under the same conditions of heat flux the first modified design did not bring about any considerable change in the thermal gradient. However using the second design, we were able to reduce the thermal gradient across the cup by more than 30% (Figure 35-36). In this case the thermal gradient was only 398 ^{o}C, signifying an improvement in the heat flow across the specimen cup.

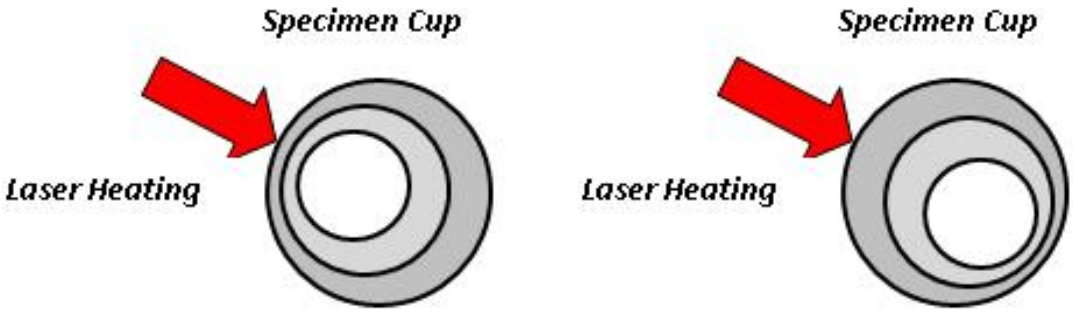

Figure 34: Schematic of the modified specimen cup used for the analysis

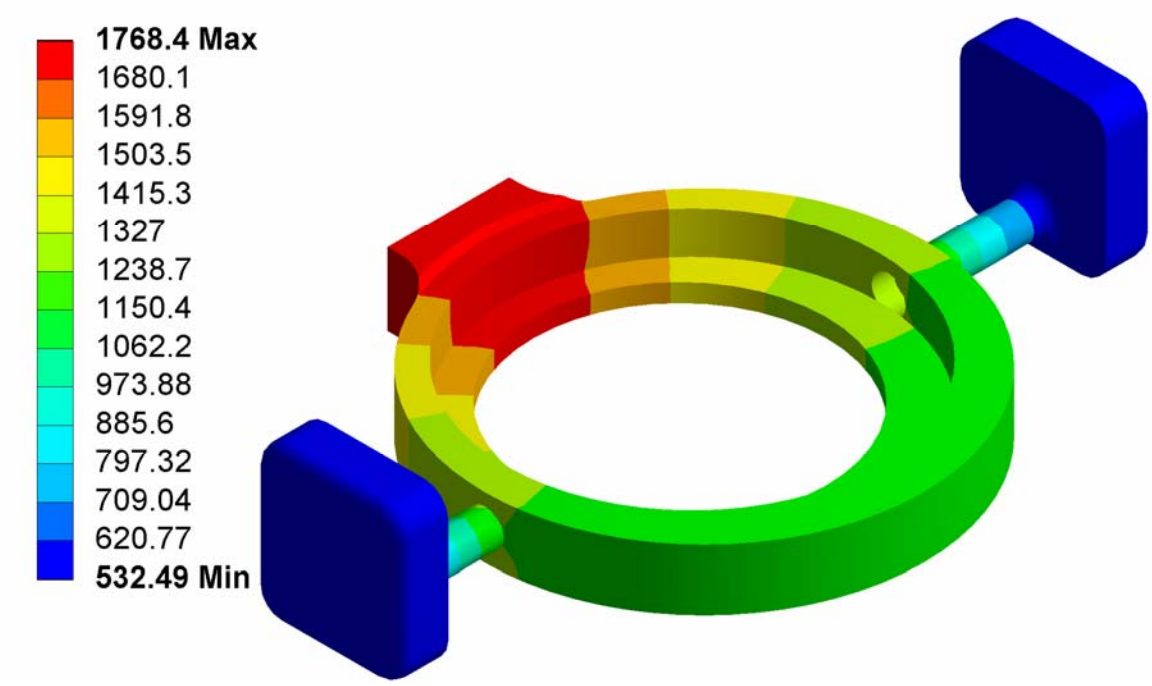

Figure 35: Steady state temperature (^{o}C) distribution within the first modified design

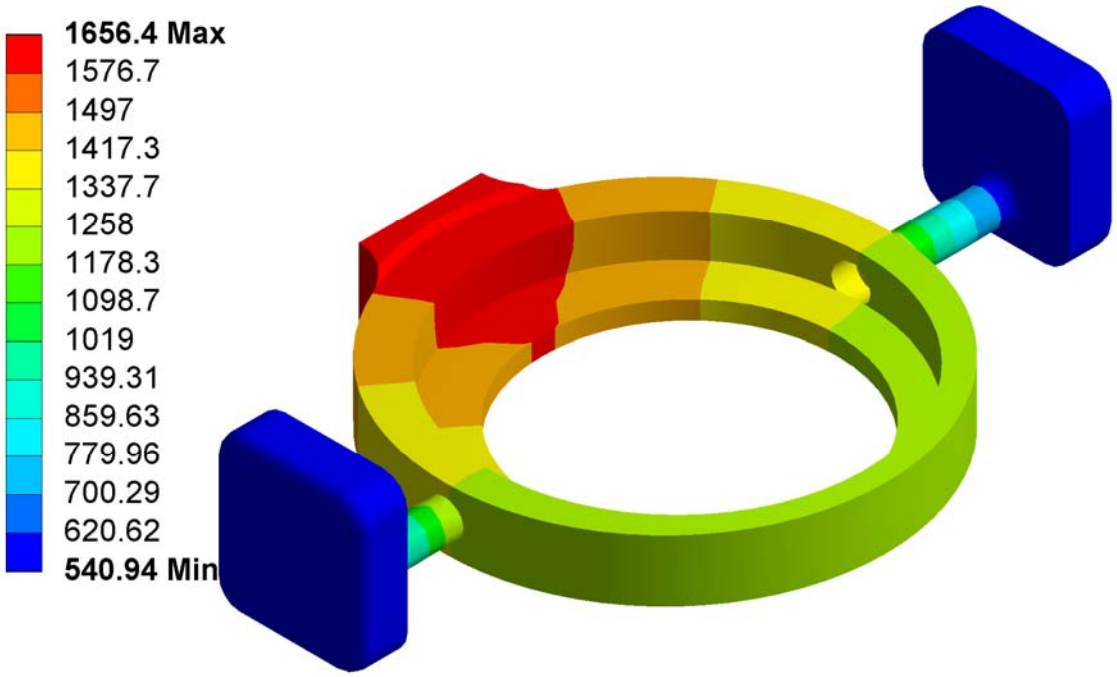

Figure 36: Steady state temperature (^{o}C) distribution within the optimized cylindrical cup

3.7 ENVIRONMENTAL CELL ANALYSIS

The specimen cup which has been optimized for heating the specimen was assembled within the environmental cell. O-rings are used to seal this environmental cell to prevent any gas from escaping into the microscope column. A good seal also helps to attain pressures as high as 1 atmosphere within the cell. The biggest drawback of this seal, for the current application, is that it can withstand a maximum temperature of only 250 ^{o}C. In order to maintain low cell temperatures when the specimen cup was heated, the cup is supported using zirconium oxide pins, which has a very low thermal conductivity and the window distance is optimized to

minimize the heat gain due to radiation. This design is shown in Figure 37 and described in detail within the next chapter.

In this study the complete assembly of the environmental cell was analyzed to observe the thermal distribution within the cell when the specimen is heated to a high temperature. It is desired to limit the cell body temperatures below 250 ^{o}C to prevent the degradation of the o-ring seal. From the results obtained (Figure 38-39) we can see that using the current design, the heat flow to the cradle body was well contained. The temperature of the cradle was only 182 ^{0}C when the specimen temperature was approximately 1200 ^{0}C.

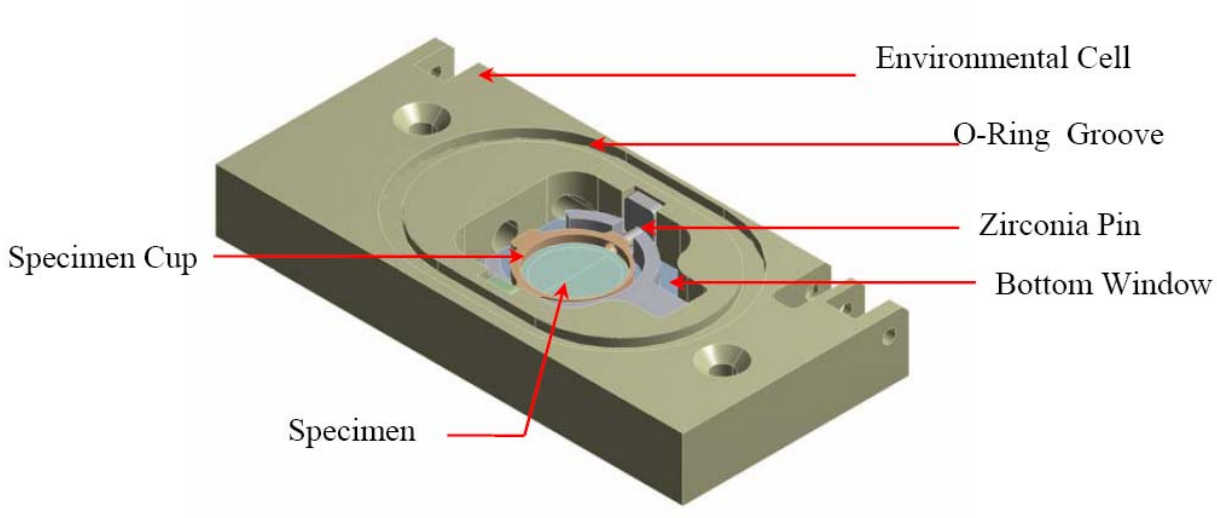

Figure 37: Model of the environmental cell assembly without the top window and the cap

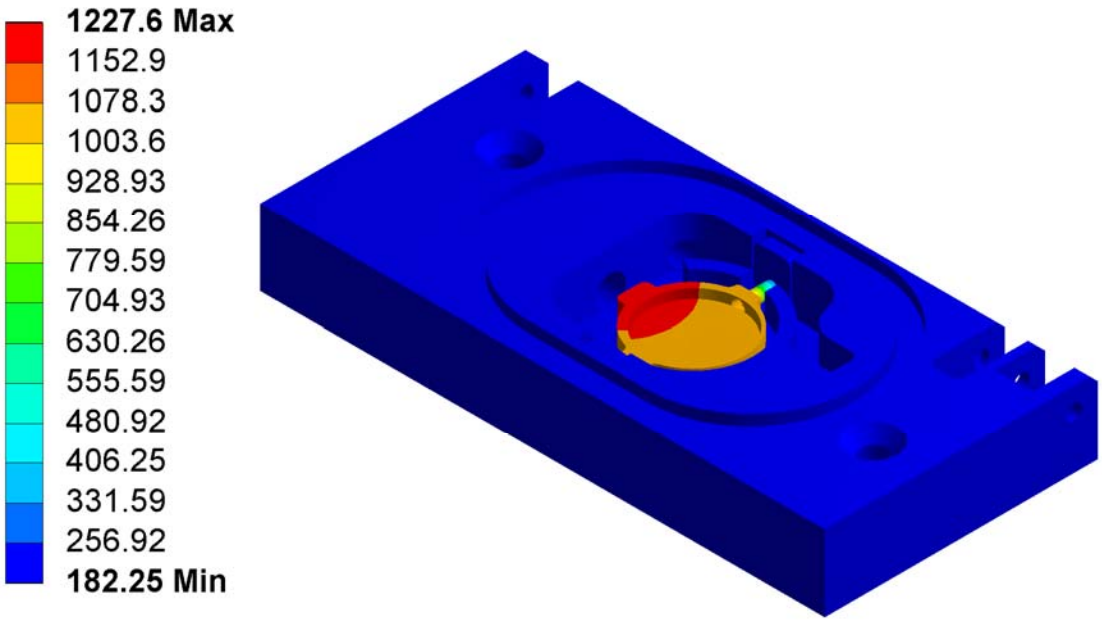

Figure 38: Heat distribution within the environmental cell (shown without the top window to view the specimen and the cup)

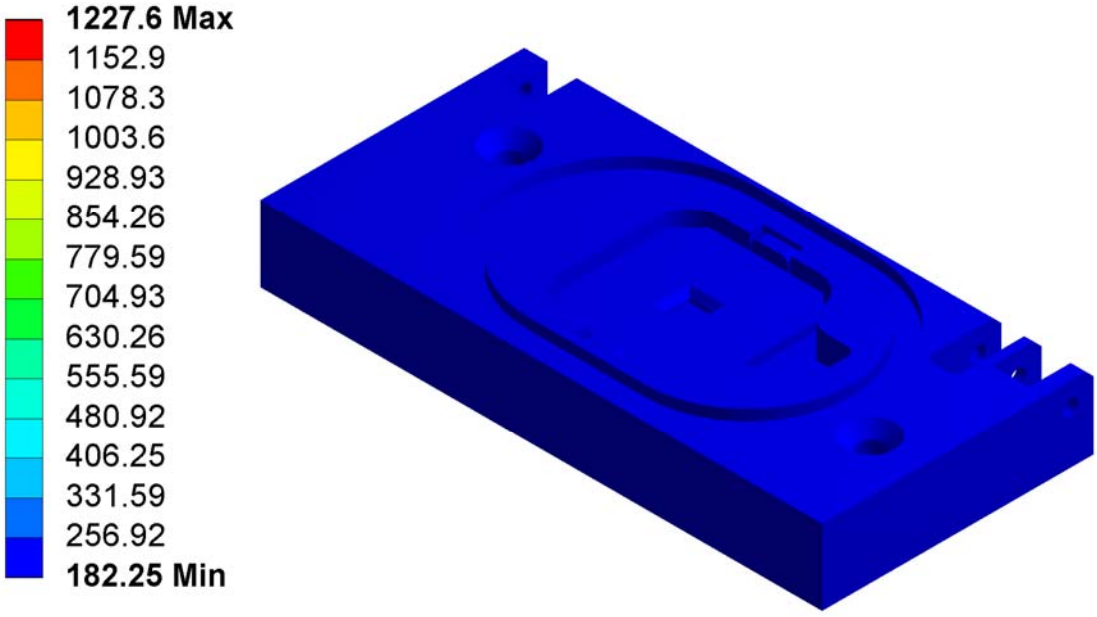

Figure 39: Heat distribution within the complete environmental cell

4.0 DESIGN AND DEVELOPMENT

The considerations given towards the design of the *in situ* gas flow and heating assembly were based on generating a portable design that was compatible with most commercially available microscopes. To assist in a wide range of experiments the design incorporated the following major components:

1. GAS FLOW ASSEMBLY
    a. Capability of flowing four different gases at a given time
    b. Gas handling system compatible with H_2, O_2, CO_2, N_2, HC and CO
    c. Environmental cell capable of withstanding pressures as high as 1 atmosphere
2. HEATING ASSEMBLY
    a. *In situ* specimen heating up to 1273 K
    b. Capability to obtain a wide range of steady state specimen temperature with accurate temperature control (+/- 10 ^oC)
3. HOLDER ASSEMBLY
    a. Capable of providing +/- 15^o specimen tilt about the primary axis (α tilt)
    b. Designed for specimen in the form of 3 mm disc
    c. Field of specimen view > 400 μm^2 at 15^o tilt of the specimen holder

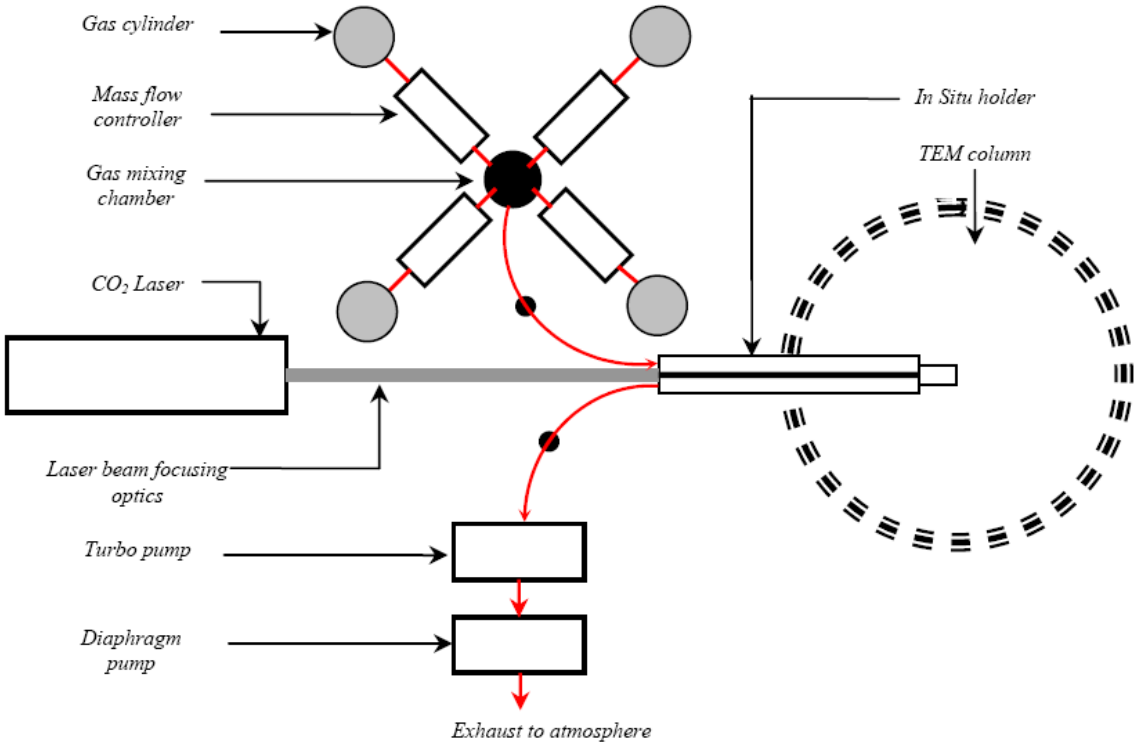

Figure 40: Schematic of the complete gas flow and laser heating assembly

The schematic of the complete assembly is shown in Figure 40. The gas cylinders are attached to a set of four different mass flow controllers and regulators. The flow controllers help to accurately control and monitor the flow of gases. Initially the gases are led into a mixing chamber. From here the gas mixture is circulated into the environmental cell through the inlet port on the holder with the help of tubes. Continuous flow of gas was maintained using the pressure differential generated between the inlet and the outlet port of the holder by the turbo molecular pump that was mounted externally. The turbo pump, along with a diaphragm pump, continuously pump the cell through tubes connected to the outlet port of the holder. The CO_2 laser along with the laser beam focusing optics (articulated arm) was used to directly focus the

laser beam onto the specimen cup that was placed in the environmental cell. The complete process is computer controlled and monitored utilizing the data acquisition boards.

4.1 *IN SITU* HOLDER

The most critical component of the complete assembly is the *in situ* holder. The major parts of the holder include:

1. Environmental cell
2. Barrel assembly
3. Holder handle

4.1.1 Environmental cell

As discussed in Chapter 2, the window and the aperture type environmental cells, each have a specific set of advantages and disadvantages. Aperture type cells have limitations on the maximum gas pressure that can be achieved and require complex design to incorporate a pumping mechanism. The window type cells, in contrast, are limited in the maximum resolution that can be attained. In order to combine the advantages of both systems, a modular design was generated. This design included amorphous silicon nitride windows to create a sealed chamber. The sealed chamber also had a simple provision by which it could be differentially pumped to generate a wide range of operating pressures. The environmental cell was comprised of the following components:

1. Specimen cup

The specimen cup was designed to hold a traditional 3mm specimen disc as shown in Figure 41. The distance between the windows determines the gas path length. Due to this, the window separation distance was set at 1mm with the specimen placed along the central plane. This limits the maximum cup height that can be assembled between the windows. The cup also acts a furnace as it is directly heated with the laser beam. In order to avoid any contact with the windows the cup height was limited to 0.5 mm. Since reduction in the thermal mass would help to achieve greater specimen temperatures for a given laser power, the cup wall thickness was limited to 0.275 mm.

Material selection was the second important criteria for the cup design. Being in the vicinity of the electron beam which passes through the specimen, it was essential that the cup be nonmagnetic. A magnetic field deflects the electrons which gives rise to astigmatism in the final specimen image generated by the TEM.

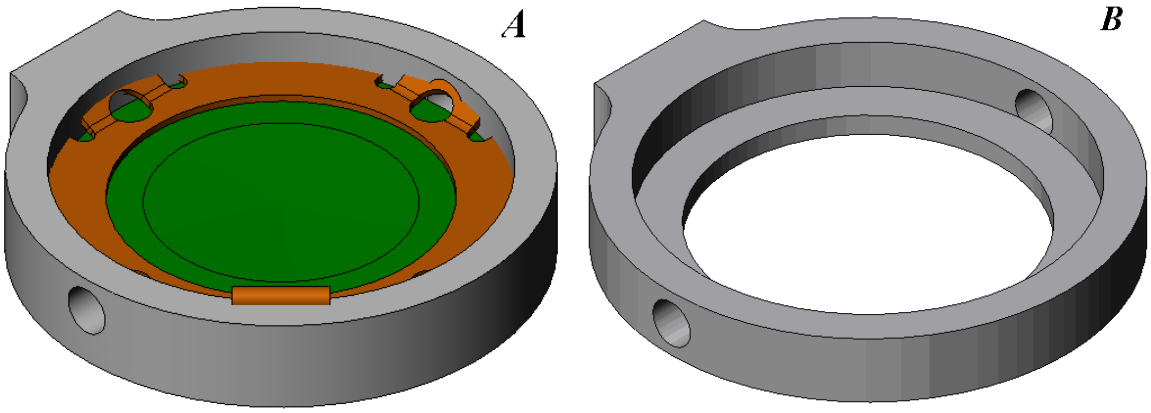

Figure 41: Specimen cup made out of tantalum, with (A) and without (B) the specimen

Since one of the factors that limit the maximum specimen temperature is the melting point of the cup material, it is important to select a material having a high working temperature. Along with this, the material should have high thermal conductivity to achieve uniform specimen temperatures. The materials considered based on the above criteria, are listed in Table 8.

Table 8: Various materials under consideration for the fabrication of the chamber

Cradle Material	Thermal Conductivity W/m-°C	Thermal Coefficient of Expansion µm/m-°C	Melting Point °C	Emissivity
Platinum	69.1	9.1	1769	0.05-0.1
316 SS	16.3	17.5	1370	0.1-0.15
Inconel	14.9	13.3	1354	0.2-0.6
Tantalum	59.4	6.5	2890	0.15-0.3
Zirconia	1.675	7	2680	0.4-0.7
Alumina	6.3	8.2	2054	0.5-0.65
Silicon	124	4.44	1412	0.6
Molybdenum	138	6	2617	0.1-0.2

Molybdenum, having the highest thermal conductivity of 138 W/m ^{o}C and the lowest coefficient of thermal expansion [51] was chosen as the preferred material. However, during the initial testing of the cup, the material degraded rapidly in the presence of an oxidizing environment. Crystals of molybdenum trioxide were observed all over the cup at a temperature of 700 ^{o}C. On further heating, the cup completely disintegrated as seen from the scanning electron microscope image in Figure 42. Molybdenum was therefore not considered further.

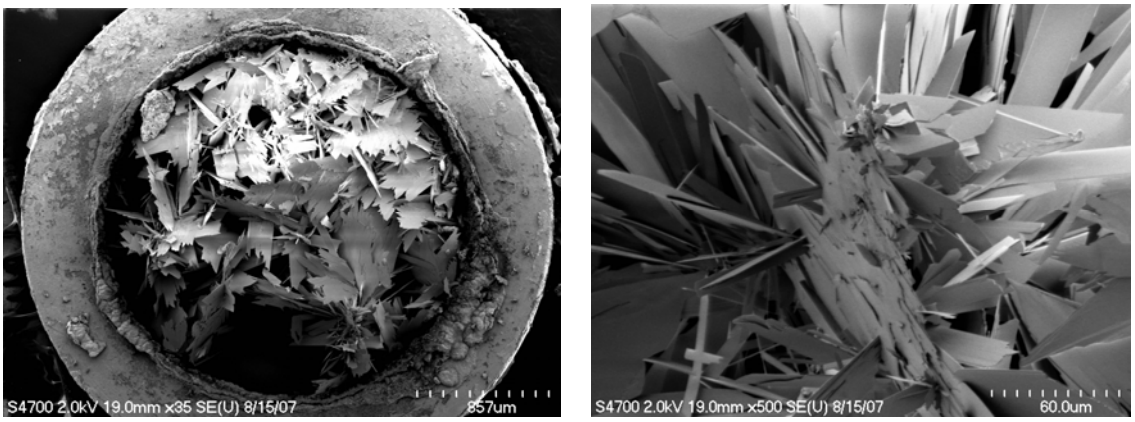

Figure 42: SEM image of molybdenum triode formed within the specimen cup at 700 ^{o}C

As listed in Table 8, silicon also had the required properties; however, it was not optimal because it was very difficult to fabricate into a cup of the desired shape. Furthermore, silicon had a very low rate of laser beam absorption and lacked sufficient fracture strength. The idea of using zirconium oxide and aluminum oxide was discarded because of their tendency to charge within the TEM in the vicinity of the electron beam. Being poor conductors they would not conduct the stray electrons which are deflected off the specimen. These stray electrons can cause the material to charge and hinder the image observation.

Tantalum was the next preferred choice. It had a low thermal coefficient of expansion (6.5 μm/m ^{o}C) and a sufficiently high thermal conductivity of 54 W/m ^{o}C. It maintained its structural rigidity at high temperatures and did not oxidize rapidly and was therefore deemed a viable candidate.

2. Cup supports

Since the current application involves heating the cup to high temperatures, it was highly desirable to isolate the cup from the rest of the holder. This minimizes thermal drift and assists in obtaining higher specimen temperatures. Pins manufactured out of zirconium oxide were used to support the specimen cup. As shown in Table 8, Zirconium oxide had the lowest thermal conductivity of 1.675 W/m ^{o}C. Its rate of thermal expansion was similar to the specimen cup and thus maintained the desired structural rigidity at the cup joints during elevated temperatures. Also, unlike the majority of the ceramics, zirconium oxide is compatible with a low pressure environment and does not evaporate in vacuum. The pins were 0.3 mm in diameter and 1.4 mm long. The only disadvantage of this material was the high machining cost associated with the required diamond tooling. Figure 43 shows the assembly of the specimen cup and the support pins.

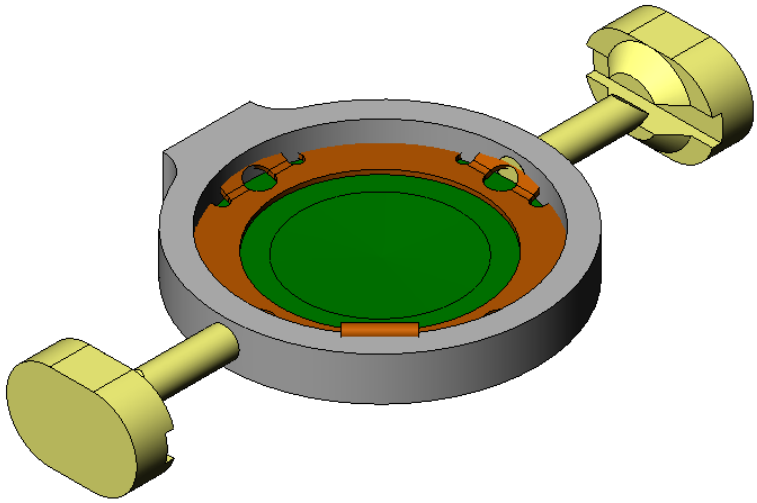

Figure 43: Specimen cup along with the specimen, clamping ring and supports.

3. Specimen Clamp

Significant heating can cause major changes in the mechanical properties of materials. Some of these effects include thermal stress, strain, and deformation. When a substance is heated, its constituent particles move around more vigorously and by doing so generally maintain a greater average separation. The degree of expansion divided by the change in temperature is called the material's coefficient of thermal expansion and generally varies with temperature. The friction between the specimen cup and the specimen resists the expansion of the specimen resulting in the generation of stresses. In order to limit this stress a unique clamping mechanism was used as seen in Figure 43. This clamping mechanism holds the specimen in place but its flexible design limits its resistance towards the expansion of specimen. The clamps were fabricated from a 0.2 mm thick tantalum sheet by the process of photo chemical etching.

4. Silicon Nitride Windows

Amorphous silicon nitride windows were placed above and below the specimen cup to form the *in situ* gas reaction chamber. The window membrane was 0.5 mm square and was supported on a 5 mm square silicon frame having a thickness of 300 microns. As illustrated in

Figure 44, these windows were completely isolated form the specimen cup with the help of spacers. The major requirements for the selection of the windows was that it must be electron transparent, it must be able to withstand high temperature as well as pressure differentials in and around the chamber, and it must be inert to gases present within the chamber. Silicon Nitride windows deposited on silicon substrate, were found to be an optimum choice to fulfill these requirements. 20nm thick silicon nitride windows were able to withstand a pressure differential of 1 atmosphere and were able to provide adequate resolution. These windows were stable up to a temperature of 1000 ^{0}C, thus the heat radiated from the heating cup did not affect them.

The silicon nitride films are generally deposited using low pressure vapor deposition techniques (LPCVD). Typically, silicon wafers are loaded in a tube furnace and nitride films are deposited by reacting dichlorosilane and ammonia at a temperature of 700 ^{0}C and a pressure of 40 KPa. Using photolithography, photo resist is applied on silicon substrate, which is patterned using UV light based on the required size of the windows. Later, the photo resist is stripped using acetone and silicon is etched in KOH. These LPCVD silicon nitride films are amorphous. The fundamental nature of the films simplifies the interpretation of TEM images and diffraction patterns. The thickness of the films determines the resolution of the images. Diffused scattering of the electrons passing through the membrane increases with increasing thickness; this degrades the attainable resolution. Figure 45 shows the degradation in the image resolution of a nickel specimen when viewed with and without a 50nm thick silicon nitride window.

Considering their high fracture strength, diamond films were also considered for this application. Their crystalline structure, however, caused a large degradation of the image quality. Presence of gases at high temperatures also rendered the film incompatible.

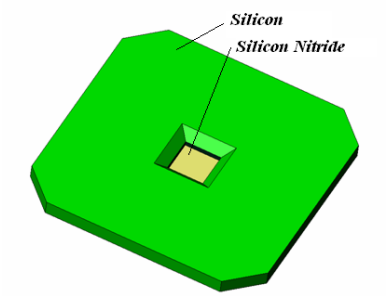

Figure 44: 20nm thick Silicon Nitride windows

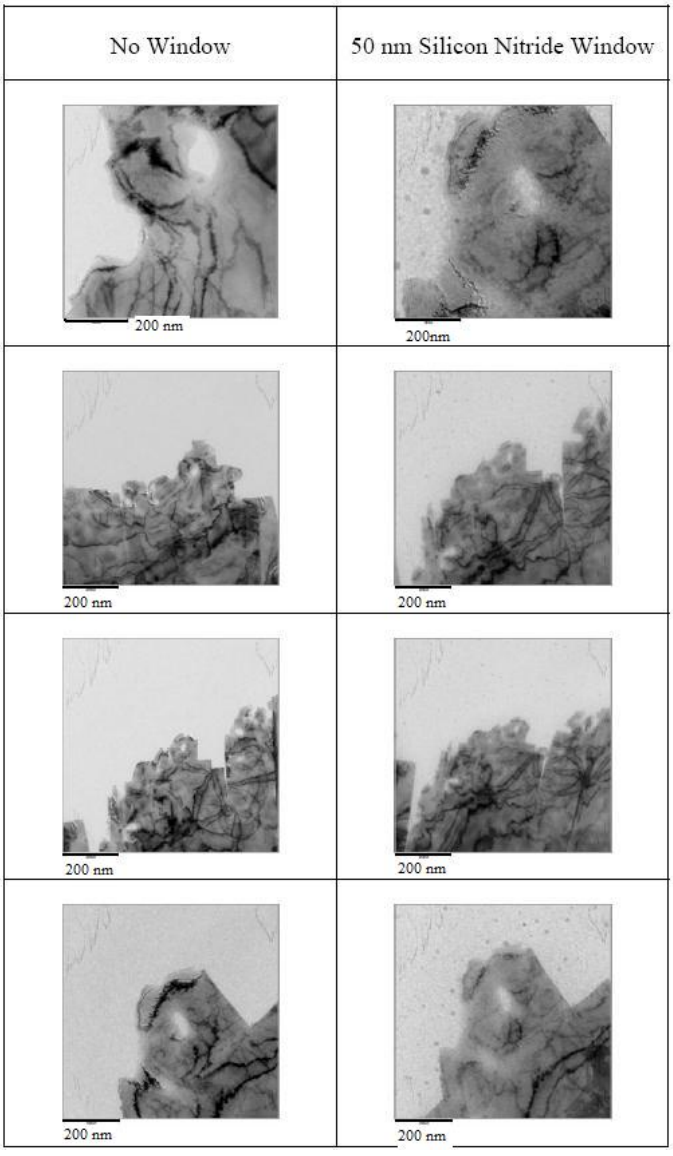

Figure 45: Reduction in image quality of a nickel sample when viewed through a 50nm silicon nitride window

5. Cradle

The cradle was used to assemble the specimen cup and the windows. Since it does not have to withstand high temperatures, it was fabricated out of non magnetic stainless steel. Its external dimensions were 15 mm X 8.5 mm and it was only 3.5 mm thick. The thickness of the cradle was limited because it determines the maximum angle by which the specimen can be tilted within the pole pieces of the microscope. A square cavity milled within the cradle is used as the gas reaction chamber. Three viton O-rings were used to provide a complete vacuum seal around the environmental cell. Viton is a fluoroelastomer manufactured by Dupont and is well known for its excellent heat resistance (~ 250 ^{O}C) and its resistance to reactive gases. Three holes were drilled along the sides of the cradle. Two of them are used as an inlet and exhaust for the gases and the third was used to allow a clear passage for the laser beam to strike the specimen cup.

Figure 46 describes the complete assembly process of the environmental cell. The first step involves placing a silicon nitride window in the cell cavity and then lowering the hinged spacer. The height of the spacer determines the separation distance between the windows. The second step involves placing the cup loaded with the specimen within the cradle. The cradle wall has the provision by which the cup was held in place without it touching the windows. The separation distance between the cup and the windows was maintained at 250 μm. A second window was then placed over the spacer. After being assembled the hinged cradle cap was lowered and clamped with the help of two screws on the cap. The set of O-rings provide the sealed environment necessary for the flow of gases over the specimen. A great deal of consideration was given toward the ease of use of the environmental cell because of the small size of the parts involved.

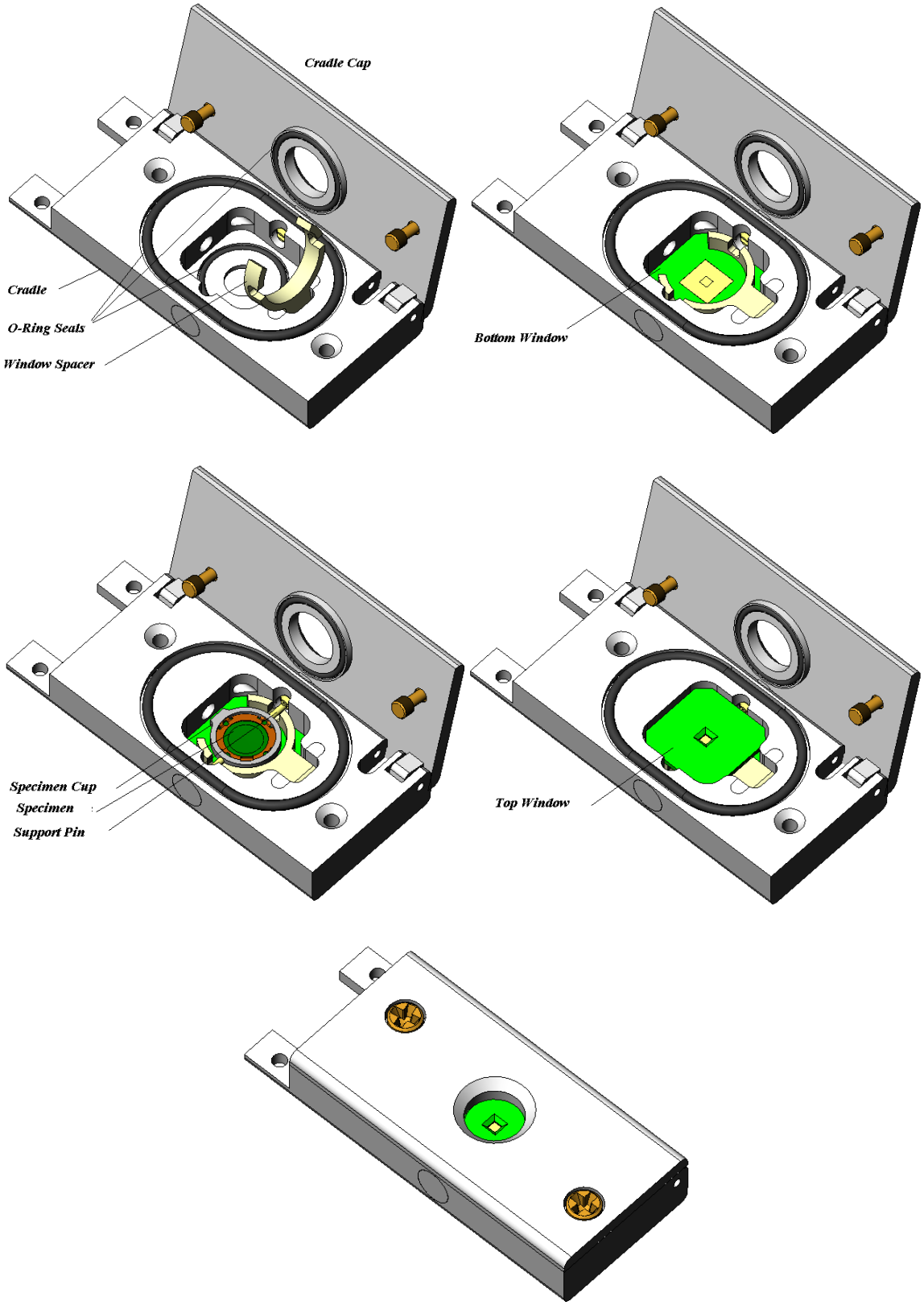

Figure 46: Complete assembly of the environmental cell

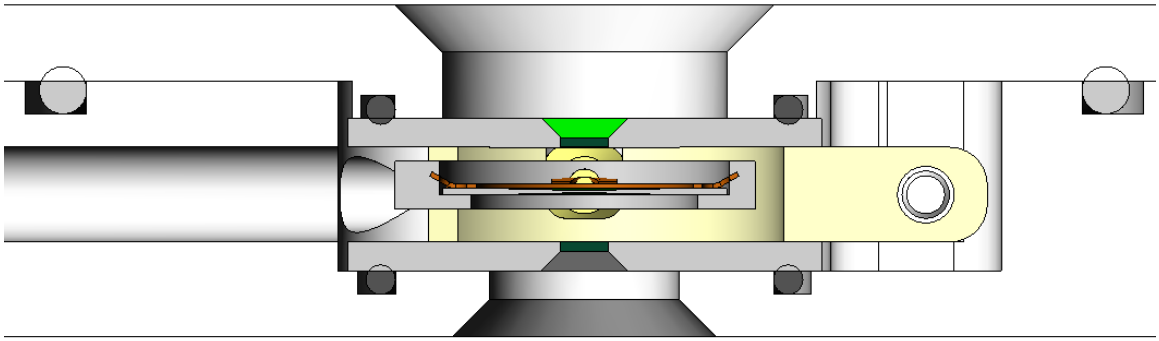

Figure 47: Sectional view of the sealed environmental cell

4.1.2 Barrel Assembly

The modular environmental cell was designed to fit onto the holder barrel of most commercially available microscopes. The size and shape of the barrel used to hold the specimen within the TEM was designated by the microscope manufacturer. It is typically made out of beryllium copper because of its non magnetic properties. Figure 48 shows the holder barrel of a prominent TEM manufacturer.

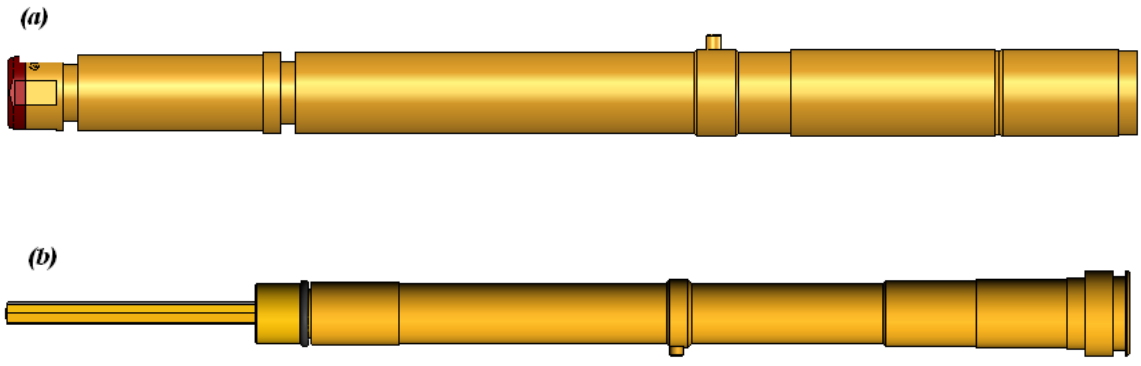

Figure 48: Holder barrels for microscopes made by JEOL Ltd.

4.1.3 Holder Handle

The holder handle includes a convex zinc selenide lens in order to focus the laser beam onto the specimen cup. The handle has the provision to mount the articulated laser arm assembly which is described later in the chapter. Two gas fittings are incorporated on the handle as shown in Figure 49. One is attached to a tube that was used to flow the desired gas mixture on to the specimen and the second was used to pump the specimen holder to maintain the desired operating pressure within the cell. A set of O-rings are used to maintain the vacuum seal at the interface of the lens and the gas tubes.

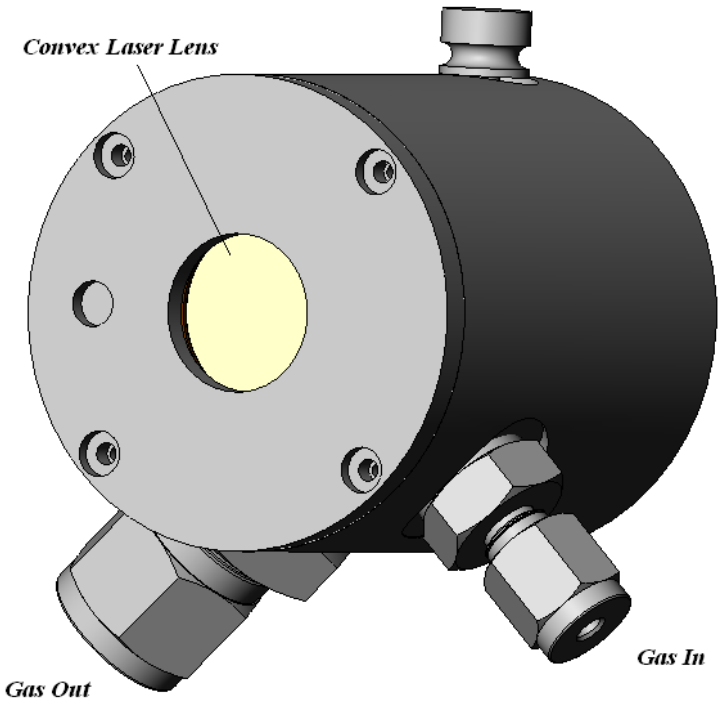

Figure 49: *In situ* holder handle

The Environmental cell, the barrel, and the handle are assembled together to form the *in situ* gas reaction and heating holder (Figure 50-51).

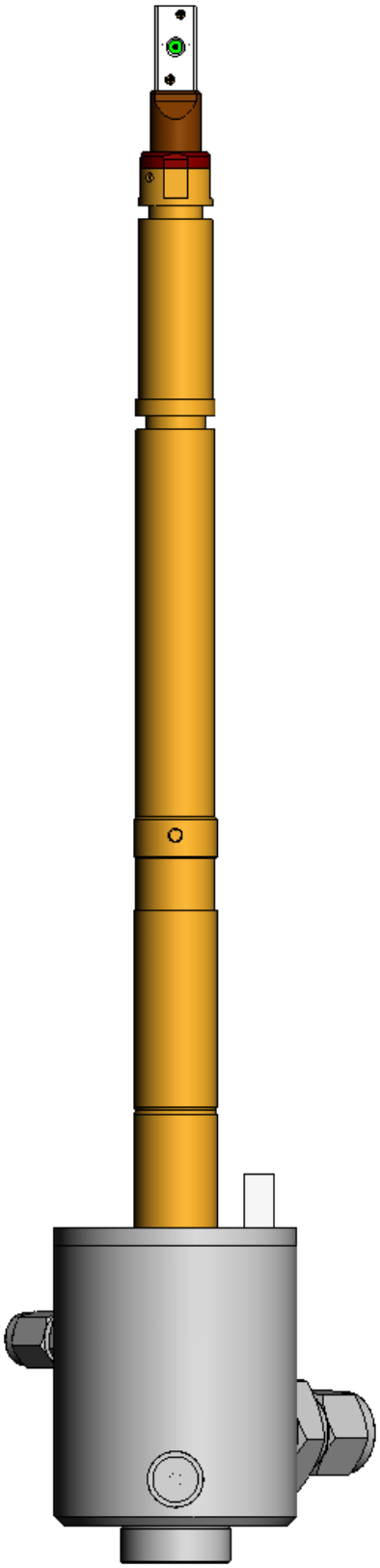

Figure 50: *In situ* gas reaction and heating holder

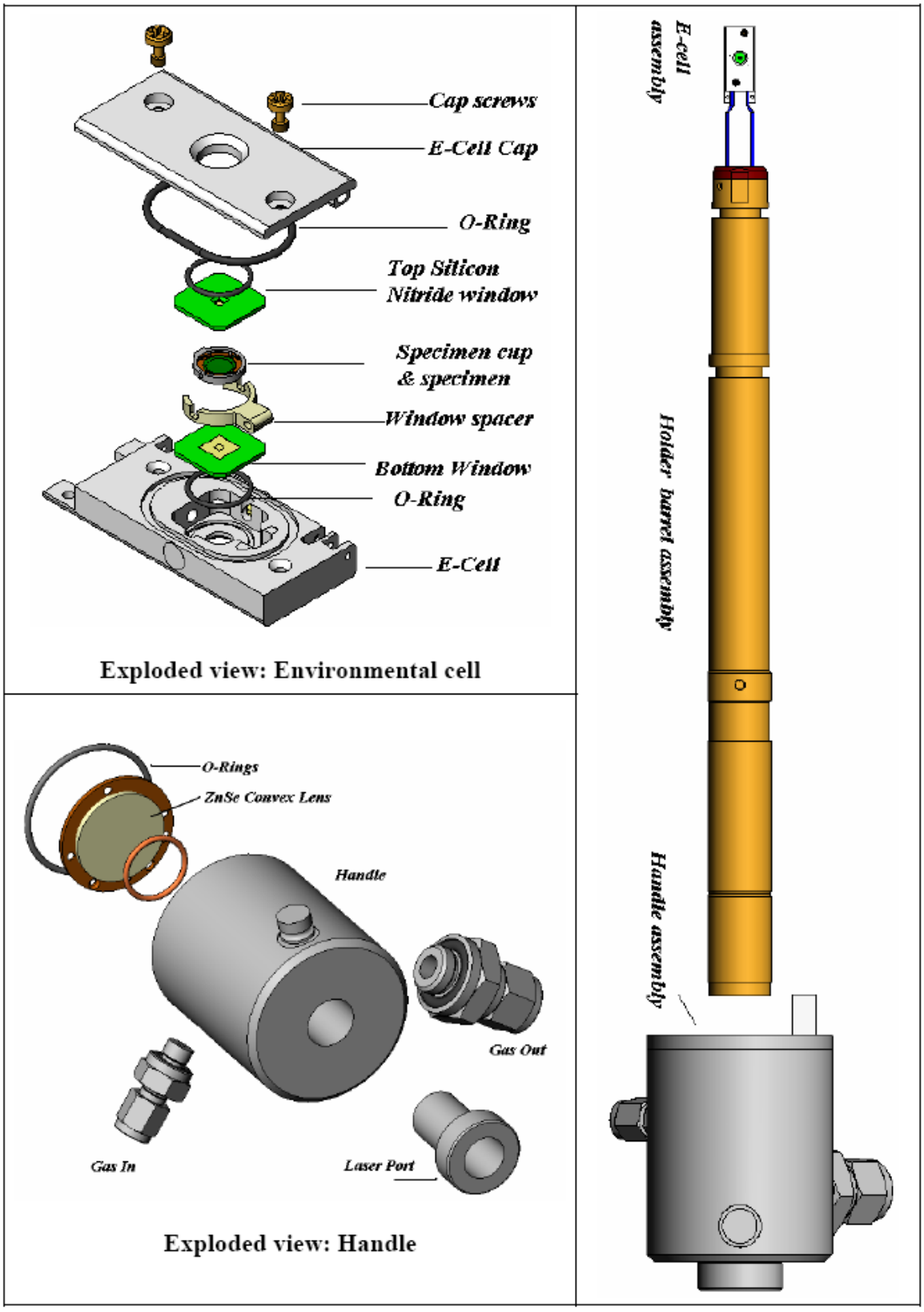

Figure 51: Exploded View-*In situ* gas reaction and heating holder

4.2 HEATING ASSEMBLY

All traditional heating holders utilized a resistive heating coil to heat the specimen within the TEM. However it has many disadvantages [9], namely:

1. The maximum temperature that can be attained is limited (< 1200 ^{0}C)
2. It has a very short life span, especially in the presence of gases (< 5 hrs at 1200 ^{0}C)
3. It requires a very complex design to incorporate this mechanism within the small space available in the environmental cell (4-5 mm in height) and it requires a skilled technician to assemble it or to replace the heating coil.
4. The electric current used to heat the specimen generates an electromagnetic field which affects the image quality. The current supplied is usually in the range of 2-3 amps.
5. It is impossible to obtain uniform specimen heating using this technique. This gives rise to uneven thermal expansion and thus limiting its use as a tool for *in situ* analysis
6. The large volume required to incorporate this design complicates its thermal isolation from the body of the holder. This often results in the need for water cooling to overcome specimen drift.

Considering these factors, a novel CO_2 laser heating mechanism was utilized to heat the specimen. The laser was mounted externally and hence required no additional parts within the environmental cell. The only consideration associated with using a laser was a means to deliver the laser beam up to the specimen cup.

Since CO_2 lasers are large compared to a TEM holder, they cannot be attached on the holder itself. The primary requirement is to select the location of the CO_2 laser such that it is not in an awkward position. It should also allow for a flexible delivery system for transmitting CO_2

laser radiation. The two common ways to deliver the CO_2 laser beam are: a) silica based glass waveguides or b) an articulated arm assembly.

4.2.1 Waveguides

Previous studies have successfully utilized hollow sapphire waveguides as an optical fiber [43-48]. The advantages of using these waveguides are listed in Chapter 2. Figure 52 shows one such commercially available waveguide [52] that was used on an experimental basis to heat the specimen within the specimen holder. It consisted of a hollow silica tube with an internal diameter of 500 μm. The inside surface of this tube was coated with silver and silver iodide to improve its performance. Its external surface was encased in an acrylate coating to protect the brittle silica tube.

Figure 52: Waveguide for transmitting CO_2 laser beam

Although the waveguide successfully transmitted the laser energy from the source to the target on a curved trajectory, it had one major disadvantage - any misalignment at the source caused the waveguide to burn (Figure 52). This burning gradually propagated along the length of the waveguide. Since a CO_2 laser beam is invisible to the naked eye, any beam reflected due to such failures could cause serious injuries to the user.

4.2.2 Articulated Arm

As seen in Figure 53 the articulated arm assembly consists of a series of hollow tubes connected by bearings, thus providing a flexible beam delivery system. Each joint includes a mirror that acts as a beam bender and is accurately positioned to keep the laser beam centered along its path. The mirrors have a gold based coating which provides very low transmittance loss (< 0.5%). The tubes create a complete sealed path for the laser beam, hence generating a safe working environment.

One of the major challenges of the laser application arises in the solution of beam alignment problems, particularly when the knowledge of the beam displacement from a reference plane is desired. In our application, the laser beam had a waist size of 3.5 mm as it exists from the laser. However as illustrated in Figure 53, the beam has to travel a long distance (1900 mm) before it reaches the TEM specimen holder. This is equal to the length of the articulated arm. The divergence rating of the laser beam by the manufacturer is 4 mrad.

The laser beam divergence is given by

$$\theta = 2\arctan\left[\frac{D_f - D_i}{2l}\right] \qquad 4.1$$

Where, D_f is the final beam diameter, D_i is the initial beam diameter, l is the length of the travel path of the beam and θ is the divergence angle of the beam. From the equation 4.1 the final diameter of the beam is calculated to be 11 mm. The height of the specimen cup is 0.5 mm. In order to heat the specimen cup using the laser, the beam size has to be reduced considerably. The distance of the specimen cup from the holder handle where the articulated arm was attached was 254 mm. In order to reduce the final beam size at the specimen cup, a convex lens having a focal length of 254 mm was incorporated into the handle. Zinc Selenide (ZnSe) was found to be the

best material for such application [35]. It had greater mechanical strength than other available lenses (KCl and NaCl) along with low absorption coefficient, thus requiring a thinner lens with low optical losses.

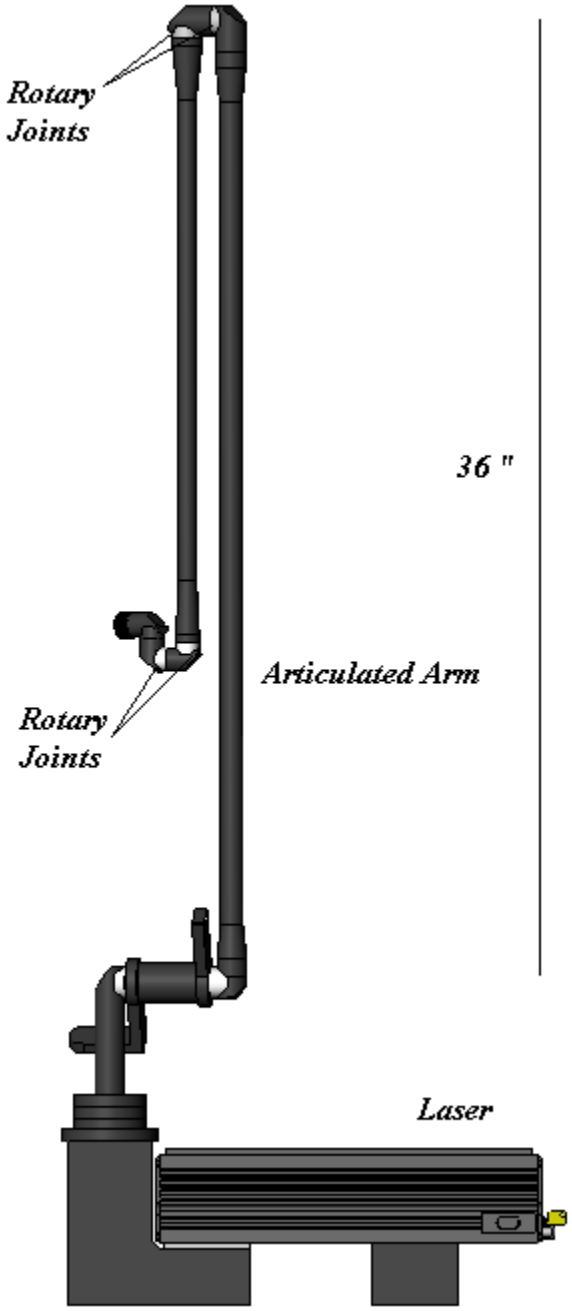

Figure 53: Laser heating assembly

Table 9: Optical properties of ZnSe window with anti reflectance coating

Angle of Incidence	0^0
Transmission	>99.4
Reflectance	0.1%
Absorption	<0.2%

The final spot size of the laser beam was calculated using the following equation:

$$D_f = \frac{4M^2 \lambda f}{\pi D_i} \qquad 4.2$$

Where, D_f is the final beam diameter, λ is the wavelength of the laser (10.6 μm for a CO_2 laser), f is the focal length of the lens (254 mm), Di is the initial beam diameter (11 mm) and M^2 is the special profile characteristics of the laser beam specified by the laser manufacturer. For the given laser M^2 was 1.2. Using the above equation the final beam spot size at the specimen cup was found to be 374 μm. From the experimental results using the laser burn card, the spot size was calculated to be approximately 300 μm as shown in Figure 54. This was slightly smaller than the theoretically calculated beam size. Such a difference is due to the Gaussian nature of the beam profile. The beam power is concentrated at the center with negligible energy at the circumference.

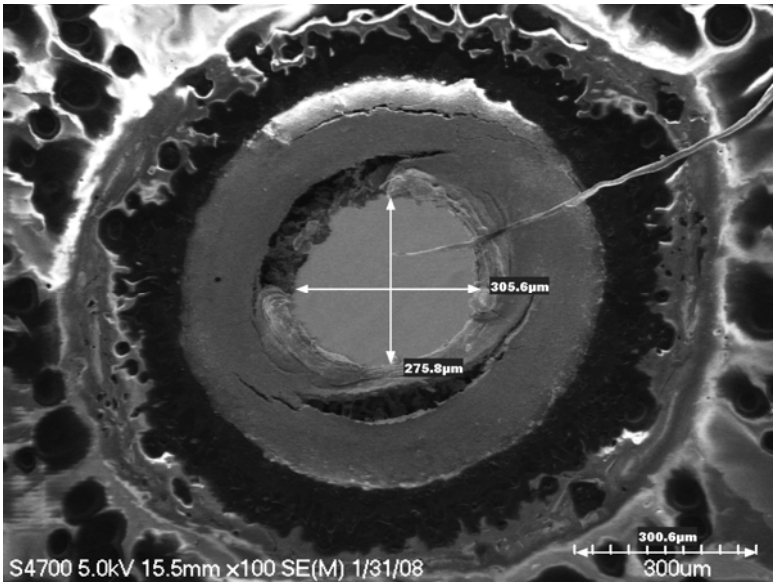

Figure 54: SEM image of the laser spot size calculated using a burn card

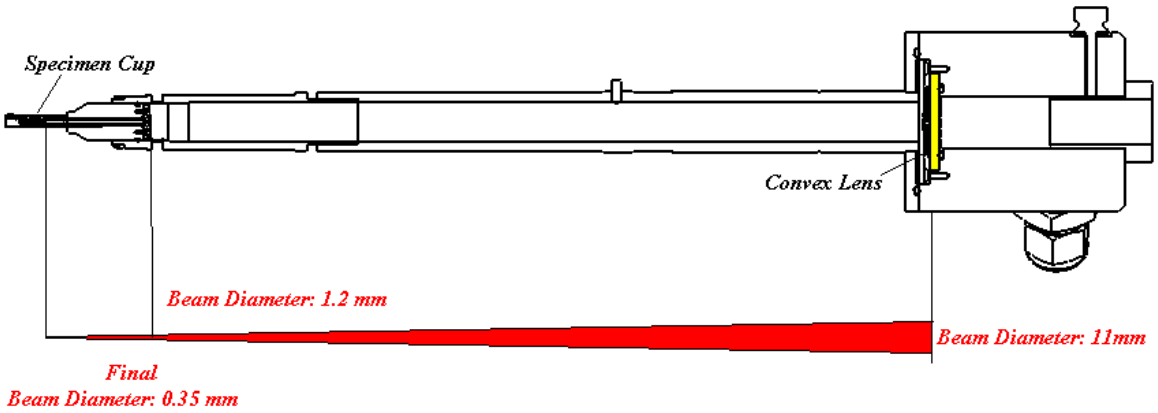

Figure 55: Laser beam profile along the holder barrel

4.3 GAS FLOW ASSEMBLY

Flow of gases over the specimen within the environmental cell is the second important phase of this research. The gas flow assembly was designed to flow a mixture of up to four different gases

within the cell at any given time. The flow rate of the gases was controlled with the help of four separate mass flow controllers as shown in Figure 56. Each mass flow controller (MFC) was calibrated to flow 0 to 5 sccm (standard centimeter cube per minute) of nitrogen. The MFC's are provided with a pneumatic shut off valve to completely seal its outlet when any particular MFC was not in use.

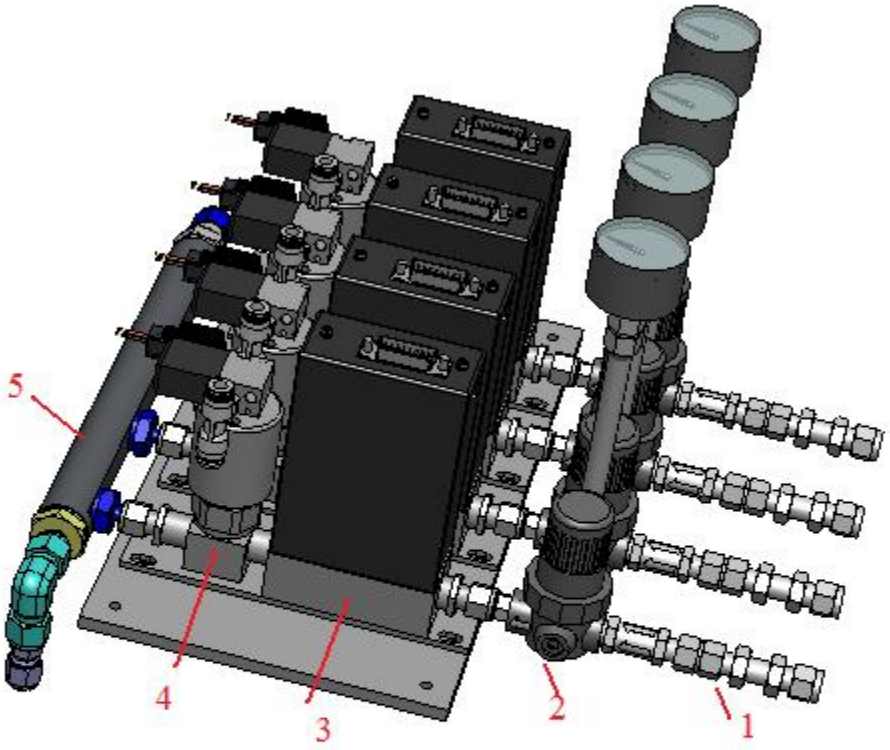

1. Bulkhead fitting
2. Regulators
3. Mass flow controllers
4. Pneumatic shut off valves
5. Gas manifold

Figure 56: Mass flow controller assembly

Gas from the MFC flows into the gas mixing manifold and this mixture was then passed onto the specimen holder though the gas inlet fitting on the holder handle. A tube assembled inside the holder leads the gas into the *in situ* environmental cell. Gases can be continuously

circulated until the desired pressure has been attained within the cell. The O-ring seals described previously prevent the gas molecules from escaping into the microscope. In order to vary the pressure within the cell a set of turbo molecular and diaphragm pumps were attached at the outlet of the holder through nylon tubing.

The pumps ability to remove the gas molecules out of the chamber was given in terms of its pumping speed (liters/s). The speed by which these gas molecules flow from the holder to the environment depends on the pressure differential between the two locations as well as the geometry of the nylon tubes. When the pressure was very low so that molecular flow conditions prevail inside the tube (Kn>1). The conductance of the gases through the tubes was directly proportional to the length and diameter of the tube; it decreases rapidly with decreasing tube diameter. There is a physical limitation on the side of the tube that can be attached to the holder. The diameter based on the design constrains was selected to be 15 mm. The distance of the holder from the gas assembly was approximately 1000 mm. The increase in the pumping capacity of the pumps did not bring about any change in the flow rate for a 15 mm tube diameter having a length of 1000 mm. In order to avoid vibrations a turbomolecular pump having a capacity of 10 liters/s was selected.

4.4 COMUPUTATIONAL CONTROL

The complete gas flow and heating assembly was operated with the help of National Instruments data acquisition boards interfaced with the LabVIEW code [59]. The layout of the LabVIEW user interface is shown in Figure 57. Once the holder was assembled and inserted into the microscope, the gas tubes and the articulated arms are attached on to the holder. The required gas

cylinders are then attached to the mass flow controllers through the bulkhead connectors. The desired flow rate of the gases and the laser power was selected using the computer interface. The pumps and the gas valves were then switched on with the help of the toggle switches provided on the LabVIEW interface. The gas flow rate and the sample temperature were continuously monitored with the help of a feed back loop. Once the sample was exposed to the required gases at the required temperature, the TEM was used to continuously monitor and record the reactions taking place on the specimen.

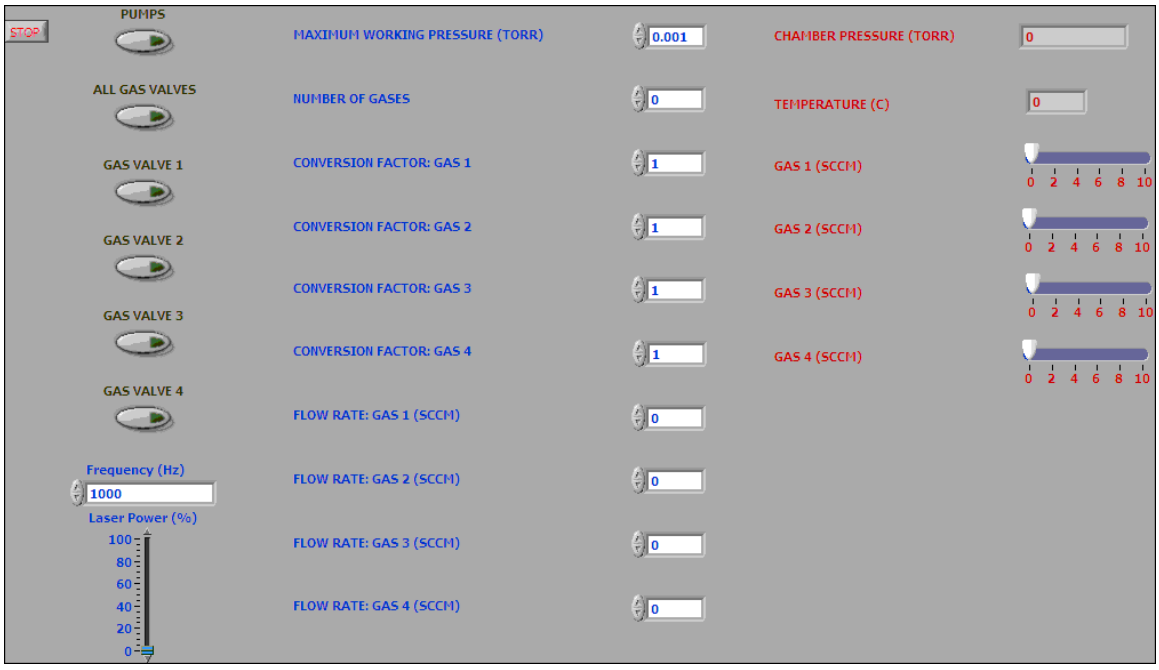

Figure 57: The user interface for the LabVIEW code used to control the gas reaction and heating assembly

5.0 RESULTS AND DISCUSSIONS

The objective of this research was to design and develop an environmental cell assembly for dynamic *in situ* observations of gas solid reactions at elevated temperatures. The requirements of *in situ* observations are best explained by Ferreira [55]. Imagine looking at two different pictures of a billiard table, taken within five seconds of each other. The first picture shows a white ball and two colored balls on the billiard table. The second picture shows the white ball alone on the table, in a different location than first pictured. If asked to figure out what happened between shots, we might assume a play was made, and colored balls are in the pockets. However, from the snapshots taken, we see only the outcome and know nothing of the process that led to it. In order to know the details, we would need to observe, *in situ* the events that took place in the five-second gap between one picture and the next.

This study was focused on bridging the gap between the desires to observe specimen reactions, to record events as they occur in real times and the scientific instrumentations available to successfully carry out these observations within a TEM.

The foremost criterion was to have a portable gas flow and heating assembly that was completely independent of the type and location of the TEM. As seen in Figure 58, the complete *in situ* assembly built on the basis of the present study, can be easily located in the vicinity of a TEM and its use does not require any modifications to the installed TEM.

One of the major limitations of using an environmental cell holder is the pole piece gap. As described previously, this is the distance between the magnetic pole pieces which comprise the magnetic electron lenses and within which the *in situ* holder is located. The *In situ* holder designed here consists of an environmental cell which is only 3.5 mm high. This makes the holder extremely flexible for use with a variety of commercially available TEM's. It can also be used to tilt the specimen through an angle of +/- 15 ^{0}.

Figure 58: The complete gas flow and heating assembly

5.1 GAS SOLID REACTIONS

To conduct gas-solid reactions at elevated temperatures, *in situ* within a TEM, it is required to confine the gaseous environment within the vicinity of the sample region, allowing the TEM column and the gun vacuum to be maintained at operable levels.

The designed *in situ* environmental cell holder was successfully tested in JEOL-2000 TEM. The effect of the gaseous environment, within the E-cell, on the microscope column pressure is shown Figure 59. The vacuum level attained within the column by the TEM pumping system was 1.5E-5 Pa when a traditional holder was used. This particular holder did not possess any gas flow mechanism. When the *in situ* holder was used and 5 sccm of argon gas was circulated through the environmental cell the microscope vacuum pressure raised to 5.2E-5 Pa. This was well within the operable TEM column pressure. However, with the use of the differential pumping system built into the *in situ* assembly, the TEM column vacuum pressure improved to 2E-5 Pa. This column pressure was equivalent to the pressure attained when a standard TEM holder was used. From these results we can conclude that the gas from the cell was confined around the specimen with the help of the series of o-ring seals built around the gas chamber. These results along with the compatibility of the cell materials clearly indicate that this environmental cell can be used for a vast range of applications that require the use of corrosive gases, without adversely affecting the TEM components.

Most gas-solid reactions require the presence of 1 atmosphere pressure (760 torr, 1.01E5 Pa) in the sample region within the environmental cell. Currently available *in situ* holders and commercial ETEM's can only generate a gas pressures in the range of 100-200 torr within the reaction chamber [9]. Higher pressures are required in order to obtain kinetic data that is compatible to real life situations. In order to test the pressure withstanding capacity of the current

holder, the gas inlet port was opened and exposed to atmosphere, when the holder was inserted within the TEM. This inlet port was directly connected to the environmental cell. By doing this the pressure within the cell was raised to 1 atmosphere. This did not bring about any major change in the TEM column pressure, indicating that the current holder can be easily used for observation and analysis of reactions that require high pressures. The maximum pressure attained within the cell is restricted due to the structural rigidity of the silicon nitride windows. In the present environmental cell the windows were 20nm thick.

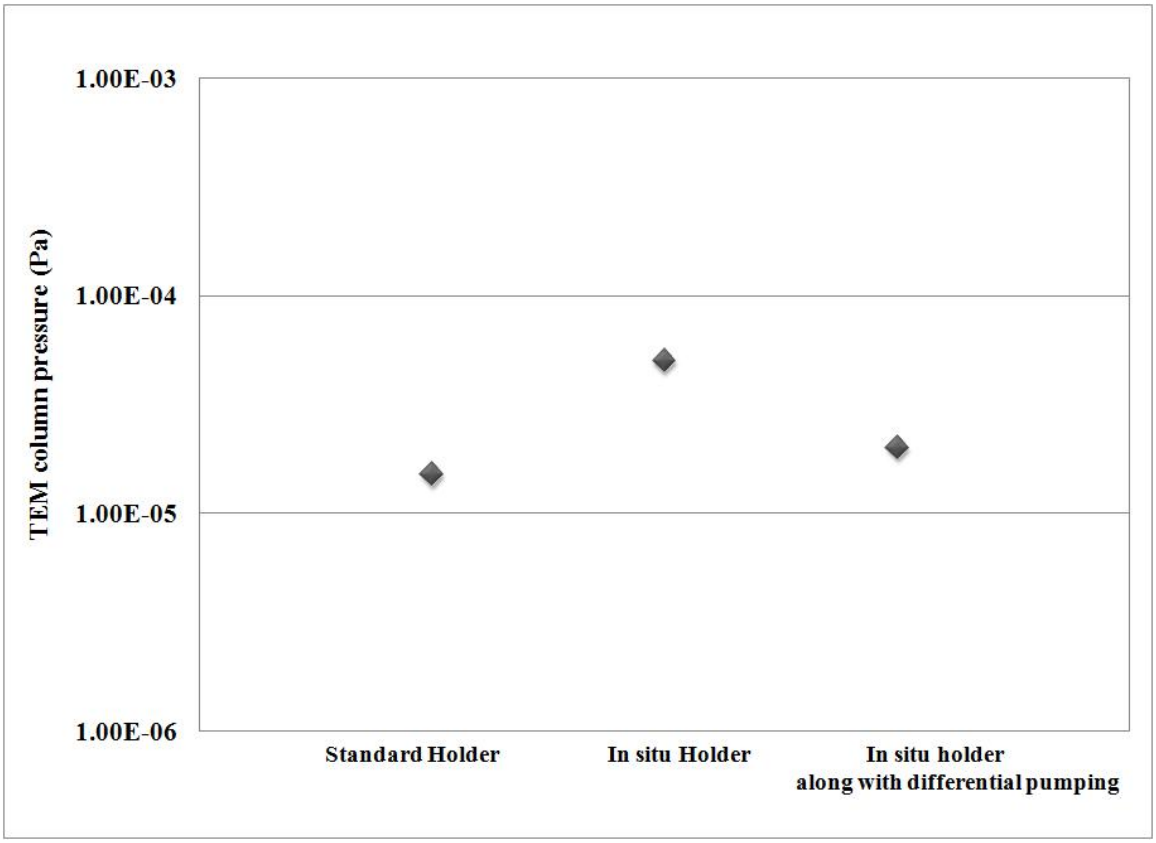

Figure 59: Effect of gas flow within the environmental cell on the TEM column pressure

These windows also play an important role when determining the desired image contrast and resolution. The current holder has a flexible design allowing for the use of the desired

window thickness which can be selected depending upon the nature of the specimen examined and what is judged acceptable image quality by the experimenter.

Investigations on the effect of amorphous silicon nitride windows on the image quality were carried out in a JEOL 2000 TEM. The test specimen used was a lacy carbon grid with Au/MgO particles suspended on it. Figure 60 shows the magnified image. From the figure it can be seen that at average magnification, the observed image was sharp and the silicon nitride window did not impose any additional structural information on the image.

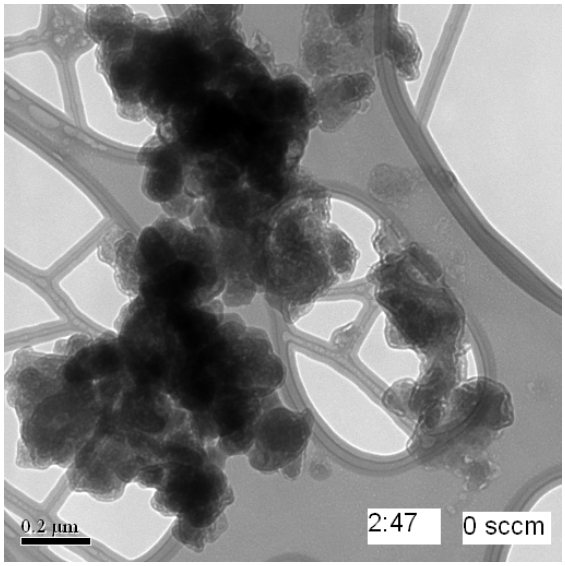

Figure 60: Magnified TEM image of Au/MgO particles suspended on a lacy carbon grid when viewed through the 20 nm silicon nitride windows using the *in situ* environmental cell holder

The distance between the windows determines the gas path length. As mentioned previously, it is important to minimize this length as it determines the amount of interaction of the electron beam with the gas molecules. The mass thickness of the gaseous environment causes scattering of the electron beam and this ultimately determines the beam intensity and image resolution. In the present holder the gas path length was less than 1 mm. The effect of gas flow

on the image resolution obtained within the *in situ* environmental cell holder was observed by passing a mixture of 5% H_2/N_2 on Au/MgO particles suspended on a lacy carbon grid.

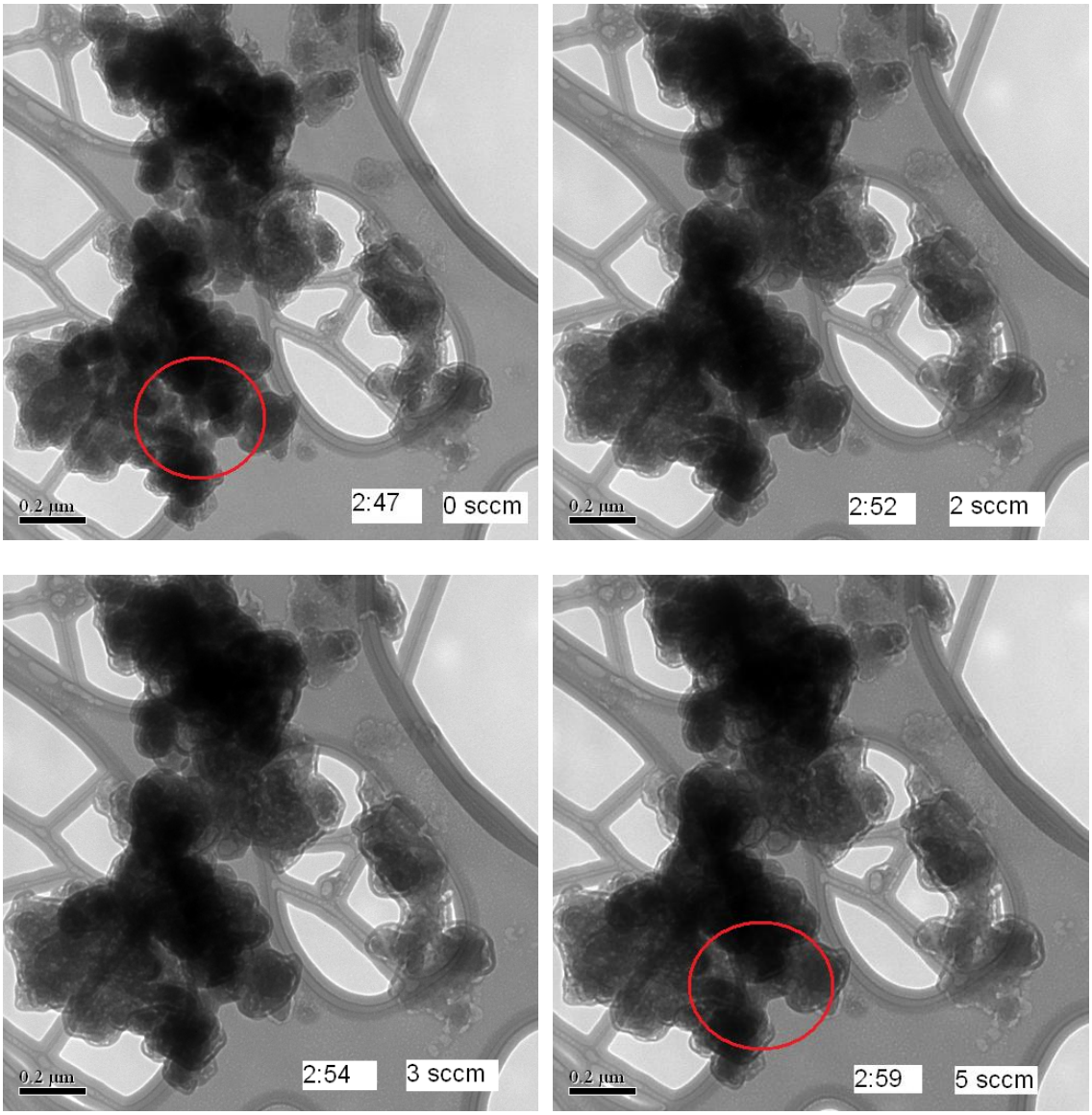

Figure 61: TEM observation of Au/MgO particles suspended on a lacy carbon grid

Figure 61 shows the variation of the of the image quality with the increase in the amount of gas circulated over the specimen. The mass flow rate of the gas mixture was accurately controlled and gradually ramped in increments of 1 sccm. From the images it can be seen that a gas path length of 1 mm did not cause a noticeable deterioration in the image contrast. It has been established that Au/MgO particles aggregate in the presence of H_2/N_2. For this reason, it is preferred to load the specimen in a vacuum environment, within a glove box. Since our holder did not have the provision where in it could be loaded with the specimen within a glove box, the specimen was handled in atmosphere. This accelerated the Au/MgO particles aggregation before it could be viewed within a TEM. As shown in Figure 61, gradual aggregation can still be observed in small regions within the image (red circle).

Image drift is an important factor to be considered, especially when dealing with environmental cell holders that require observations for a prolonged duration of time. The major causes of image drift are thermal, mechanical and electrical stability. Detailed studies [56-57] have been carried out in the past to understand the major sources that attribute to image drift. Suggestions with respect to electromagnetic, thermal and vibration drift have been factored into the design of our environmental cell holder. The biggest challenge was to obtain image stability under the influence of gas flow around the specimen within the environmental cell.

In order to calculate the drift rate generated due to the flow of gases with the environmental cell, Au/MgO particles were observed for extended duration of time within the TEM. A steady flow of 5 sccm of gas mixture consisting of 5% H2/N2 was maintained within the *in situ* environmental cell. From the magnified images in Figure 62, it can be seen that during the 300 seconds of continuous gas flow over the specimen the image drifted by only 20 nm and 40 nm in the x and y direction, respectively. Based on this reasonable interpretation of

the images it can be stated that the overall drift rate due to the mechanical stability of the specimen holder and the gas flow were 0.65 Å/s in the x direction and 1.3 Å/s in the y direction.

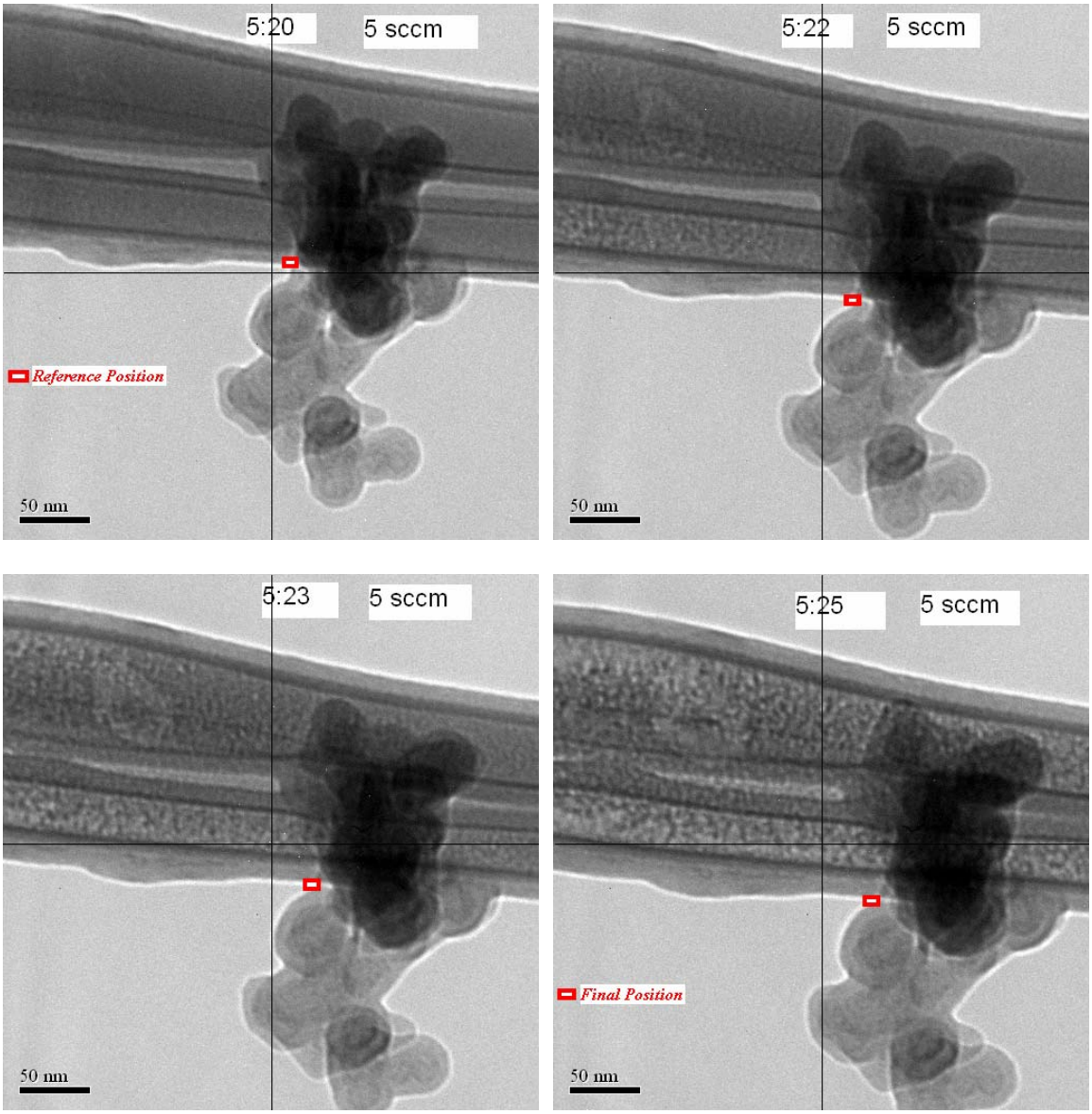

Figure 62: Drift observations using Au/MgO in 5% H2/N2

5.2 THERMAL REACTIONS

Design consideration of gas flow, which involves minimum gas path length, is often conflicting in terms of space with respect to the second objective of this research, elevating the specimen to high temperatures. The two important considerations for *in situ* heating involve the ability of the specimen to reach high temperatures as well as to attain thermal and mechanical stability.

Finite element analysis was used extensively to model heat flow and to minimize thermal drift. The use of laser heating has also expanded the range of applications for the *in situ* environmental cell assembly. Most commercially available heating holders can heat the specimen only up to 1000 ^{0}C [16]. To study specimen reactions, including ceramic materials, higher temperatures are desired. The *in situ* environmental cell assembly designed on the basis of this study incorporates a novel CO_2 laser which can provide energy to heat the specimen in excess of 2000 K. The maximum temperature that can be attained is limited only by the material of the specimen cup and ability of the surrounding windows to withstand heat radiation.

Figure 63, shows the SEM image of the *in situ* specimen cup that was used to heat the specimen in the presence of an oxidizing environment. As mentioned previously the specimen cup was made of tantalum which has a melting temperature in excess of 2500 ^{0}C. The laser energy focused on the cup was ramped continuously in order to observe the maximum temperature that can be achieved. As observed from Figure 63, the laser beam was strong enough to melt a hole within the tantalum cup.

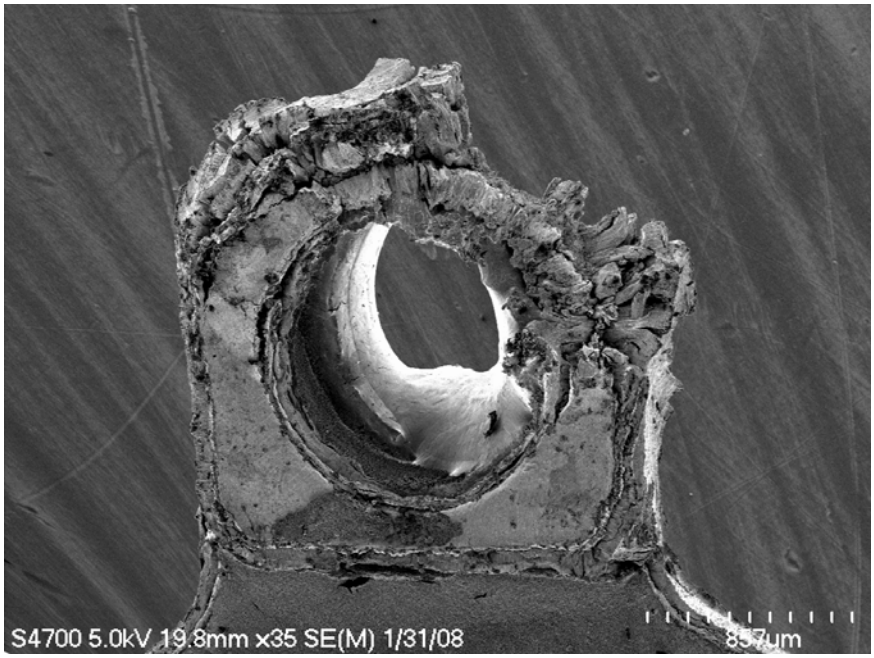

Figure 63: SEM image showing the effect of high power CO_2 laser heating on the specimen cup

Traditional heating holders require water cooling in order to minimize inadvertent heating of the surrounding holder components. However, the use of focused CO_2 laser beam has completely eliminated the need of complex heating and water cooling mechanism. The *in situ* specimen cup is isolated from the rest of the environmental cell, thus concentrating the energy only in the desired region of interest. Also traditional heating holder takes 1-2 hrs for the specimen temperature to stabilize after high temperature is reached. From the experimental results described in this study we have a clear advantage of using the focused laser energy. Using laser heating technique, it took less than 60 seconds to attain high, steady state specimen temperature.

6.0 CONCLUSION

In this dissertation a transmission electron microscope specimen holder assembly has been successfully designed and developed that would facilitate *in situ* observations of gas solid reactions at elevated temperatures for a wide range of applications.

The National Science Foundation workshop held in January 2006 clearly outlines the need for dynamic *in situ* electron microscopy as a tool to meet the challenges of the nano world. The advantages of these modern *in situ* techniques include

1. Following the evolution of transformation mechanism at the atomic-level, allowing different steps of nucleation and growth processes to be identified from the time resolved images and spectra
2. Identification of both stable and meta-stable intermediate phases
3. Determination of thermodynamic and kinetic data for individual nanostructures
4. Synthesis and structural characterization is performed simultaneously and this dynamic feedback may allow synthesis conditions to be rapidly optimized

Although the future research goals had been clearly demarcated, what was clearly lacking was the provision by which the researchers could achieve these objectives. This dissertation was focused on providing a tool to accomplish this requirement.

The *in situ* assembly designed in this dissertation incorporated a gas flow and heating mechanism along with a window-type environmental cell. It has the provision to circulate a

controlled mixture of up to four different gases over the specimen within the cell. The cell can easily withstand a gas pressure differential of up to 1 atmosphere. The unique heating mechanism provided within the assembly can heat the specimen beyond 1500 °C. The novel carbon dioxide laser heating technique offered major advantages over conventional heating methods in terms of product life, specimen heating time and design size. Finite element analysis was used extensively to optimize the thermal performance of the cell. The deep understating of radiation and conduction pattern within the cell helped in retaining the heat within the region of interest, thus minimizing thermal drift at elevated temperatures.

The cell design incorporates a gas reaction chamber less than 1 mm in height, enclosed between a pair of 20 nm thick silicon nitride windows. The overall height of the environmental cell was 3.5 mm. This cell height can be easily incorporated within the pole pieces of most commercial transmission microscopes, making the design highly flexible in terms of usability. The chamber can accommodate standard specimens or a grid having a diameter of 3 mm and thickness in the range of 50 to 100 microns. The amorphous nature of the silicon nitride windows helped in retaining image contrast without the introduction of any extraneous information.

With the advent of the atomic-resolution environmental transmission electron microscope (ETEM), researchers now have a tool to directly image–at atomic scale-the dynamic structure, morphology and composition of heterogeneous catalysts in their functioning state. However ETEM's are very expensive and only few large organizations have the privilege to install one in their facility. With the development of the current *in situ* assembly, a cutting edge tool for dynamic electron microscopy will be within the reach of all educational and research institutions in terms of portability and cost. Institutions having an ETEM would also benefit from this development as the use of this *in situ* assembly along with their microscope would help them

achieve the desired gas pressure and specimen temperature. It is envisioned that this tool would profoundly impact the way *in situ* experiments are performed in applications ranging from nano scale observations to biological interactions.

6.1 FUTURE WORK

6.1.1 Pressure within the Environmental cell

In order to control the environment within the *in situ* cell, it is essential to continuously monitor the gas pressure within the specimen chamber. The biggest challenge in doing so arises from the space constraints imposed due to factors involving TEM pole piece gap, image resolution and thermal compatibility. Currently the pressure at the inlet and the outlet ports of the holder is monitored in order to approximately calculate the pressure within the cell. This pressure is further correlated with some experimental results that are known to occur at a certain pressure.

Due to the complex gas flow mechanism leading to the environmental cell it is difficult to formulate a theoretical equation that could be used to accurately monitor the gas pressure within the environmental cell. Tools such as the residual gas analyzer (RGA), which is a type of mass spectrometer, have been used for process control and contamination monitoring in semiconductor industries. RGA's can easily be used to detect traces of gases in low pressure gas environment. However, the size of the analyzer prohibits its use in our current application.

In order to devise a mechanism to measure the pressure within the cell, research will be carried out in the field of micro electro mechanical devices (MEMS). This technology combines microelectronics with tiny mechanical systems such as valves and gears, all on one

semiconductor chip using nanotechnology to measure pressure. Efforts are underway to collaborate with Technical University of Denmark, Center of Electron Naoscopy. It is envisioned to mount a MEMS pressure sensor on the 300 nm thick silicon nitride window which forms the environmental cell.

Along with pressure calibration, direct simulation Monte Carlo method (DSMC) will be utilized in order to optimize molecular distribution of the gas within the environmental cell. The degree of rarefication of the gas is generally expressed in terms of Knudsen number (Kn), which is the ratio of the mean free path of the gas molecules to a characteristic dimension. For the free molecular flow regime the Kn number approaches infinity. DSMC is a well established method that has been successfully used to simulate high Kn number gas flow problems. The DSMC method stores the position, velocity and the initial states of the gas molecules and modifies in time, the process of particles moving, colliding among themselves and interacting with boundaries in the simulated physical space. The environmental cell geometry will be further optimized by studying the results obtained from these simulations. The molecular distribution within the chamber will be analyzed and the gas impingement rate on the specimen will be improved. These parameters are essential to perform atomic scale observations of gas solid reactions.

6.1.2 Specimen Temperature

It is critical to know the specimen temperature within the environmental cell. In order to observe reactions at predetermined temperatures, the user should be able to continuously monitor and control the specimen temperature. In the current holder design the specimen is heated indirectly through the laser heating of the specimen cup. In the initial prototype of the specimen holder, a

thermocouple was attached to the specimen cup and the temperature was controlled through a feedback loop controlling the laser power with the help of data acquisition boards. Although the laser power can be controlled precisely, the specimen temperature obtained was not very accurate. Because of the small size of the specimen cup, the thermocouple mounted on it acted as a heat sink complicating the thermal balance of the environmental cell. Also, there is a limitation on the type of thermocouple that can be used for recording high temperatures (2000 K). The maximum temperature attained by the specimen for a given laser power depends upon the properties of the material. In the future, a detailed study will be conducted by melting various materials within the specimen cup. Depending upon the melting temperature of the material, the laser power will be correlated to temperature for the given material. Also, it is envisioned to mount a MEMS sensor along with the pressure sensor on the silicon nitride window.

The current holder is designed to observe a 3mm specimen disc. As new specimen preparations techniques such as the focused ion beam method (FIB) evolve, there is a need to provide provisions within the environmental cell to clamp specimens of various shapes and sizes. This environmental cell design will be further modified to incorporate such TEM specimens for a wider range of applications.

BIBLIOGRAPHY

1. D. B. Williams and C. B. Carter, "Transmission Electron Microscopy", *Plenum Press*, 1996

2. S. B. Newcomb, C. S. Baxter and E. G. Bithell, "The preparation of cross-section TEM specimens", *Proceedings of the 9th European Conference on Electron Microscopy*, Volume 1, Pages 43-48, 1988

3. G. Thomas and M. J. Goringe, "Transmission Electron Microscopy of Materials," *John Wiley and Sons,* 1979

4. R. D Schoone and E. A. Fischione, "Automatic unit for thinning transmission electron microscopy specimens of metals," *Review of Scientific Instruments*, Vol. 37, No. 10, 1351-1353, 1966

5. P. E. Fischione, T. K. Kelly, A. Dalley, L Holzman and Dawson-Elli, "Advances in ultrasonic disk cutting and precision dimpling," *Mater Res Soc Symp Proc*, Volume 254, 79-97, 1991

6. P. B. Hirsch, A. Howie, R. B. Nicholson, D. W. Pashley and M. J. Whelan, "Electron microscopy of thin crystals", *The Butterworth Inc*, 1965

7. P. J. Goodhew, "Thin foil preparation for electron microscopy", Elsevier Science Publications, 1985

8. "Dynamic *in situ* electron microscopy as a tool to meet the challenges of the nanoworld", *NSF workshop report, Tempe, Arizona*, 2006

9. E. P. Butler, K. F. Hale, "Dynamic Experiments in the Electron Microscope", *North-Holland Publishing Company, New York*, 1981

10. P. R. Swann and N. J. Tighe, "Performance of differentially pumped environmental cell in the AE1 EM7", *Proc. 5th Eur. Congr. Electron Microsc*., *Manchester,* pp. 360, 1972a

11. P. R. Swann and N. J. Tighe, "Voltage and pressure dependence of the electron transmission through various gases", *Proc. 5th Eur. Congr. Electron Microsc*., *Manchester*, pp. 436, 1972b

12. M. J. Flower, "High voltage electron microscopy of environmental reactions", *J. Microsc*., 97, 171, 1973

13. J. N. Turner, C. W. See, A. J. Ratkowski, B. B. Chang and D. F. Parsons, "Design and Operation of a Differentially Pumped Environmental Chamber for the HVEM", *Ultramicroscopy*, 6, 267-280, 1981

14. T. C. Lee, D. K. Dewald, J. A. Eades, I. M. Roberstson, and H. K. Birnbaum, "An environmental cell transmission electron microscope", *Rev. Sci. Instrum*., 62 (6), 1438-1444, 1991

15. R. Sharma and K. Weiss, "Development of a TEM to Study *In Situ* Structural and Chemical Changes at an Atomic Level During Gas-Solid Interaction at Elevated Temperatures", *Microscopy Research and Technique*, 42, 270-280, 1998

16. R. Sharma, "Design and Application of Environmental Cell Transmission Electron Microscope for In Situ Observation of Gas-Solid Reactions", *Microscopy and Microanalysis,* 7, 494-506, 2001

17. R. Sharma, "An environmental transmission electron microscope for in situ synthesis and characterization of nanomaterials", *Journal of Materials Research*, 20 (7), 1695-1707, 2005

18. E. D. Boyes, P. L. Gai, "Environmental high resolution electron microscopy and applications to chemical science", *Ultramicroscopy*, 67, 219-232, 1997

19. P. Gai, K. Kourtakis and S. Ziemecki, "In Situ Real-time Environmental High Resolution Electron Microscopy of Nanometer Size Novel Xerogel Catalysts for Hydrogenation Reactions in Nylon 6,6", *Microscopy and Microanalysis*, 6, 335-342, 2000

20. P. Gai and E. D. Boyes, "Pioneering Development of Atomic Resolution *In Situ* Environmental Transmission Electron Microscopy for Probing Gas-Solid Reactions and *In Situ* Nanosynthesis", *Mater. Res. Soc. Symp. Proc.,* 876E, 2005

21. M. Zhang, E. A. Olson, R. D. Twesten, J. G Wen, L. H Allen, I. M. Robertson, "*In situ* transmission electron microscopy studies enabled by microelectromechanical system technology", *Journal of Materials Research*, 20 (7), 1802-1807, 2005

22. D. Teter, P. Ferreira, I. M. Robertson, and H. K. Birnbaum, "An environmental Cell TEM for studies of gas-solid interactions", *New Techniques for Characterizing Corrosion and Stress Corrosion, TMS Warrendale, PA*, 53-72, 1995

23. I. M. Robertson and D. Teter, "Controlled Environmental Transmission Electron Microscopy", *Microscopy Research and Technique*, 42, 260-269, 1998

24. Tyrone L. Daulton, Brenda J. Little, Kristine Lowe, and Joanne Jones-Meehan, "In Situ Environmental Cell–Transmission Electron Microscopy Study of Microbial Reduction of

25. M. Komatsu and H. Mori, "In situ HVEM study on copper oxidation using an improved environmental cell", Journal of Electron Microscopy, 54(2), 99-107, 2005

26. H. Konishi, A. Ishikawa, Y-B. Jiang, P. Buseck and H. Xu, "Sealed Environmental Cell Microscopy", *Microscopy and Microanalysis*, 9(2), 902-903, 2003

27. P. A. Crozier, "Gas-Solid reactions and Nanomaterials Research", *IMC16, Sapporo*, 909, 2006

28. T. Kamino, T. Yaguchi, M. Konno, A. Watabe, T. Marukawa, T. Mima, K. Kuroda, H. Saka, S. Arai, H. Makino, Y. Suzuki and K. Kishita, "Development of a gas injection/specimen heating holder for use with transmission electron microscope", *Journal of Electron Microscopy*, 54(6), 497-503, 2005

29. R. T. Hodgson, G. S. Boebinger, and P. E. Batson, "In situ laser heating in a scanning transmission electron microscope", *Appl. Phys. Lett*., 43 (9), 881-883, 1983

30. O. Bostanjoglo and E. Endruschat, "Kinetics of Laser-induced Crystallization of Amorphous Germanium Films", *Phys. Stat. Sol. (a),* 91, 17 (1985)

31. H. Domer and O. Bostanjoglo, "High-speed transmission electron microscope", *Rev. Sci. Instrum*., 74 (10), 4369-4372, 2003

32. A. Takaoka, N. Nakamura, K. Ura, H. Nishi, and T. Hata, "Local Heating of Specimen with Laser Diode in TEM", *J. Electron Microsc*., Vol. 38, No. 2, 95-100, 1989

33. V. A. Lobastov, R. Srinivasan, and A. H. Zewail, "Four-dimensional ultrafast electron microscopy", *PNAS*, Vol. 102, No. 20, 2005

34. T. LaGrange et. al., "Single-shot dynamic transmission electron microscopy", *Appl. Phys. Lett*., 89, 044105, 2006

35. S. Patel, "Optical suitability of window materials for CO_2 lasers", *Applied Optics*, 16 (5), 1232-1235, 1977

36. M. Prokhorov, V. I. Konov, I. Ursu, I. N. Mihailescu, "Laser Heating of Metals", *Adam Hilger,* 1990.

37. A. Mehmetli, K. Takahashi, and Shunichi Sato, "Direct measurement of reflectance from aluminum alloys during CO_2 laser welding" *Applied Optics*, 35 (18), 3237-3241, 1996

38. E. Bernal, "Heat Flow Analysis of Laser Absorption Calorimetry", Applie Optics, 14 (2), 314-321, 1975

39. L. K Ang, Y. Y. Lau, R. M. Gilgenbach and H. L. Spindler, "Analysis of laser absorption on a rough metal surface" *Appl. Phys. Lett*., 70 (6), 696-698, 1997

40. P. A. A. Khan and T. Debroy, "Absorption of CO_2 Laser Beam by AISI 4340 Steel" *Metallurgical Transactions B,* 16B, 853-856, 1985

41. M. Bramson, "Infrared Radiation: A Handbook for Applications", *Plenum Press*, p-127, 1968.

42. J. F. Ready, "Industrial Applications of Lasers", Academic Press, 1997

43. E. A. J. Marcatili and R. A. Schmeltzer, "Hollow metallic and dielectric wave guides for long distance optical transmission and lasers" *Bell Syst. Tech. J*., 43, 1783-1809, 1964

44. J. A. Harrington, C. C. Gregory, "Hollow sapphire fibers for delivery of CO_2 laser energy" *Opt. Lett*, 15, 541-543, 1990

45. C. C. Gregory and J. A. Harrington, "High peak power CO_2 laser transmission by hollow sapphire waveguides", *Appl. Opt*., 32, 3978-3980, 1993

46. T. Abel, J. Hirsch, J. A. Harrington, "Hollow glass wave guides for broad band infrared transmission" *Opt. Lett*., 19, 1034-1036, 1994

47. R. K. Nubling and J. A. Harrington, "Hollow wave guide delivery systems for high-power industrial lasers", *Appl. Opt*., 34, 372-380, 1996

48. J. Dai and J.A. Harrington, " High-peak-power, pulsed CO_2 laser light delivery by hollow glass waveguides", *Appl. Opt*., 36, 5072-5077, 1997

49. ANSYS, Inc. Release 10.0 Theory Reference, Canonsburg, PA, USA: ANSYS Inc., 2005

50. *SolidWorks 3D CAD software*, D'S SolidWorks, Concord, Massachusetts, USA, 2007

51. www.matweb.com

52. www.polymicro.com

53. www.lasermech.com

54. J. F. O'Hanlon, "A users guide to vacuum technology" 2nm Edition, John Wiley and Sons, New York, NY, 1989

55. P. J. Ferreira, K. Mitsuishi, and E. A. Stach, "*In Situ* Transmission Electron Microscopy", MRS Bulletin, 33, No.2, 83-85, 2008

56. J. Adler and S.N. Pagakis, “Reducing image distortions due to temperature-related microscope stage drift”, *Journal of Microscopy*, 210(2), 131-137, 2003

57. A. Muller and J. Grazul, “ Optimizing the environment for sub-0.2 nm scanning transmission electron microscope”, *Journal of Electron Microscopy,* 50(3), 219-226, 2001

58. B. Khalid, “Development of Precision TEM Holder Assemblies for Use in Extreme Environments”, *PhD Dissertation*, University of Pittsburgh, 2005

59. www.ni.com

60. Z. Wang, et al., ”Fiber-Guided CO_2 Laser Surgery in an Animal Model”, *Photomedicine and Laser Surgery*, 24(5), 646-650, 2006

61. R. Van Hillegersberg, “Fundamentals of laser surgery”, *Eur. J. Sur*., 163, 3–12, 1997

62. ncem.lbl.gov/TEAM-project